

ABSTRACT

Title of Document: CHARACTERIZATION OF RIBOSOMAL
PROTEIN L2 AND ANALYSIS OF
MISSENSE CODON DISCRIMINATION IN
THE YEAST *SACCHAROMYCES CEREVISIAE*

Johnathan Robert Russ, Ph.D., 2007

Directed By: Associate Professor Dr. Jonathan D. Dinman,
Department of Cell Biology and Molecular
Genetics

Translational fidelity is of vital importance to the ribosome as it strikes an optimal balance between speed and accuracy. The study of factors contributing to the structure and function of the ribosome by assaying effects on fidelity yields important insights into the mechanism of the ribosome. Ribosomal protein L2 is vital to the structure and function of the ribosome with importance in RNA interaction and positioning, ribosomal subunit binding, and peptidyl transfer. Sixteen unique alleles of the *RPL2A* gene were studied for their effects on translational fidelity and general ribosome function. Mutations at V48D and L125Q of the highly structured globular domain proved generally deleterious to growth, but resistant to anisomycin, and markedly increased -1 programmed ribosomal frameshifting. H215Y, a mutation at the site of interaction with H93 of the peptidyl transferase center (PTC), was both sparsomycin and anisomycin resistant, indicating a functional impact on the PTC structure. Mutations at F185L and

W195C border conserved rRNA binding regions and proved hyperaccurate in misincorporation studies. Understanding of fidelity and proper tRNA selection in translation requires analysis of how the ribosome discriminates between cognate, near-cognate, and non-cognate tRNAs. Measuring misreading of several codon substitutions in the context of paromomycin as well as mutations and deletions of contributing elongation factors and ribosome structural elements allowed further understanding of interactions governing tRNA selection and tRNA misincorporation events. A mutant of eEF1B α , the nucleotide exchange factor for eEF1A, promoted a general increase in fidelity. Interestingly, a mutated ribosomal protein L5, though distant from the decoding center, also stimulated hyperfidelity in both near- and non-cognate cases. Distinction between near- and non-cognate tRNA interactions on the ribosome was observed in tests using paromomycin, and in studying mutations of eEF1B γ with both demonstrating increased misreading of near-cognate codons but hyperaccurate decoding of non-cognate codons.

CHARACTERIZATION OF RIBOSOMAL PROTEIN L2 AND ANALYSIS OF
MISSENSE CODON DISCRIMINATION IN THE YEAST *SACCHAROMYCES*
CEREVEVISIAE

By

Johnathan Robert Russ

Dissertation submitted to the Faculty of the Graduate School of the
University of Maryland, College Park, in partial fulfillment
of the requirements for the degree of
Doctor of Philosophy
2007

Advisory Committee:

Associate Professor Jonathan D. Dinman, Ph.D., Chair

Adjunct Associate Professor James Culver, Ph.D.

Associate Professor Jeffery DeStefano, Ph.D.

Assistant Professor Jocelyne DiRuggiero, Ph.D.

Associate Professor Jason Kahn, Ph.D., Dean's Representative

© Copyright by
Johnathan Robert Russ
2007

Dedication

To Rosemary, thank you for putting up with me, none of this would have happened without you.

To Madeline, soon you'll be here to see what your mother has had to put up with.

To Chris, RIP, I miss you my friend, you just barely missed the celebration...

Acknowledgements

Thanks to all the members of the Dinman lab, past and present, and the boss man himself, JD. Thanks to all the many friends who have kept me sane through the years. Special props to the redhead and my partner-in-crime 337 for staying close and still wanting to know me after 5 years!

Table of Contents

Dedication	ii
Acknowledgements	iii
Table of Contents	iv
List of Tables.....	vi
List of Figures	vii
List of Abbreviations	ix
Chapter 1: Background	1
Introduction	1
Initiation	2
Elongation	4
<i>Aminoacyl-tRNA selection and accommodation</i>	4
<i>Peptidyl transfer</i>	5
<i>Translocation</i>	6
Termination	7
Translational recoding	8
<i>Programmed -1 ribosomal frameshifting</i>	8
<i>Programmed +1 ribosomal frameshifting</i>	11
<i>Missense incorporation and nonsense suppression</i>	13
Chapter 2: Ribosomal protein L2	14
Introduction	14
Materials and methods	16
<i>Strains, plasmids, and media</i>	16
<i>L2 knockout strain construction</i>	17
<i>Mutation library creation</i>	18
<i>Temperature response, drug sensitivity, and growth curves</i>	20
<i>Translational fidelity assays</i>	23
<i>Polysome profiles</i>	24
<i>Computational analysis</i>	25
Results.....	26
<i>rpl2A alleles</i>	26
<i>Temperature variable dilution spots and growth curves</i>	28
<i>Mutant pharmacological response</i>	32
<i>-1 PRF and +1 PRF measurements with killer phenotypes</i>	36
<i>Further translational defect analysis</i>	37
<i>Polysome profiles</i>	41
Discussion	43
Chapter 3: Differentiating between near- and non-cognate codons in <i>Saccharomyces cerevisiae</i>	47
Introduction	47
Materials and methods	52
<i>E. coli and yeast strains and genetic methods</i>	52
<i>Plasmid constructs</i>	52

<i>Dual luciferase assays</i>	53
Results.....	54
<i>Baseline and Paromomycin-stimulated rates of missense suppression suggest a functional difference between the near- and non-cognate tRNAs</i>	54
<i>eEF1A mutants generally affect utilization of near-cognate aa-tRNAs</i>	57
<i>A mutation in eEF1Ba promotes general hyperfidelity</i>	60
<i>Codon-specific misreading in the absence of eEF1Bγ</i>	61
<i>The K27E mutant of ribosomal protein L5 promotes a general enhancement of fidelity</i>	62
Discussion	64
<i>Influence of eEF1A and associated elongation factors in translational fidelity</i>	68
<i>Ribosomal protein L5: Coordination of tRNA exit from the E-site with aa-tRNA entrance at the A-site</i>	72
<i>Kinetics: the difference between near- and non-cognate interactions may occur at the GTPase activation step</i>	73
<i>Using Paromomycin to functionally distinguish between ‘near-‘ and ‘non-cognate’ codon:anticodon interactions</i>	75
Chapter 4: Conclusions and future directions	78
Introduction	78
The extension and tip of ribosomal protein L2	78
Other mutations in ribosomal protein L2	80
An intersubunit bridge in L2	82
Significance of near- and non-cognate tRNA differentiation	83
Misincorporation of tRNA and ribosome structure.....	84
Appendix A: L2 mutation strains generated	85
Appendix B: Primers used in L2 study	90
Reference list.....	92

List of Tables

Table 2.1: List of yeast strains used in L2 study.....	18
Table 2.2: Effects of mutations in ribosomal protein L2 on rates of -1 and +1 frameshifting.....	37
Table 2.3: Effects of mutations in ribosomal protein L2 on rates of non- and near-cognate tRNA misincorporation.....	39
Table 2.4: Effects of mutations in ribosomal protein L2 on nonsense suppression rates..	40
Table 3.1: Baseline levels and effects of Paromomycin on suppression of missense mutations at codon 218 of firefly luciferase.....	54
Table 3.2: Effects of selected alleles of genes on mis-reading of non-cognate and near- cognate mutations at codon 218 of firefly luciferase.....	60
Table 3.3: Survey of isogenic wild-type and mutant pairs of strains with seven different Codons at codon 218 of firefly luciferase.....	62
Table 3.4: Yeast strains used in this study.....	76

List of Figures

Figure 1.1: Eukaryotic cap-dependent translation initiation.....	3
Figure 1.2: Kinetic proofreading in aminoacyl-tRNA selection.....	5
Figure 1.3: The hybrid states representation of the translocation cycle.....	7
Figure 1.4: L-A and M ₁ virus propagation in yeast and the “killer assay”.....	10
Figure 1.5: The integrated model for programmed ribosomal frameshifting.....	12
Figure 2.1: Amino acid sequence alignment of ribosomal protein L2.....	15
Figure 2.2: Locating L2 in the ribosome.....	16
Figure 2.3: Schematic of RPL2A cassette.....	18
Figure 2.4: Structures of ribosome binding drugs.....	21
Figure 2.5: Dual luciferase assay.....	24
Figure 2.6: Single mutations of L2.....	28
Figure 2.7: Variable temperature dilution spots of L2 single mutation strains.....	30
Figure 2.8: Growth curves of single mutation L2 strains.....	31
Figure 2.9: Anisomycin variable dilution spots of L2 single mutation strains.....	33
Figure 2.10: Paromomycin variable dilution spots of L2 single mutation strains.....	34
Figure 2.11: Drug filter disc assays for mutants of ribosomal protein L2.....	35
Figure 2.12: Dual luciferase measurements of PRF efficiency in single mutation strains.....	36
Figure 2.13: Dual luciferase measurements of translational fidelity characteristics.....	38
Figure 2.14: Polysome profiles of L2 mutant strains.....	42
Figure 3.1: The decoding center and dual-luciferase reporters for determining rates of translational misreading in yeast.....	51

Figure 3.2: Proposed basis for near-cognate codon-anticodon interactions.....	57
Figure 3.3: Effects of the eEF1 complex mutants on mis-reading of near- and non- Cognate codons.....	59
Figure 3.4: Characteristics of alleles of RPL5.....	64
Figure 3.5: Modeling of mutations in eEF1A and eEF1B α that influence misincorporation of missense aa-tRNAs.....	71
Figure 4.1: Mutated residues in the tip of L2.....	80
Figure 4.2: Alignment of L2 from <i>S. cerevisiae</i> and <i>H. marismortui</i>	82

List of Abbreviations

5-FOA	5-fluoroorotic acid
aa-tRNA	Aminoacyl-tRNA
ALS	Amyotrophic lateral sclerosis
ASL	Anticodon stem loop
CFU	Colony forming unit
CMO⁵	Oxyacetic acid modification at position 5 of uridine
DLA	Dual luciferase assay
dsRNA	Double stranded RNA
EDTA	Ethylenediaminetetraacetic acid
eIF	Eukaryotic initiation factor
eEF	Eukaryotic elongation factor
eRF	Eukaryotic release factor
GAC	GTPase associated center
GTP	Guanosine triphosphate
H-	Hartwell's synthetic medium, minus indicated amino acid
KSI	K120R S121Δ I122Δ
LSU	Large subunit of the ribosome
mRNA	Messenger RNA
4.7 MB	YPAD medium pH 4.7 with methylene blue
OD	Optical density at specified wavelength
ORF	Open reading frame
PABP	Poly-A binding protein
PMSF	Phenylmethylsulfonyl fluoride
PTC	Peptidyl transferase center
PRF	Programmed ribosomal frameshifting
RDRP	RNA dependent RNA polymerase
RF	Release factor
RM	Random mutagenesis
RPL	Ribosomal protein of the large subunit

rRNA	Ribosomal RNA
SC	Synthetic complete medium
SDM	Site directed mutagenesis
SH3	Src homology 3 domain
SSU	Small subunit of the ribosome
TEF	Translation elongation factor
tRNA	Transfer RNA
UTR	Untranslated region
YPAD	Yeast extract – peptone – dextrose medium + adenine

Chapter 1: Background

Introduction

The ribosome is a large ribonucleoprotein complex responsible for carrying out the process of protein synthesis in all living cells. In the yeast *Saccharomyces cerevisiae*, the ribosome is composed of 78 unique proteins and 4 different ribosomal RNA (rRNA) molecules (Planta and Mager, 1998). The ribosome complex is comprised of a small and a large subunit. The small subunit sediments at 40S in eukaryotes and 30S in prokaryotic organisms and is the location for the messenger RNA (mRNA) decoding function of the ribosome. The larger subunit (60S in eukaryotes and 50S in prokaryotes) performs the central catalytic action of the ribosome, peptidyl transfer.

The 46 proteins of the yeast large ribosomal subunit surround a core of three rRNA molecules, 25S, 5.8S, and 5S. With the solution of the atomic level structure of the *Haloarcula marismortui* ribosome, the peptidyl transferase center (PTC) active site proved to consist entirely of RNA (Ban et al, 2000). Observation of additional crystals bound with active site substrate analogs led to the assertion that the ribosome is a ribozyme (Nissen et al, 2000) displacing ribosomal proteins as the purported source of catalysis.

Initiation

The process of translation can be divided into three sections: initiation, elongation, and termination. While a variety of initiation mechanisms exist, eukaryotic cap-dependent initiation will be described here, as it is used in the majority of cellular message translation in *Saccharomyces cerevisiae*. As shown in figure 1.1, the 5' ends of most mRNAs have a 7-methylguanosine cap and poly-A tails which are recognized by translation factors in the cell (Shatkin, 1976; Rau et al., 1977). The 43S pre-initiation complex is created when eIF2, GTP and Met-tRNA^{Met} bind the 40S ribosomal subunit allowing eIF1, eIF1A, eIF3, and eIF5 to bind. eIF4F, itself composed of 4 subunits (eIF4A, eIF4B, eIF4E, and eIF4G), binds the 7-methylguanosine cap of the mRNA, interacts with the poly-A binding proteins, and recruits the 43S pre-initiation complex to the 5' end of the message (Grifio et al., 1983; Kozak, 1999; Le et al., 1997). ATP-dependent scanning of the mRNA proceeds from 5' to 3' until reaching the start codon (Kozak, 1980). The start codon is an AUG sequence in the proper context for recognition, a specificity that is poorly understood. At this point, GTP hydrolysis by eIF5 and eIF2 displaces the initiation factors and the 60s ribosomal subunit joins to form a functional 80s ribosome (Sachs et al., 1997).

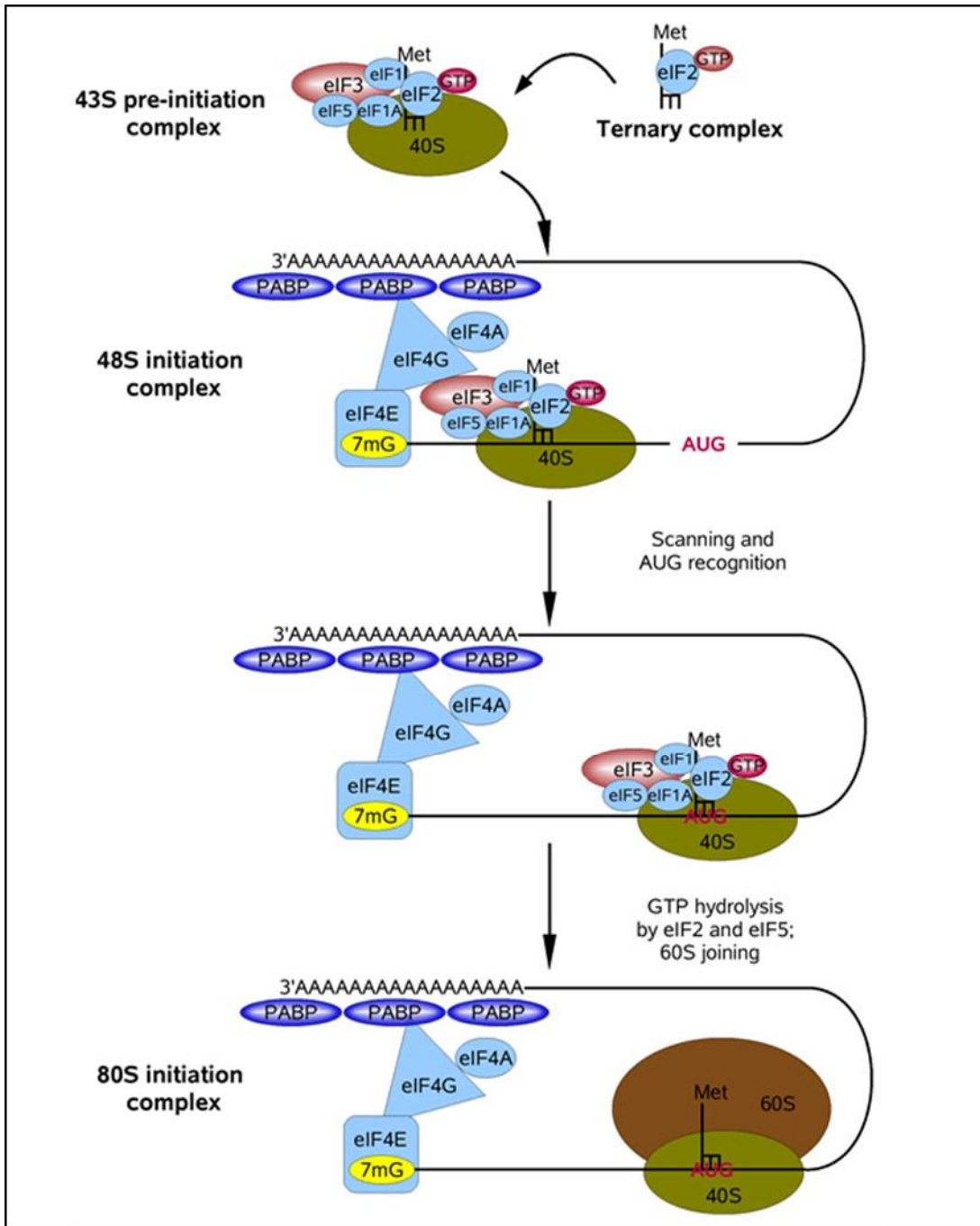


Figure 1.1: Eukaryotic cap-dependent translation initiation

Cap-dependent translation initiation in eukaryotes is a multistep process mediated by many initiation factors. Initiation factors are responsible for connecting the 5' cap of the mRNA with the 3' polyA tail (with PABP), and bringing the pre-initiation complex to the cap where it can begin scanning the message from 5' to 3'. Finally, initiation factors facilitate assembly of the 80s ribosome with an initiator tRNA at the translation start codon of the mRNA.

Elongation

Elongation consists of several steps, divided here as aminoacyl-tRNA selection and accommodation, peptidyl-transfer, and translocation. With the P-site of the ribosome already occupied by tRNA, an aminoacyl-tRNA is accepted and accommodated into the A-site. This is followed by transfer of the nascent peptide chain to the amino acid on the 3' end of the A-site tRNA, and translocation of that same A-site tRNA to the P-site.

Aminoacyl-tRNA selection and accommodation

The “kinetic proofreading” model for tRNA selection identifies two distinct points of discrimination for tRNA selection by the ribosome, and divides the process into six intermediate steps (Ogle and Ramakrishnan, 2005). Initial binding of the tRNA occurs rapidly as the anticodon end of the aminoacyl-tRNA is sampled by the ribosome until a codon match and recognition occurs. This is the first discriminatory step of selection, as non-cognate tRNAs that do not match the codon sequence in the A-site are rejected. When a proper matching tRNA binds and forms base pairs in the A-site, the complex is stabilized as a network of interactions between the small and large subunit rRNA and the tRNA triggers conformational change, GTPase activation, and GTP hydrolysis by eEF1A.

During accommodation, a cognate tRNA is fully accepted into the ribosome as the 3' end of the aminoacyl-tRNA moves into the peptidyl transferase center (computer simulation by Sanbonmatsu et al., 2005). As the tRNA must unbend and allow its 3' end to shift significantly along a specific pathway through two accommodation ‘gates’ to arrive at the PTC, the ribosome is afforded a second point of discrimination. While this

mechanism isn't fully understood, it is possible that near- and non-cognate tRNAs that reach this step are in an incorrect configuration such that the trajectory of the 3' end of the tRNA is unable to pass through the pathway to the PTC, and the tRNA is rejected. (Sanbonmatsu et al., 2005).

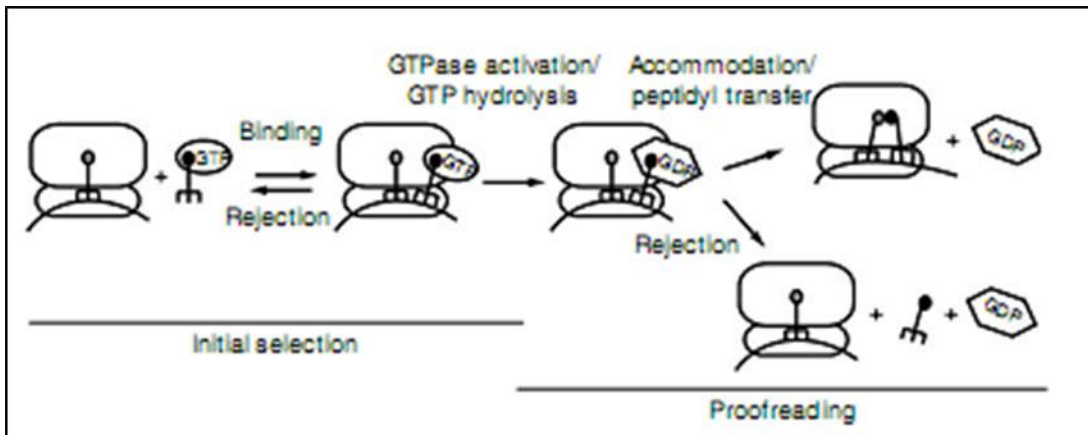


Figure 1.2: Kinetic proofreading in aminoacyl-tRNA selection

This simplified scheme demonstrates the two irreversible steps necessary in kinetic selection of tRNA. Irreversible steps are indicated with only forward arrows. The first opportunity to reject tRNA based on an improper codon:anticodon match occurs at initial binding and selection. Once the irreversible GTPase activation and GTP hydrolysis steps have occurred, initial selection is done. The second and final chance to reject an incompatible tRNA occurs prior to accommodation. If the tRNA is not rejected and is accommodated fully into the A-site, the ribosome is committed to moving forward with peptidyl transfer.

Figure from Cochella et al., 2007

Peptidyl transfer

Following accommodation of aminoacyl-tRNA into the A-site, the main catalytic function of the ribosome, peptidyl transfer, occurs in the PTC. As crystal structures of the ribosome have come available, the active site for peptidyl transfer has proven to be composed entirely of rRNA (Ban et al., 2000). The mechanism of peptidyl transfer is

currently unknown, though many possibilities have been presented. The process is possibly activated by an induced fit mechanism as the PTC structurally rearranges after accommodation (Schmeing et al., 2005). However it is catalyzed, the post-accommodation arrangement of the PTC allows the amino group of the aminoacyl-tRNA to proceed with nucleophilic attack on the carbonyl of the ester connecting the nascent peptide chain to the peptidyl-tRNA. Suggested mechanisms for peptidyl transfer have spanned from acid-base catalysis (Katunin et al., 2002), to substrate assisted catalysis (Weinger et al., 2004), to proximity scenarios (Sievers et al., 2004). In *E. coli*, A2451 (*S. cerevisiae* A2841) has most often been implicated in catalysis (Nissen et al., 2000), as well as the 2'-OH of peptidyl-tRNA A76 (Weinger et al., 2004).

Translocation

Translocation is the process of shifting the translational apparatus in the 3' direction by three nucleotides. The hybrid states model of the entire translocation cycle is represented schematically in figure 1.3. Following peptidyl transfer, the tRNAs shift such that the former peptidyl-tRNA is displaced into the E-site and the aminoacyl-tRNA (now the peptidyl-tRNA) is shifted from an A-site/P-site hybrid state fully into the P-site and the cycle can begin again with aminoacyl-tRNA selection and accommodation into an empty A-site. The translocation step requires EF-G and GTP hydrolysis to proceed efficiently but its specific mechanism is unknown. Structural rearrangements have been observed on both the small and large subunits during translocation (Wilson and Noller, 1998; Gabashvili et al., 1999; Agrawal et al., 1999). There also appears to be a role for the shifting positions of the various bridges between the subunits as a large distance

ratchet-like movement of the small subunit relative to the large subunit has been observed during and is required for translocation (Frank and Agrawal, 2000; Spahn et al., 2004; Horan and Noller, 2007).

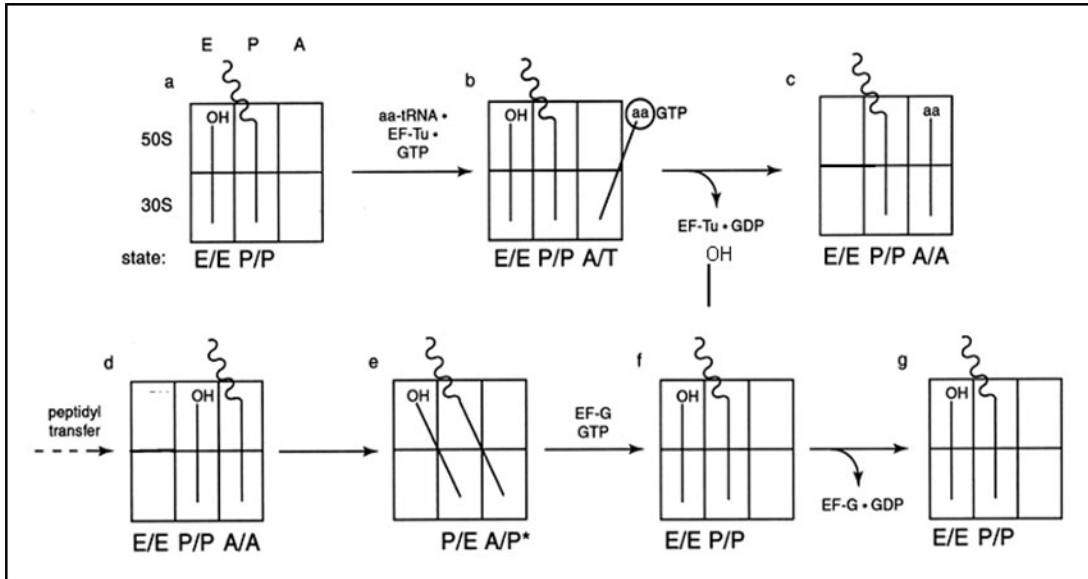


Figure 1.3: The hybrid states representation of the translocation cycle

Each square panel represents the ribosome with the large subunit on top and small subunit on the bottom. The A, P, and E sites of the ribosome are each delineated by the vertical rectangles in each step. The lines represent tRNA and their location during each step in translocation is indicated schematically and in the text below.

Figure from Noller et al., 2002

Termination

Termination occurs as the polypeptide chain is released from the ribosome by hydrolysis of the ester bond attaching it to the peptidyl-tRNA. Release factors recognize the arrival of a stop codon (UAA, UAG or UGA), in the A-site decoding center of the ribosome and trigger the peptide release and subsequent dissociation of release factors from the ribosome. While the mechanism of translation termination is not fully

understood, it is known that a water molecule must be allowed into the PTC of the ribosome for ester bond hydrolysis and eRF1 most likely directs the introduction of this molecule (Song et al., 2000).

Translational recoding

The ribosome serves to translate mRNA into protein within all cells. It has evolved to perform this function with an effective balance of accuracy and speed; incorporating 10-20 amino acids per second with only 1 mistake for 3000 codons translated (Laughrea, 1981). Coding mistakes by the ribosome can manifest themselves as shifts in reading frame, or in events such as missense incorporation and termination readthrough (nonsense suppression).

Programmed -1 ribosomal frameshifting

Programmed -1 frameshifting (-1 PRF) was first identified in the Rous sarcoma virus where, as in many viral systems, it serves to regulate the relative abundance of two products: an abundant Gag (major capsid) protein encoded by the 5' region of the first open reading frame, and a Gag-pol protein encoded as a fusion of the 5' gag and the 3' pol genes (Jacks and Varmus, 1985). The L-A virus of yeast and the HIV-1 virus exhibit the best studied examples of -1 PRF, but signals can be found in genomes of many organisms, including humans (Dinman et al., 1991; Jacks et al 1988; Wills et al., 2006). The most common cis-acting signals required for -1 PRF contain a 5' heptameric slippery site, a downstream mRNA secondary structure (usually an mRNA pseudoknot),

and an intervening spacer region to ensure proper positioning of the ribosome. The heptameric slippery site can be represented as N NNW WWH, where N is any 3 of the same base; W is an A or U; and H is A, C, or U. When the ribosome encounters the pseudoknot it pauses, allowing the ribosome to shift frame and re-pair in the -1 frame. (Somogyi et al., 1993; Tu et al, 1992). The spacer region is thought to direct the ribosome to pause with its aminoacyl and peptidyl tRNAs positioned over the slippery site.

As mentioned above, the yeast L-A virus is a well understood model of -1 PRF. This single segment double stranded RNA genome has two overlapping ORFs connected by a -1 PRF signal. *Gag* is the capsid protein, encoded by the first ORF and the sequence for *Pol*, the viral RNA dependent RNA polymerase, is found in the second ORF (Dinman et al., 1991). In most cases, no frameshift occurs and *Gag* is produced; but in the event of a frameshift, *Gag-Pol* fusion protein is produced. The proper efficiency of frameshift events and resulting ratio of structural to enzymatic protein is necessary for optimal propagation of the L-A virus. The L-A virus also supports a satellite virus identified as M_1 , which codes for only a toxin and immunity to the same toxin, and is thus completely dependent on the packaging and enzyme capabilities of L-A. The toxin is secreted by yeast harboring both L-A and M_1 viruses, providing a growth advantage by killing nearby cells that do not have M_1 . While both L-A and M_1 propagation are dependent on a particular rate of frameshifting, M_1 is more sensitive to translational defects that may interfere with virus particle formation and can be used as an assay for such defects (Dinman and Wickner, 1992).

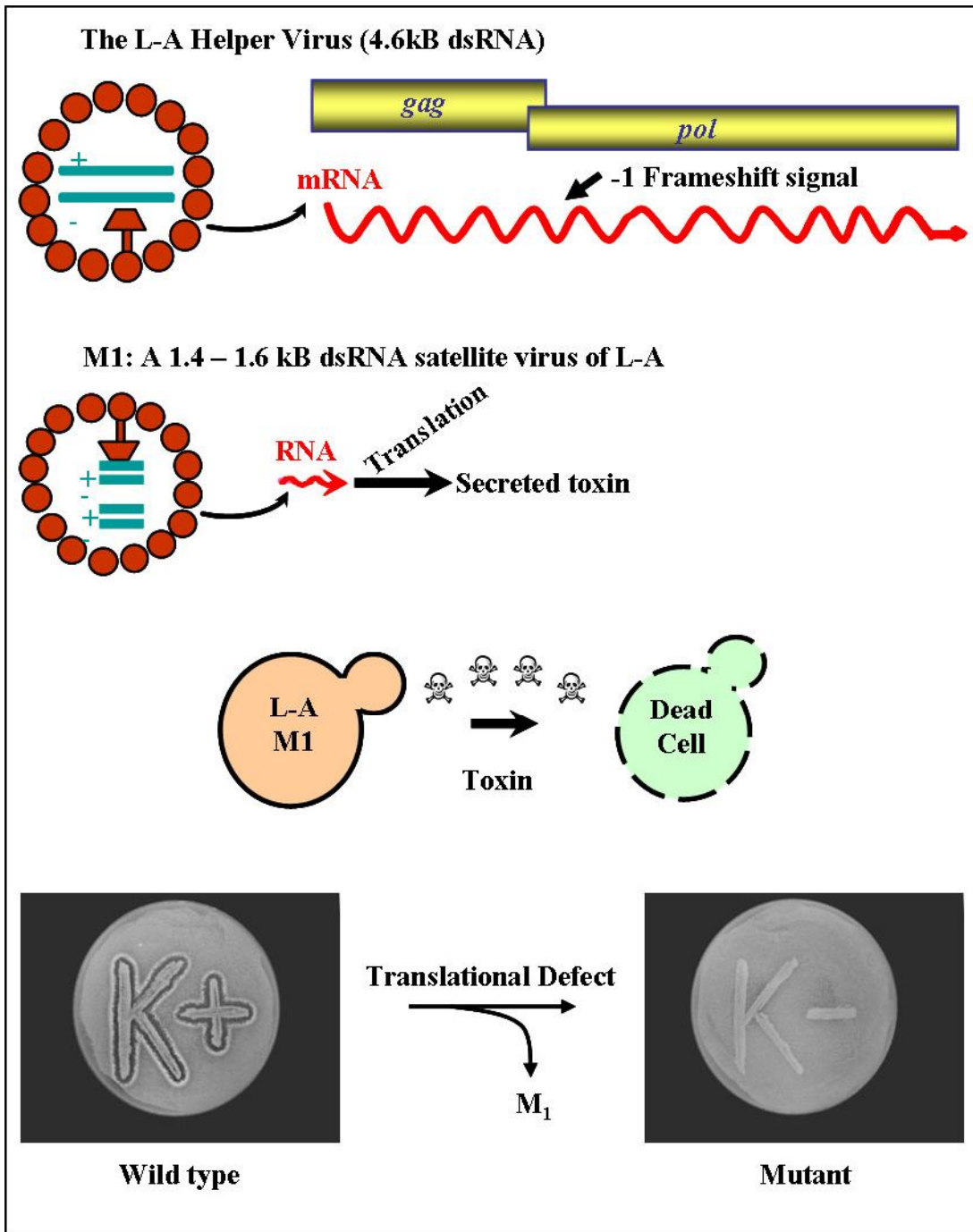


Figure 1.4: L-A and M₁ virus propagation in yeast and the “killer assay”

The M₁ satellite RNA of the ubiquitous yeast L-A virus is affected by translational defects and its presence is easily detected as a zone of clearing in toxin-susceptible 5X47 cells.

Programmed +1 ribosomal frameshifting

Certain cis-acting elements on mRNAs are able to program ribosomes to shift reading frame by 1 base in the 3' direction. Programmed +1 frameshifting (+1 PRF) signals are used by both prokaryotic and eukaryotic genes, as well as several Ty retrotransposons in yeast where it is used to create an enzymatic fusion protein at a relatively low frequency (Belcourt and Farabaugh, 1990; Farabaugh et al., 1993; Wilson et al., 1986). +1 PRF occurs simply at a heptameric slippery site that contains a non-abundant A-site codon. In this kinetically driven process, these “hungry” codons pause the ribosome, allowing the more abundant +1 frame A-site tRNA to bind (Farabaugh et al., 1993). The *Ty1* retrotransposable element was the first example of +1 PRF identified in eukaryotes; where similar to -1 PRF, it regulates the ratio of production for *TYA* (gag) and *TYB* (pol) genes. The slippery site is CUU AGG C, such that the previously described “hungry” codon is AGG, which encodes a rare aa-tRNA^{Arg}; in the +1 frame GGC codes for an abundant Glycine tRNA. This kinetic model of +1 PRF was supported when overexpression of Arg-tRNA^{CCU} decreased +1 PRF 43-fold and its deletion generated almost 100% efficient frameshifting (Belcourt and Farabaugh, 1990; Kawakami et al., 1993).

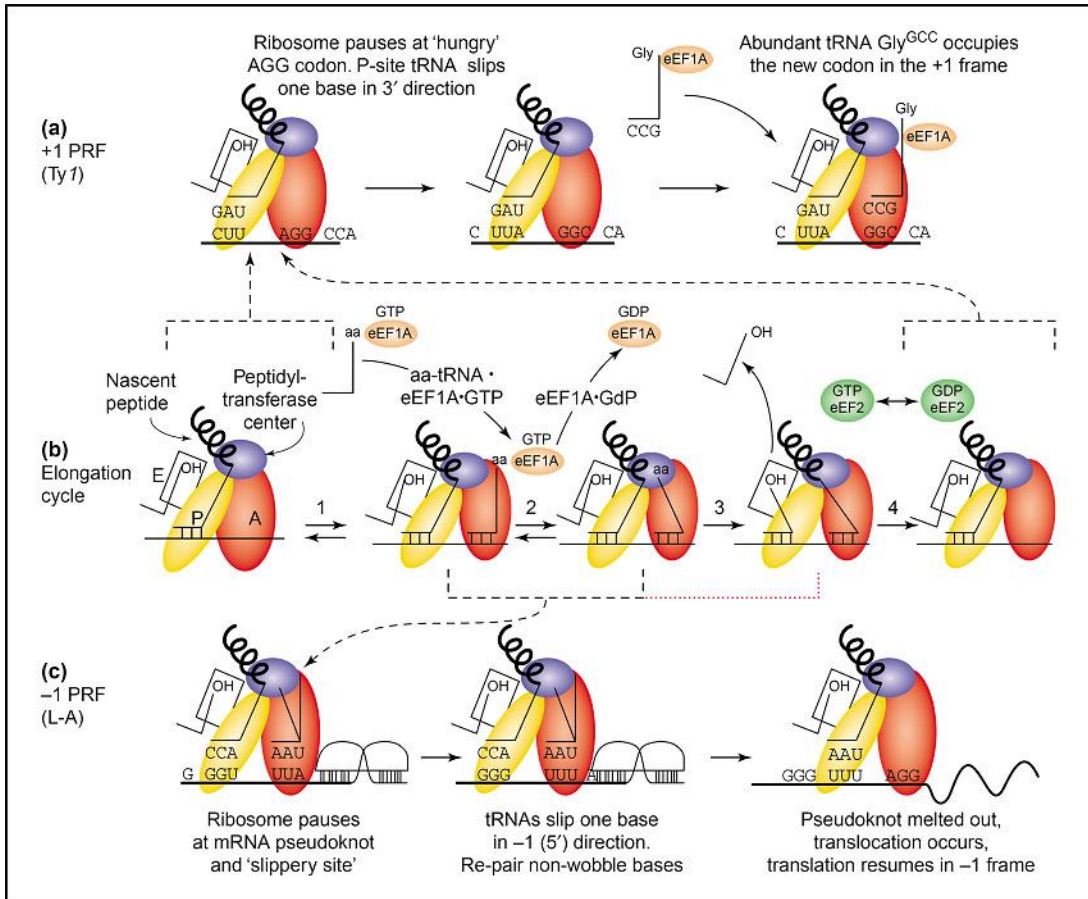


Figure 1.5: The integrated model for programmed ribosomal frameshifting

Brackets indicate points where +1 PRF (a) and -1 PRF (c) events are integrated into the elongation cycle (b). Ty1 directed +1 PRF (a) occurs during the elongation cycle when the p-site is occupied but the a-site remains open as the ribosome pauses for delivery of the rare CCU-tRNA^{Arg} tRNA. When 1 base slippage in the 3' direction occurs, the highly abundant CCG-tRNA^{Gly} is accepted into the A-site and elongation continues in the +1 reading frame. In the case of -1 PRF in the L-A virus (c), the shift in frame occurs during the elongation cycle when both the A- and P-sites are occupied. Upon pausing at an inhibitory downstream pseudoknot structure, the ribosome slips on a heptameric slippery site 1 frame in the 5' direction such that non-wobble bases re-pair appropriately. The pseudoknot is melted out and elongation occurs in the -1 reading frame.

Figure from Harger et al., 2002

Missense incorporation and nonsense suppression

Missense incorporation is simply the incorrect decoding of the messenger RNA such that a near- or non-cognate tRNA is used for a certain codon, leading to the incorrect amino acid in the peptide chain. Missense incorporation is discussed in greater detail in chapter 3. Nonsense suppression is an error that results in readthrough past a prescribed termination codon. This readthrough occurs when a termination codon is decoded with a suppressor tRNA and the ribosome continues to translate in the 3' direction (Beier and Grimm, 2001).

Chapter 2: Ribosomal protein L2

Introduction

Ribosomal proteins have consistently proven to be more than mere scaffolds for ribosomal RNA assembly. Ribosomal protein L2 in particular participates in a number of interesting intermolecular interactions and possible functions. L2 makes contact with multiple domains of the large subunit rRNA (Klein et al, 2004) and forms an intersubunit bridge with the 18S rRNA of the small subunit (Spahn et al, 2001). L2 falls into a group of ribosomal proteins containing acidic globular domains at the periphery and highly basic extensions penetrating into the rRNA core of the ribosome (Klein et al, 2004). Its SH3 β -barrel globular domain participates in the intersubunit bridge, and interacts mainly with rplL43, and helices 79 and 65. The middle bridge region of the protein L2 is encased in rRNA, making extensive contacts with many separate helices, including H33, H65, H66 and H67. The extension region closely approaches the peptidyl-tRNA in a particularly strong interaction with the major groove of helix 93 at the PTC.

Previous research on L2 was primarily performed in *Escherichia coli*. Its contacts and structure are remarkably conserved, such that *E. coli* expressing *Haloarcula marismortui* L2 is viable despite significant sequence variation (Wittman-Liebold et al, 1995). L2 is one of the few proteins absolutely required for peptidyl transfer (Schulze and Nierhaus, 1982). In fact, mutation of the universally conserved Histidine 229 (*E. coli* numbering) was shown to abolish peptidyl transfer (Cooperman et al, 1995). This study aims to perform analyze the role of ribosomal

protein L2 in the structure and function of the ribosome by studying the effects of mutations on many assayable characteristics of translational fidelity. After this initial foray into L2 mutagenesis, the groundwork will be laid for further mutation of specific residues and regions known to be important for translational fidelity in the ribosome.

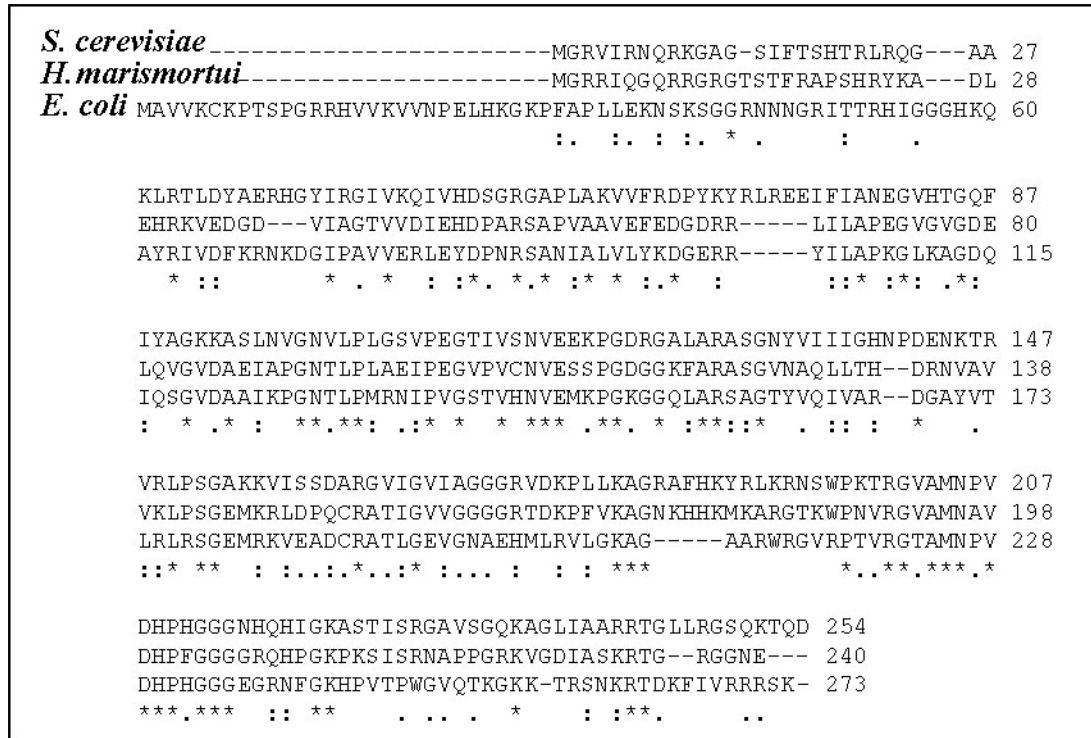


Figure 2.1: Amino acid sequence alignment of ribosomal protein L2

A clustalW alignment of the amino acid sequence of ribosomal protein L2 from *S. cerevisiae*, *H. marismortui*, and *E. coli*. Symbols below each position indicate identical residues (*), conserved substitutions (:), or semi-conserved (.) substitutions.

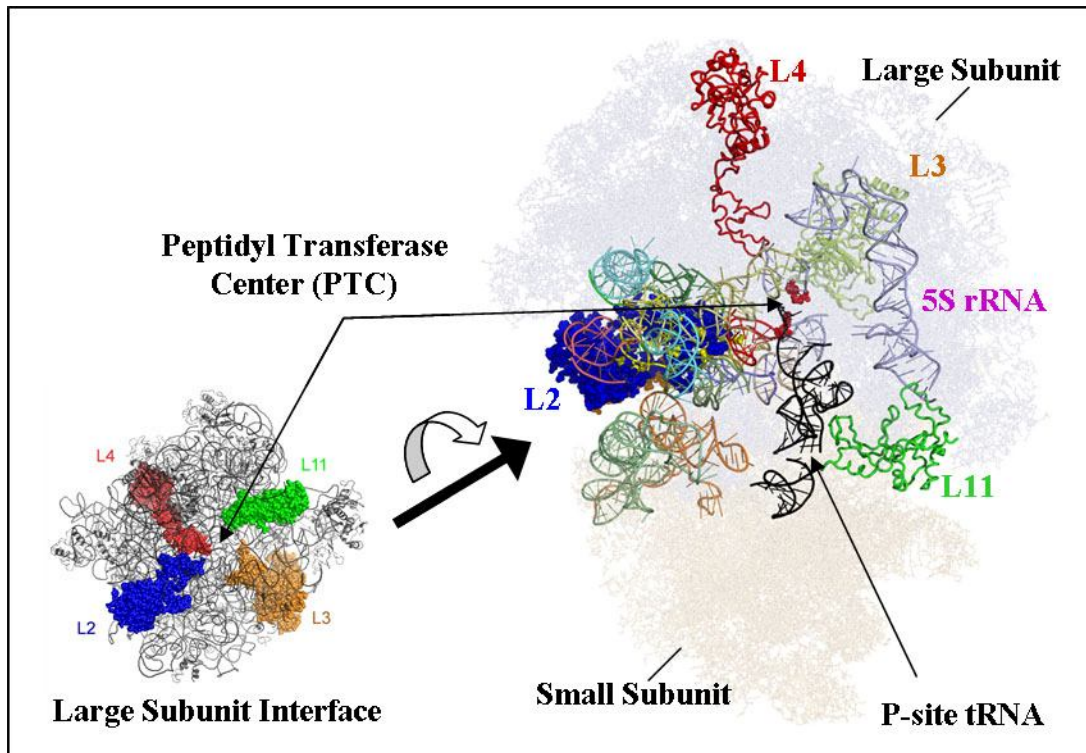


Figure 2.2: Locating L2 in the ribosome

Ribosomal protein L2 (blue) is located at the interface of the large and small subunits. Much of L2 is buried in contacts with the 25S ribosomal RNA, and the protein also makes contacts with the small subunit rRNA across the subunit interface. L2 is one of several proteins (L3, L4, L11 labeled for reference) with regions extending towards the functional core of the ribosome.

Materials and methods

Strains, plasmids, and media

Table 2.1 and Appendix A catalogue the *S. cerevisiae* strains used in this study. Plasmids were amplified in *Escherichia coli* strain DH5 α . Oligonucleotides obtained from IDT (Coralville, IA) which were used in plasmid construction and sequencing are listed in Appendix B. *E. coli* were transformed using a calcium chloride method

(Sambrook et al., 1989) and yeast were transformed with an alkali cation protocol (Ito et al., 1983). YPAD, synthetic complete (SC), synthetic dropout medium (H-), 4.7 MB plates for testing the killer phenotype were used as previously described (Wickner and Leibowitz, 1976; Dinman and Wickner, 1994).

L2 knockout strain construction

In yeast, L2 is encoded by two identical genes (*RPL2A* and *RPL2B*). *RPL2A* was cloned in three segments (5' UTR, ORF, and 3' UTR) each separated by unique restriction sites added during PCR, and inserted into the pRS316 (*CEN6-URA3*) plasmid in which *URA3* is available for auxotrophic selection. The pRS series of yeast shuttle vectors were described previously (Christianson et al., 1992; Sikorski and Hieter, 1989). The 5'UTR fragment is 815 bp, the ORF is 949 basepairs, and the 3'UTR was 270 basepairs. The product was named pRPL2A-URA3. The three-segment *RPL2A* cassette was also cloned into the pRS315 plasmid (*CEN6-LEU2*) to generate pRPL2A-LEU2. In parallel, haploid strains of opposite mating type each with a knockout of one copy were obtained commercially (Resgen #1411 and 15712), and one of these was transformed with pRPL2A-URA3. The two strains were then mated, sporulated, and tetrads dissected to obtain a haploid *rpl2A*, *rpl2B* double knockout strain supported by a plasmid borne copy of the gene from pRPL2A-URA3. The strain was confirmed by inability to grow on 5-fluoroorotic acid (5-FOA).

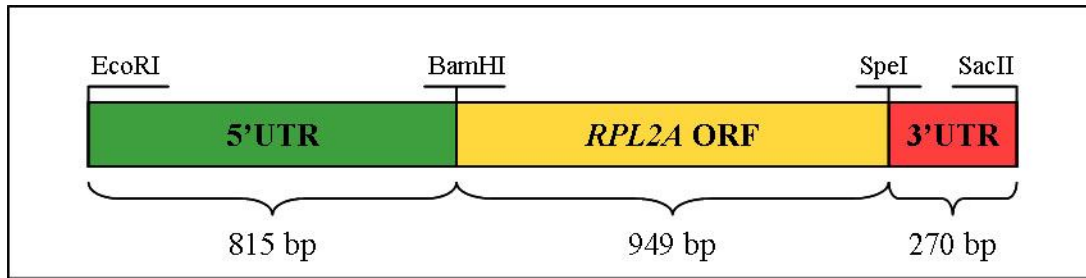


Figure 2.3: Schematic of RPL2A cassette

Tripartite cassette clones into polylinker of pRS315 and pRS316 to create pRPL2A-LEU2 and pRPL2A-URA3, respectively.

Strain	Description	Source
5X47	<i>MATa/MATα his1/+ trp1/+ ura3/+ K⁻</i> ; Standard diploid killer tester	JD Dinman*
JD1205	<i>MATα his3Δ1 leu2Δ0 met15Δ0 ura3Δ0 rpl2b::KAN^R K⁺</i>	BY4741/ #1411**
JD1207	<i>MATα his3Δ1 leu2Δ0 met15Δ0 ura3Δ0 rpl2a::KAN^R K⁺</i>	BY4742/ #15712**
JD1269	<i>MATα his3Δ1 leu2Δ0 met15Δ0 ura3Δ0 rpl2b::KAN^R rpl2a::KAN^R + RPL2A in pRS316 K⁺</i>	BY4742/ This Study
JD1273	<i>MATα his3Δ1 leu2Δ0 met15Δ0 ura3Δ0 rpl2b::KAN^R rpl2a::KAN^R + RPL2A in pRS316 K⁺</i>	BY4741/ This Study
JD1315	<i>MATα his3Δ1 leu2Δ0 met15Δ0 ura3Δ0 rpl2b::KAN^R rpl2a::KAN^R + RPL2A in pRS315 K⁺</i>	BY4742/ This Study

*Reference: Wickner, 1974 **Yeast Genome Deletion Project (Winzeler et al., 1999; Brachmann et al, 1999) via Invitrogen, Inc.

Mutation library creation

Mutations in the ORF of *RPL2A* were generated by both random mutagenesis and site-directed mutagenesis techniques. Random mutagenesis of the *RPL2A* ORF was

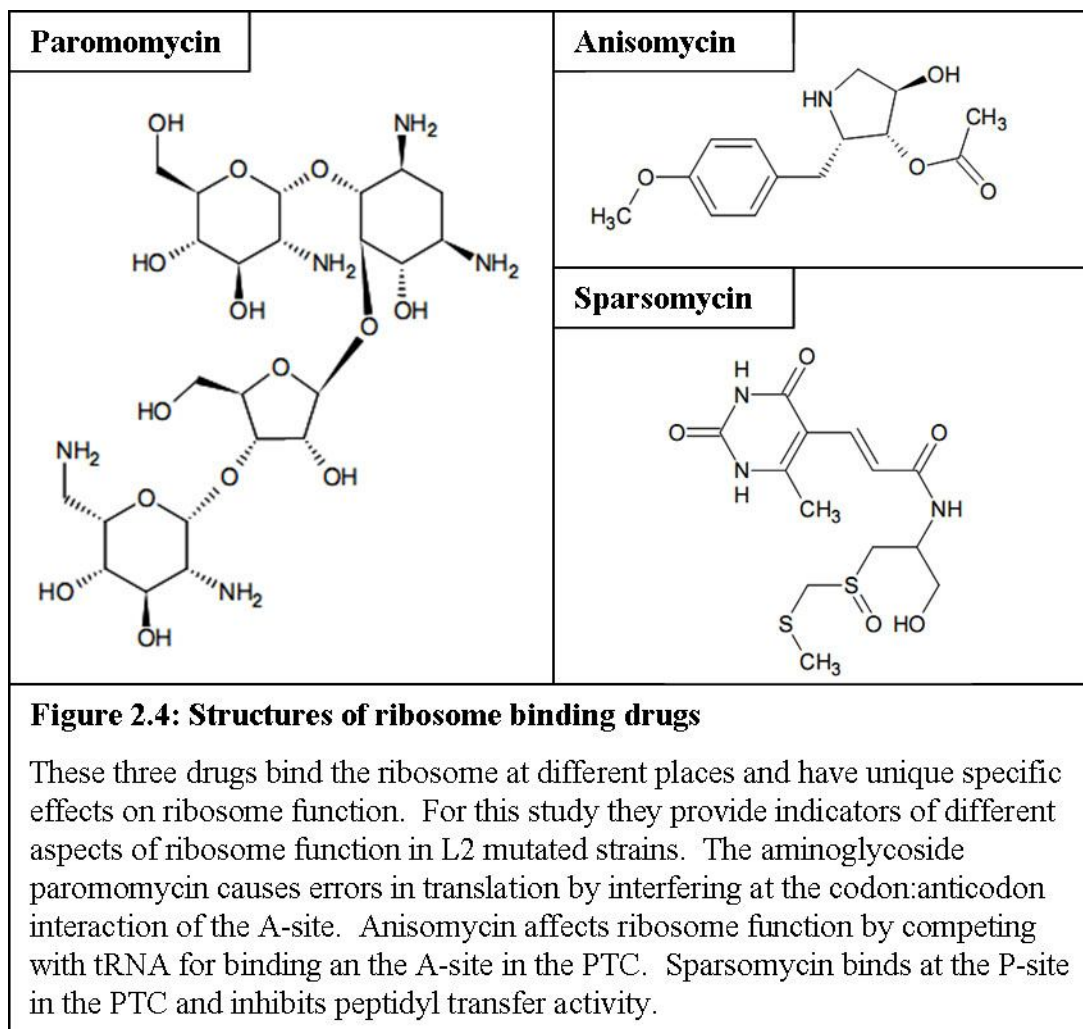
performed using an error-prone PCR and gap-repair procedure (Muhlrad et al., 1992). The Stratagene Genemorph II Random Mutagenesis Kit (Stratagene, La Jolla CA) was utilized and reaction conditions were optimized for 1-3 mutations per thousand nucleotides. The primers used (forward: RPL2ARMF and reverse: RPL2ARMR, Appendix B) include the start and stop codons and are complimentary to the 5' and 3' untranslated regions of *RPL2A*. Following the PCR reaction, mutated fragments were cotransformed into yeast with linearized and agarose gel purified pRPL2A-LEU2 with the ORF removed such that it contained only the 5' and 3' UTR regions of *RPL2A*. Cells were then selected for growth on medium lacking leucine (-leu). Under these conditions, cells can only grow consequent to homologous recombination events between the linearized plasmid and the PCR products to regenerate covalently closed plasmids. After initial selection on -leu media, cells were replicated to media containing 5-FOA to select for cells that had lost pRPL2A-URA3, leaving colonies with only the mutant-bearing pRPL2A-LEU2. As an initial screen of the population, these colonies were tested for their ability to maintain the killer virus, a general indicator of translational defects. The killer assay was performed with the tested colonies replica plated onto an even lawn of killer-susceptible 5X47 indicator cells spread over 4.7MB (Dinman and Wickner, 1992). Colonies that showed killer phenotypes (Killer loss, K⁻; or Killer reduction K^f) were subjected to a plasmid rescue. Plasmids taken from the yeast were amplified in *E. coli* and then retransformed into strain JD1269, the wildtype pRPL2A-URA3 was eliminated on 5-FOA, and the Killer assay was repeated.

Site-directed mutagenesis was carried out using the Stratagene Quikchange XL site directed mutagenesis kit. The method utilizes two inverse primers harboring the

same base change to generate new full-length plasmid sequence with the desired mutation. *DpnI* is used to digest and eliminate the methylated parental plasmid DNA and when the reaction mixture is transformed into *E. coli*, nicks in the new plasmids are repaired and mutated plasmid is amplified. Site directed mutagenesis primers are used are listed in Appendix B.

Temperature response, drug sensitivity, and growth curves

The ribosomal binding sites of each drug tested are well understood and their phenotypic effects have long been examined. Paromomycin binds to the small subunit rRNA, changing the structure of the of the A-site decoding center (Moazed and Noller, 1987; Fourmy et al, 1998; Vicens and Westhof, 2001). This interaction increases the rate of tRNA misincorporation. Sparsomycin and anisomycin both bind at the peptidyl transferase center of the ribosome large subunit, inhibit protein synthesis, and affect -1 PRF (Dinman et al, 1997; Hansen et al, 2003). Sparsomycin binds the P-site bound tRNA in the peptidyltransferase center, increasing the ribosome's affinity for P-site tRNA. Anisomycin competes and interferes with the binding of aminoacyl tRNA to the A-site of the peptidyl transferase center (Hansen et al, 2003).



Dilution spot assays were used to test growth at various temperatures and drug concentrations. For all conditions, yeast cells were grown to the logarithmic growth phase and then diluted to 1×10^6 colony forming units per milliliter. 10-fold dilutions of each strain were spotted in sequence on YPAD, or YPAD containing various concentrations of paromomycin or anisomycin (Sigma Aldrich, St. Louis, MO). Each serial dilution was spotted onto 8 different plates, three were for temperature testing at 15°, 30°, and 37°C, and the other 5 plates contained paromomycin at 1500, 3000, or 5000 µg/ml; or anisomycin at 10 or 20 µg/ml and were incubated at 30°C for 2 days.

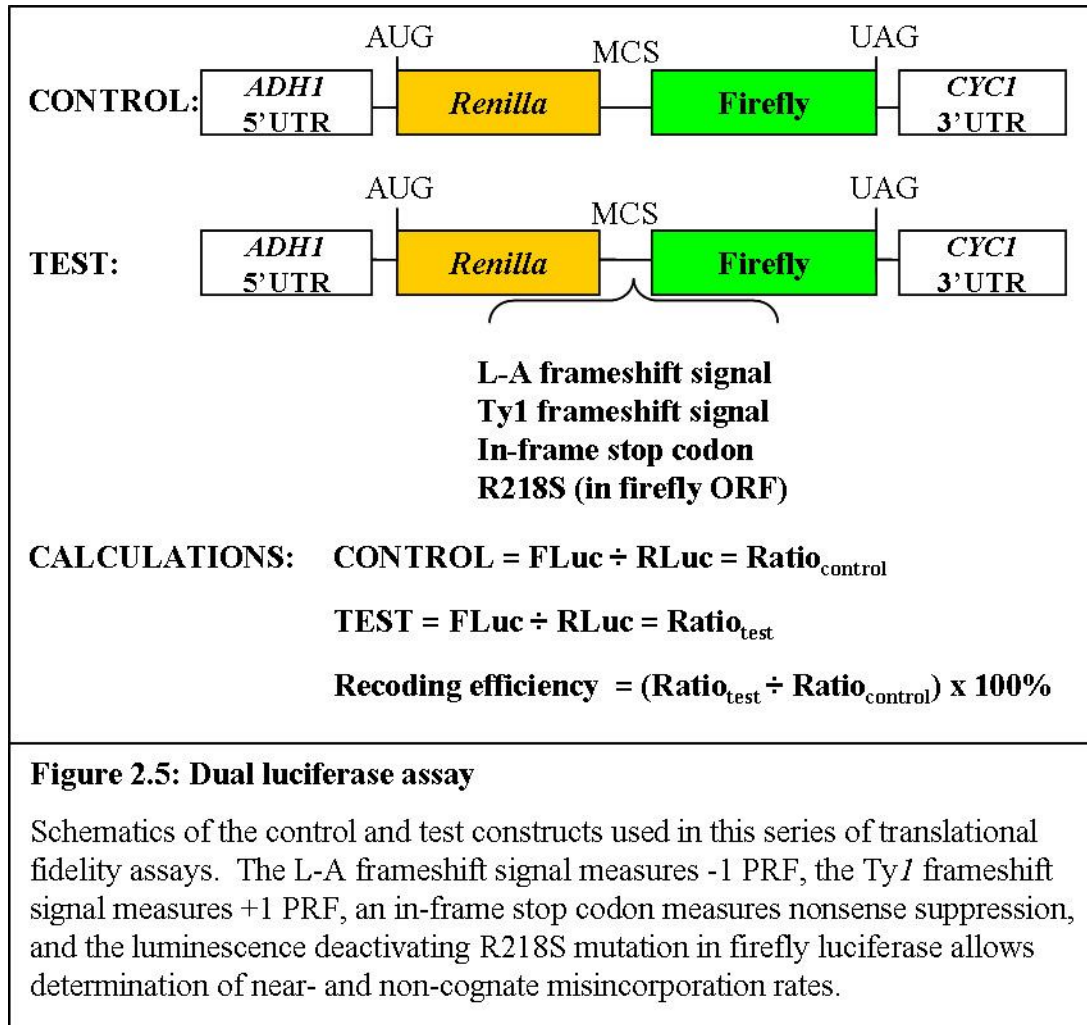
Drug sensitivity was also tested using a filter disc assay (Dinman and Kinzy, 1997). Yeast cells were grown overnight to saturation, OD₅₉₅ was measured, and the culture was diluted to a concentration of 0.2. 300µl of the solution was spread evenly onto freshly prepared YPAD plates and allowed to dry. Anisomycin, Paromomycin, and Sparsomycin solutions were prepared, allowing each drug concentration to be applied in 10µl volume to sterile Whatman paper discs which are subsequently placed on the tested lawn of yeast. Following optimization for the strain background, discs were prepared containing 40µg Anisomycin, 30µg Sparsomycin, and 6 mg Paromomycin.

Growth curves were generated in quadruplicate in a Synergy HT micro-plate reader (Bio-Tek Instruments, Inc., Winooski, VT), utilizing the KC4 software package. Yeast growth at 30° was measured in 48 well plates starting at an optical density of 0.5 at 595nm in 0.5ml of H-leucine media. Cultures were subjected to constant high intensity shaking and automatic OD₅₉₅ readings of each well were taken every 20 minutes for 40 hours. Cultures were tested in duplicate on each of 2 different plates to generate a growth curve for each strain and the 4 readings were averaged for each timepoint. Data analysis for the automated growth curves was performed as previously described (Warringer and Blomberg, 2003; Jasnos et al, 2005; and Touissant et al, 2006). Blank control well values were subtracted from the raw optical density data, which was then smoothed and log transformed to generate growth curves and allow calculation of doubling times and a lag phase estimation for each strain. Doubling times were determined by calculating the slope over 3 data points and using the average of the lower 5 of the 7 highest slopes to generate the mean_{DT}. Doubling time is equal to the log₁₀ of 2 divided by the mean_{DT}.

Translational fidelity assays

Translational fidelity characteristics of each strain were measured by testing efficiencies of -1 PRF, +1 PRF, nonsense suppression, and near- and noncognate missense incorporation using dual luciferase assays. Constructs are pictured in figure 2.5. The test construct for -1 PRF includes a -1 frameshift signal from the yeast L-A virus and the downstream Firefly luciferase gene in the -1 frame, and the +1 PRF test construct includes a *TyI* yeast retrotransposon +1 frameshift signal and the downstream firefly gene in the +1 frame. The control, -1 PRF, and +1 PRF plasmids were described previously (Harger and Dinman, 2003). Plasmids to measure near and non-cognate missense incorporation were generated by mutating Arginine 218 in the catalytic center of the firefly luciferase gene such that a misincorporation of arginine at the site is required for expression of the functional luciferase protein (Rakwalska and Rospert, 2004). AGC (Serine) or TCT (Cysteine) codons replace the wild-type AGA (Arginine) codon at the position in near- and non-cognate test constructs, respectively. Nonsense suppression was measured by simply inserting an in-frame stop codon such that a readthrough event is necessary for expression of the downstream firefly luciferase. Reaction reagents were from the Dual-Luciferase® Reporter Assay System (Promega Corporation, Madison, WI) and luminescence readings were measured by a TD20/20 luminometer (Turner Designs Inc. Sunnyvale, CA). Each individual assay compares a ratio of two luciferase (firefly and renilla) intensities from the test construct to a 0-frame control plasmid. The ratio of this test to the control was calculated and normalized to the wild-type value, with enough replicates for >95% confidence (minimum of 9 replicates).

All calculations and standard errors were determined as described by Jacobs and Dinman (2004).



Polysome profiles

To generate polysome profiles, cytoplasmic extracts were prepared from yeast growing at mid-logarithmic phase with OD₅₉₅ between 0.5 and 0.7 (protocol adapted from Baim et al 1985). Ice cold solution containing 200 µg/ml cyclohexamide, 20 mM

Tris-HCl pH 7.0, 50 mM KCl, 12 mM MgCl₂ and 1 mM β-mercaptoethanol was used for cell lysis and to arrest elongating ribosomes on mRNAs. Cells were maintained at 4°C as they were harvested using tabletop centrifugation and through disruption with glass beads in a Mini Beadbeater. Extracts were clarified by centrifugation at 14000 rpm for 10 minutes at 4°C in a tabletop centrifuge, and supernatant fractions containing polysomes were aliquoted as 6.0 optical units at OD₂₈₀ in total volumes of 200μl. Aliquots were applied to 13 ml linear 7%-47% sucrose gradients containing the same components as the lysis buffer described above. An SW41 rotor was used to spin the gradients at 40,000 rpm for 135 minutes at 4°C. An ISCO-5 gradient fractionator was used to read continuously at 254 nm across the gradient.

Computational analysis

The molecular visualization tool Pymol (Delano, 2002) was used to view and examine available crystal structures of the ribosome. Images in this document are based primarily on structures from Spahn et al., 2001, in which atomic resolution crystal structures from *Haloarcula marismortui* and *Thermus thermophilus* were docked into cryo-EM structures from *Saccharomyces cerevisiae* (pdb accession numbers 1s1h and 1s1i).

Results

rpl2A alleles

Random PCR mutagenesis was used to generate a library of *rpl2a* alleles. PCR products and linearized *Eco* RI/*Spe* I digested pPRL2A-LEU2 were introduced into JD1315 cells, transformants were initially selected for growth on –leu medium, and then replica plated to medium containing 5-FOA. Preliminary analysis using 5-FOA revealed that approximately **30%** of the mutants were not viable as the sole form of *rpl2a*. All mutations created both in random mutagenesis and later site-directed mutagenesis are catalogued in Appendix A. Killer virus maintenance was employed as a general indicator to identify mutants conferring general translational defects. Approximately 10,000 candidate colonies were screened, with 79 initially displaying Killer loss (K^-) or Killer reduced (K^r) phenotypes. Plasmids were rescued from these colonies, reintroduced into JD1315 cells, and taken again through the selection and killer analysis protocols. This analysis revealed that 16 of the mutants truly promoted the K^- phenotype, while 13 conferred K^r phenotypes. In all, plasmids from 36 selected strains (including the 29 promoting killer phenotypes) were sequenced.

The majority of the killer defective *rpl2A* alleles contained multiple mutations and resulting amino acid changes, with 22 of the alleles having 3 or more mutations. Two alleles had mutations in their stop codons, resulting in C-terminal extensions containing an extra 4 amino acids (YIMY). Six strains generated only had double mutations and 6 alleles contained single point mutations. Oligonucleotide site-directed mutagenesis was used to generate a bank of single mutations for further analysis. Residues were selected

for mutation based on the frequency with which individual mutations occurred, and their locations within the structure of L2. Examination of the L2 structure reveals that it can be generally divided into three domains: 1) a highly structured globular domain that abuts the solvent accessible side of the large subunit; 2) a C-terminal “finger” that extends deep into the core of the large subunit; and 3) “bridge” region that connects the globular and finger domains. Figure 2.6 shows the 16 single rpl2A alleles and the rRNA and tRNA features in the region surrounding the protein. Amino acid residues corresponding to mutations in the globular domain are colored green, those in the bridge are red, and mutants in the extension are shown as yellow spheres.

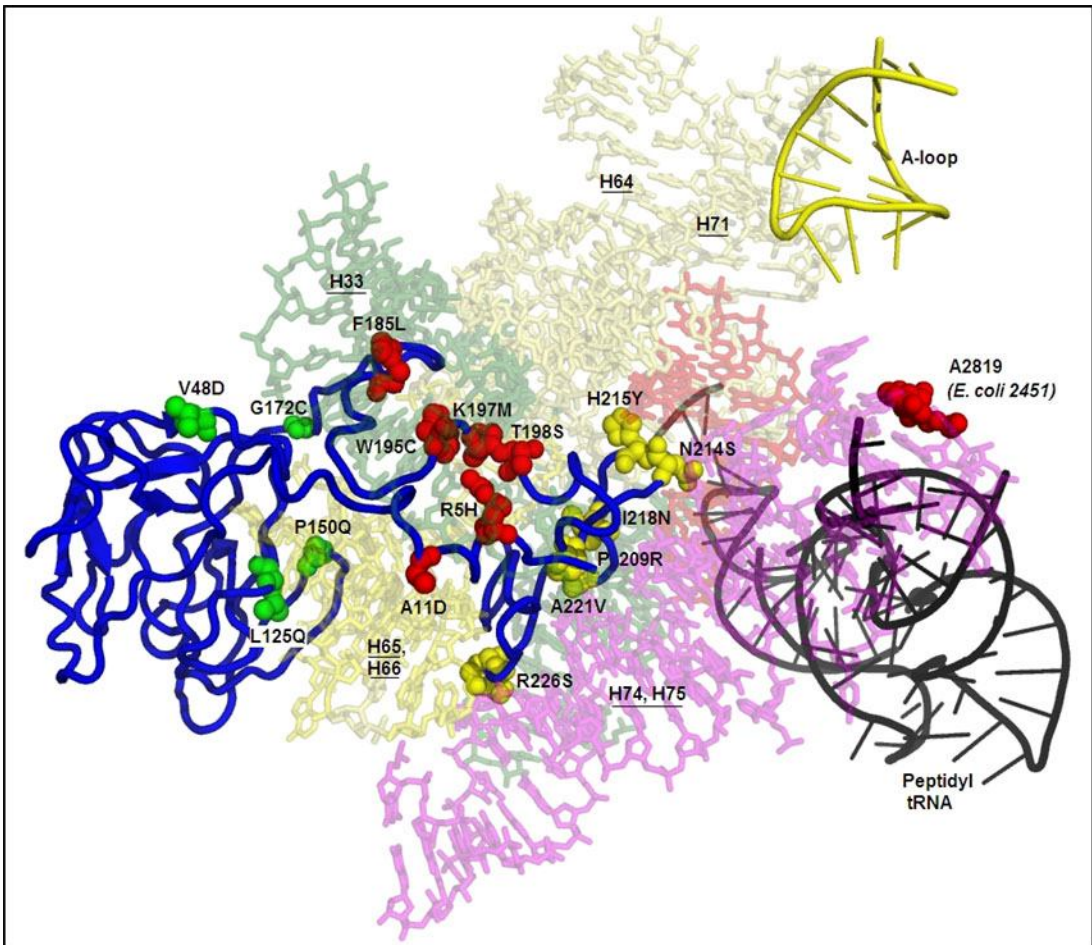


Figure 2.6: Single mutations of L2

Mutations are displayed in 3 different colors to reflect different regions of L2. Residues mutated in the globular domain are colored green, those in the bridge region are red, and mutants in the extension are shown as yellow spheres. Helices that contact the extension and tip of L2 are labeled, as are functional sites of the ribosome and peptidyl tRNA. RCSB Protein Data Base entries shown: 1S1I, 1K5X (tRNA).

Temperature variable dilution spots and growth curves

Growth characteristics for all single mutation strains were determined at 15°, 30°, and 37°C using dilution spot assays and growth curves were generated at 30°C, allowing comparisons of growth and doubling times. Conditions of 15° C were designed to test

cold-sensitivity and 37° C was selected to indicate heat sensitivity; however, no significant temperature-associated phenotypes were identified in mutant strains via dilution spot assay (Figure 2.7). Mutations associated with the globular, structured domain of the protein (V48D and L125Q) grew most poorly in dilution spot assays across all tested temperatures.

Growth curves provide a qualitative impression of growth for each strain as well as quantitative doubling time information (Figure 2.8). Several strains (R5H, W195C, K197M, T198S, P209R, A221V, and R226S) displayed a flat growth phenotype with little defining characteristics and doubling times near or greater than 3 hours. The flat growth curve and slower doubling times indicate a lack of exponential growth characteristic of a wild-type yeast strain in culture. Other strains (A11D, V48D, L125Q, P150Q, G172C) provided a somewhat classic growth curve shape, with reasonable doubling times (between 1.83 and 2.5 hours), but failed to approach the density of the saturated wildtype cultures. The most interesting growth phenotypes were in the F185L and N214S hyper-growing strains. These strains had shorter doubling times than wild-type, and grew to a higher saturation concentration before entering the liquid-culture death phase. H215Y and I218N demonstrated growth similar to wild-type yeast in terms of both saturation concentration and doubling time.

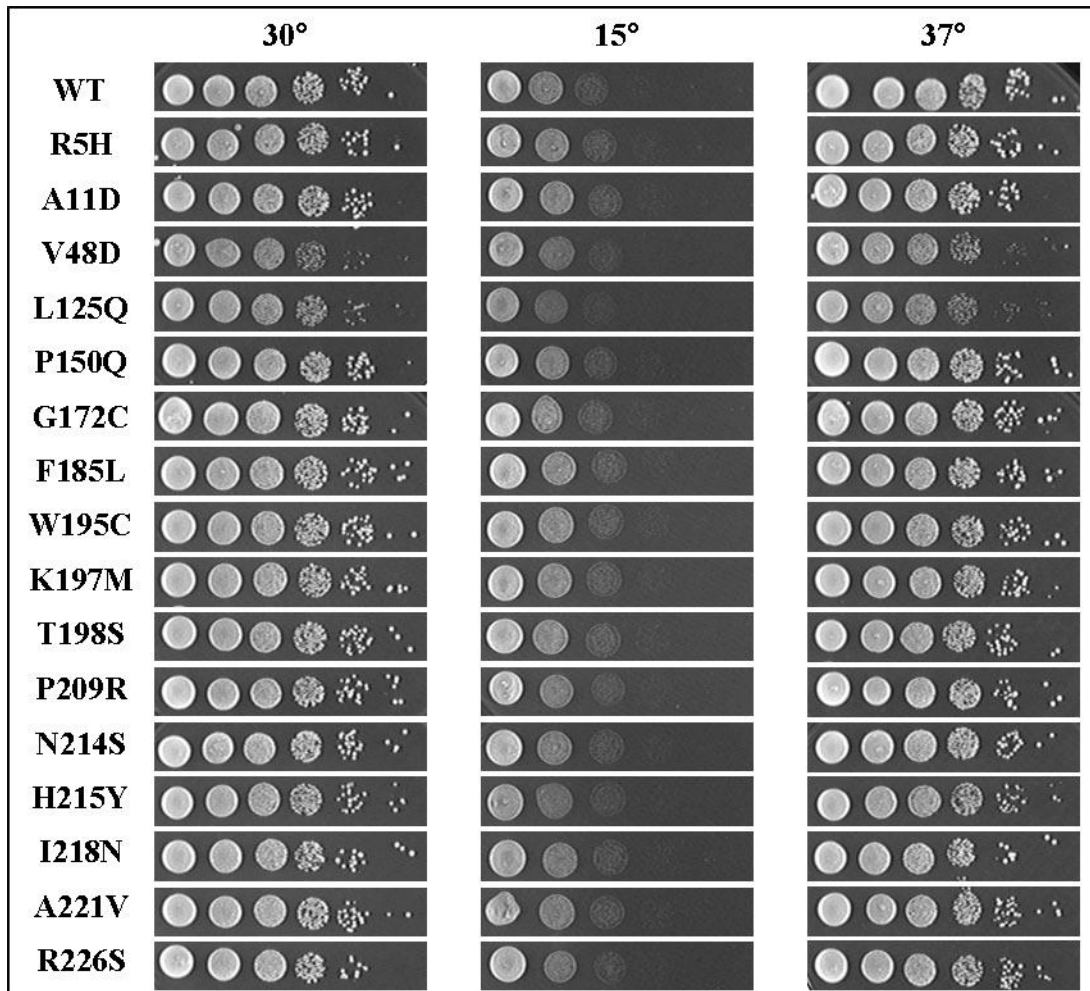


Figure 2.7: Variable temperature dilution spots of L2 single mutation strains

Ten-fold dilutions ($10^6 \rightarrow 10^1$ CFU) of logarithmically growing cells were arrayed onto YPAD plates and grown at 30°C, 15°C, 37°C for two days.

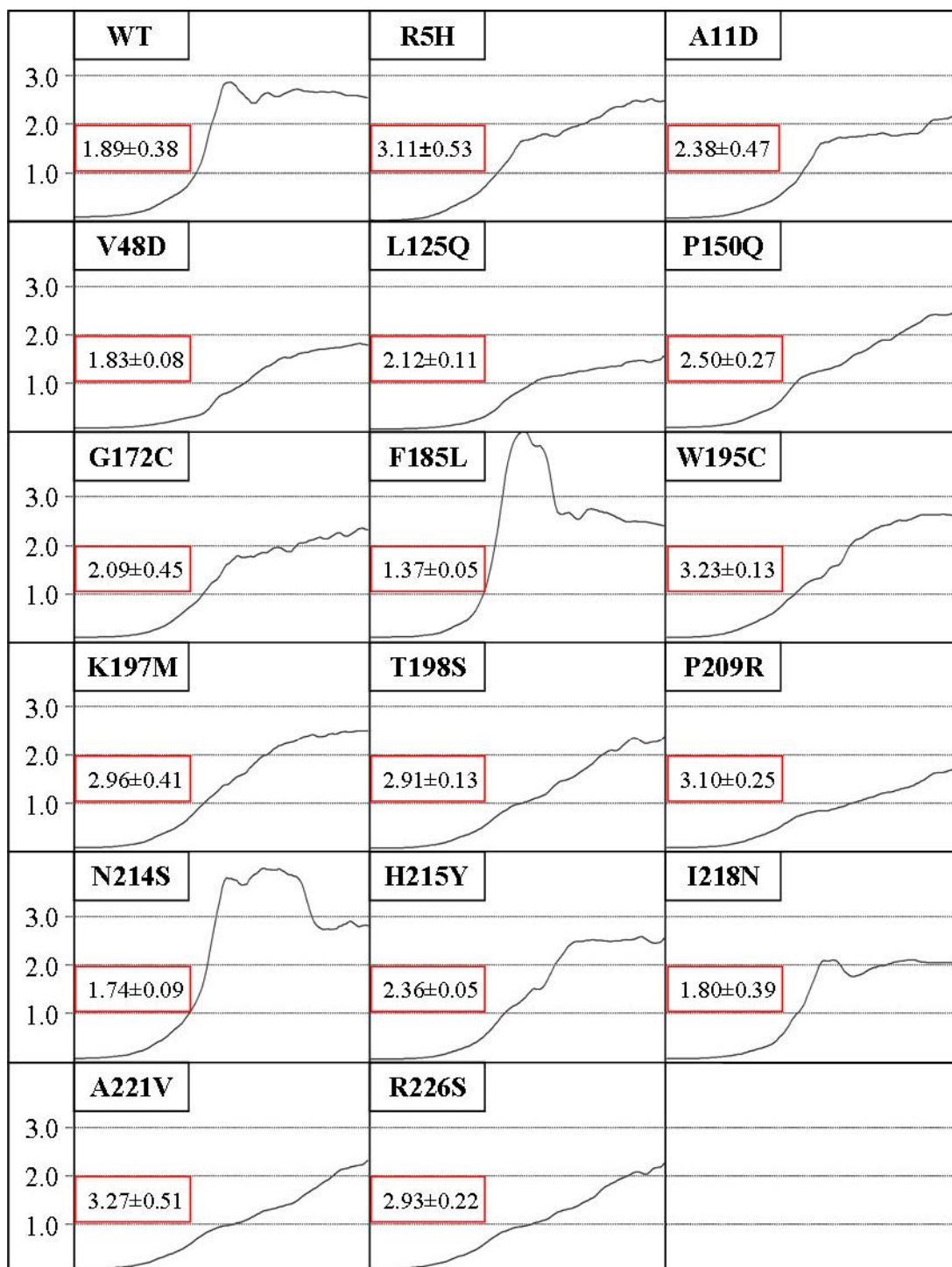


Figure 2.8: Growth curves of single mutation L2 strains

All curves show growth (average curves from 4 replicates) at 30° C in H-leucine liquid media with constant shaking and readings every 20 minutes for 40 hours. The Y-axis is marked at OD₅₉₅ values of 1.0, 2.0, and 3.0. Peak doubling times (hrs) with standard deviation are reported in red boxes.

Mutant pharmacological response

Each single mutation strain was tested for sensitivity to the drugs anisomycin, paromomycin, and sparsomycin. Dilution spot assays on paromomycin at concentrations up to 5 mg/ml did not reveal any definitive phenotypes (Figure 2.10). However, when tested using a filter disc assay, the G172C mutant proves sensitive to paromomycin (Figure 2.11). When anisomycin response was tested using the dilution spot assay, several strains (V48D, L125Q, H215Y) displayed anisomycin resistant phenotypes relative to wild type (Figure 2.9). The phenotype is indicated as more serial dilution spots survive relative to wild type as the drug concentration increases. The anisomycin resistant phenotype was generally confirmed by smaller zones of growth inhibition in the filter disc assay. Sparsomycin availability limited its use to testing growth effects using filter disc assays (Figure 2.11). The only clear sparsomycin response is a strong resistance phenotype in the H215Y strain.

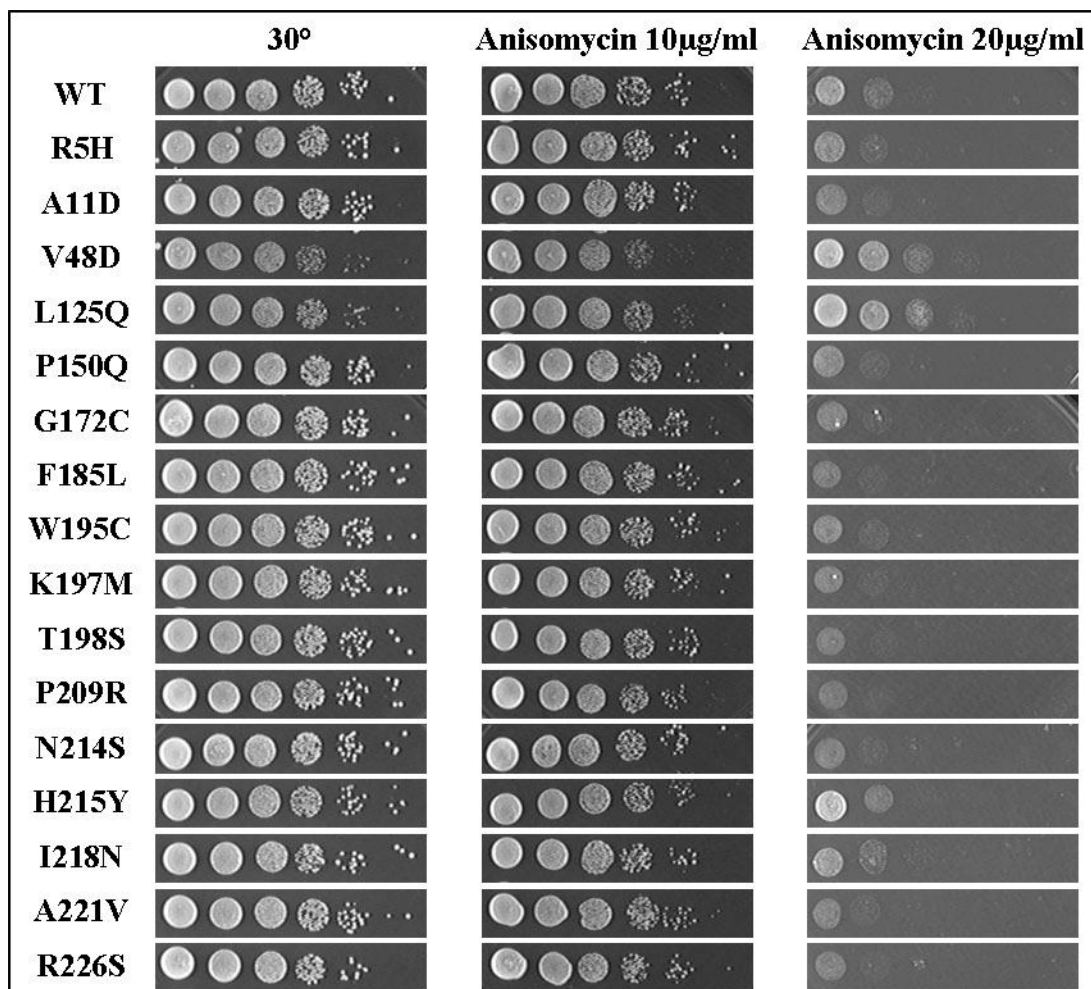


Figure 2.9: Anisomycin variable dilution spots of L2 single mutation strains

Ten-fold dilutions ($10^6 \rightarrow 10^1$ CFU) of logarithmically growing cells were arrayed onto YPAD plates containing 10 µg/ml anisomycin, 20 µg/ml anisomycin, and a no-drug control and grown at 30°C for two days.

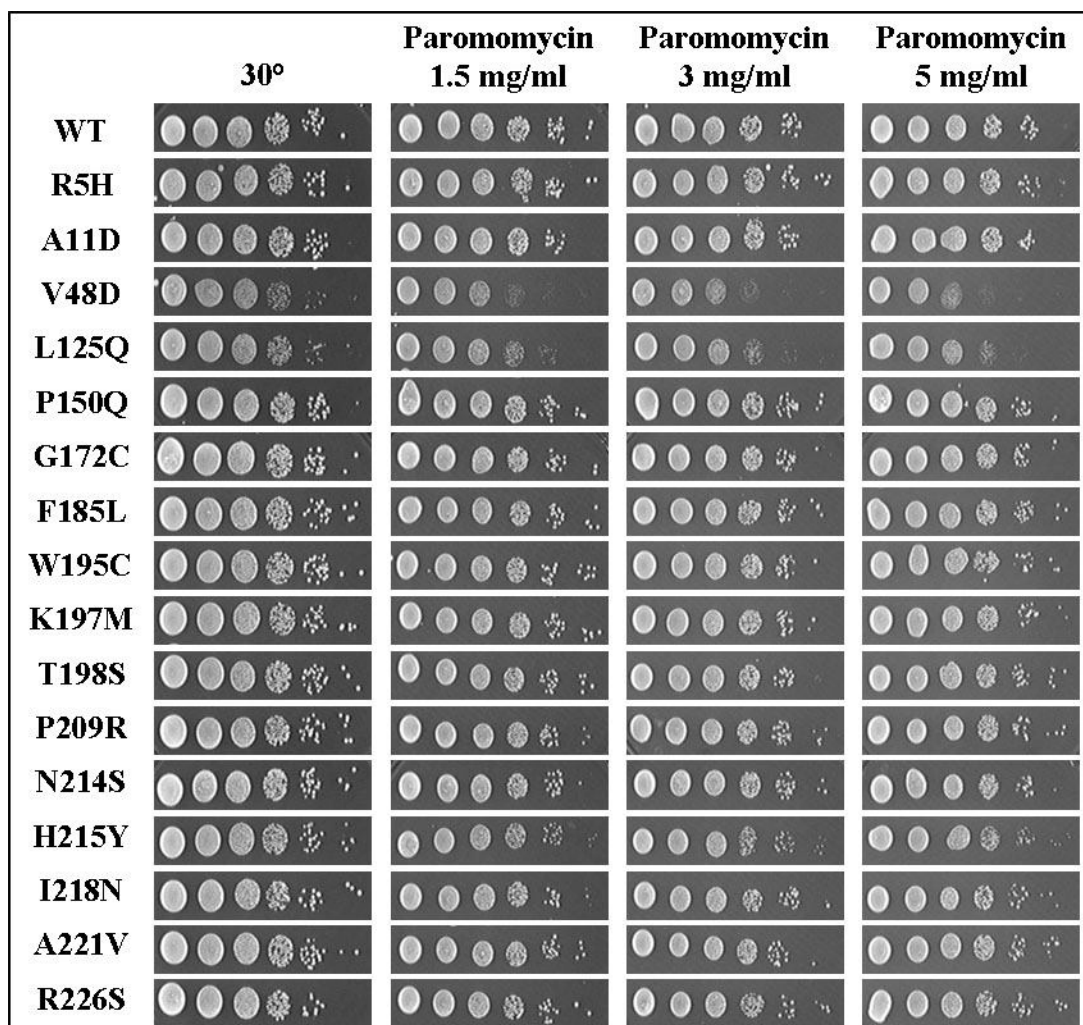


Figure 2.10: Paromomycin variable dilution spots of L2 single mutation strains

Ten-fold dilutions ($10^6 \rightarrow 10^1$ CFU) of logarithmically growing cells were arrayed onto YPAD plates containing 1.5 mg/ml paromomycin, 3 mg/ml paromomycin, 5 mg/ml paromomycin, and a no-drug control and grown at 30°C for two days.

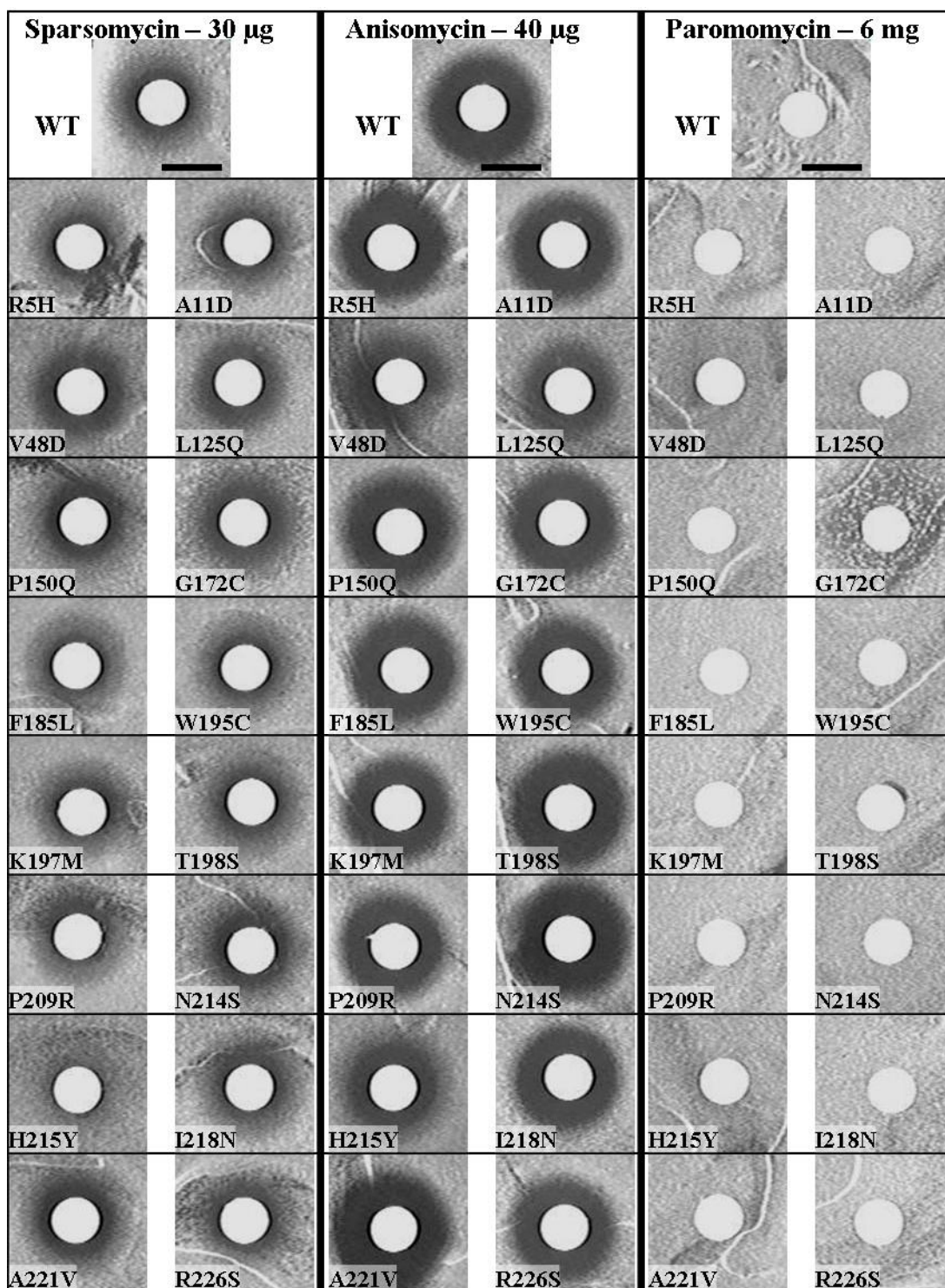


Figure 2.11: Drug filter disc assays for mutants of ribosomal protein L2

Filter discs soaked in the indicated quantity of drug dissolved in a 10 μ l volume were placed on YPAD plates seeded with 300 μ l of cells with an OD_{595} of 0.2 and grown for 2 days at 30°C. The black bar in the WT pictures represents 1 cm.

-1 PRF and +1 PRF measurements with killer phenotypes

None of the tested strains exhibited strong changes in +1 programmed frameshifting efficiency as measured by the dual luciferase assay. Interestingly, only 3 of the single mutation strains consistently lose killer and those 3 strains (V48D, L125Q, and H215Y) have the largest increase in -1 PRF relative to wild type (Figure 2.12). Specifically, fold changes of 1.61 and 1.35 for V48D and L125Q, respectively, indicate a significant increase in -1 PRF rates over the wild-type. The baseline -1 PRF rate measured for this strain was 6.29 ± 0.15 %, while the measured +1 PRF rate was 13.65 ± 0.43 % (Table 2.2).

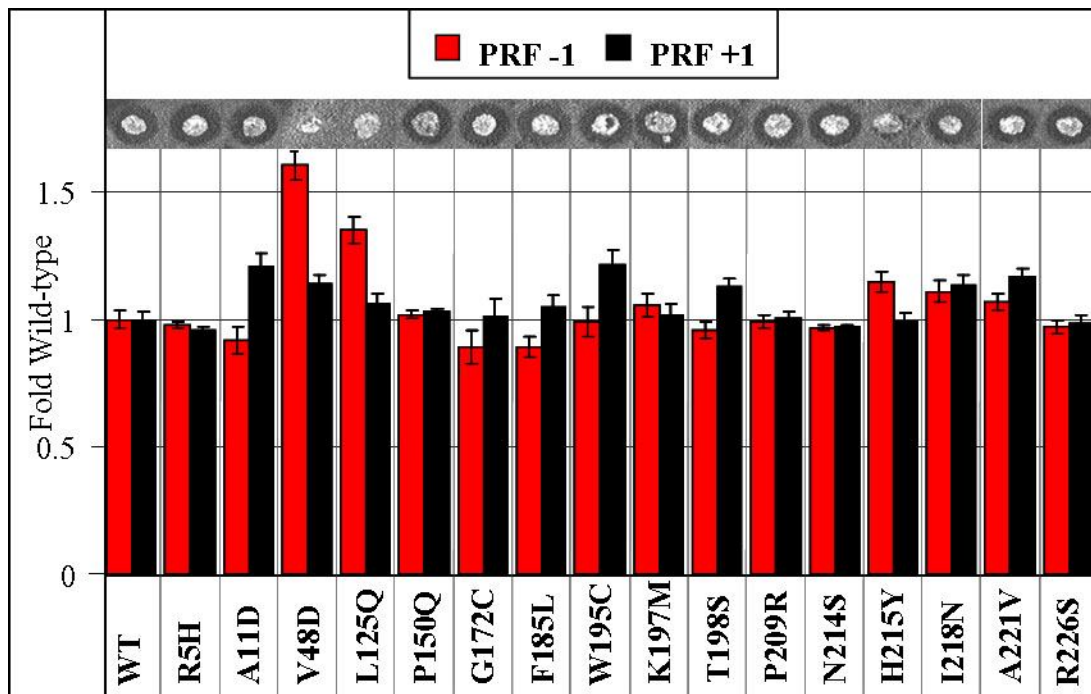


Figure 2.12: Dual luciferase measurements of PRF efficiency in single mutation strains

Effects on -1 PRF (red) and +1 PRF (black) efficiency in *rpl2* mutation strains are depicted as fold of wild-type cells. Error bars indicate standard error. Killer assay results for each mutant strain are pictured directly above each column.

Table 2.2: Effects of mutations in ribosomal protein L2 on rates of -1 and +1 frameshifting

The PRF value is reported with standard error and indicates the frequency of programmed ribosomal frameshifting events. Fold wild-type provided is reported graphically in figure 2.11.

Strain	-1 PRF			+1 PRF		
	PRF (x 10 ⁻²)	Fold WT	P-value	PRF (x 10 ⁻²)	Fold WT	P-value
WT	6.29 ± 0.15	1.00	1.00	13.65 ± 0.43	1.00	1.00
R5H	6.16 ± 0.10	0.98	0.62	13.06 ± 0.21	0.96	0.21
A11D	5.78 ± 0.26	0.92	0.15	16.44 ± 0.42	1.21	9.10E-4
V48D	10.10 ± 0.52	1.61	8.54E-5	15.55 ± 0.64	1.14	0.04
L125Q	8.49 ± 0.42	1.35	2.20E-3	14.45 ± 0.82	1.06	0.41
P150Q	6.42 ± 0.11	1.02	0.57	14.01 ± 0.52	1.03	0.56
G172C	5.62 ± 0.40	0.89	0.21	13.74 ± 0.47	1.01	0.90
F185L	5.61 ± 0.18	0.89	0.06	14.34 ± 0.31	1.05	0.30
W195C	6.24 ± 0.31	0.99	0.90	16.52 ± 0.35	1.21	1.00E-3
K197M	6.65 ± 0.34	1.06	0.46	13.90 ± 0.59	1.02	0.76
T198S	6.03 ± 0.17	0.96	0.32	15.37 ± 0.47	1.13	0.03
P209R	6.23 ± 0.18	0.99	0.76	13.71 ± 0.32	1.00	0.90
N214S	6.09 ± 0.08	0.97	0.45	13.20 ± 0.27	0.97	0.33
H215Y	7.23 ± 0.31	1.15	0.01	13.52 ± 0.53	0.99	0.84
I218N	6.98 ± 0.25	1.11	0.10	15.52 ± 0.29	1.14	9.37E-3
A221V	6.72 ± 0.19	1.07	0.16	15.94 ± 0.50	1.17	0.01
R226S	6.12 ± 0.18	0.97	0.43	13.47 ± 0.34	0.99	0.73

Further translational defect analysis

The dual luciferase system was used to test further translational fidelity qualities of the mutant strains. In nonsense suppression and misincorporation assays, values lower

than wild type indicate a hyper accurate strain. Several strains were hyperaccurate in one or both tRNA misincorporation assays (F185L, W195C, P209R, I218N). More promiscuous misincorporation strains were those with mutations at the extreme N or C termini (R5H, I218N, A221V). Nonsense suppression testing did not yield as many definitive results, but strains with mutations of V48D and L125 showed increased rates of stop-codon readthrough, as did G172C, W195C, and I218N to lesser degrees (Figure 2.13, Table 2.3, Table 2.4).

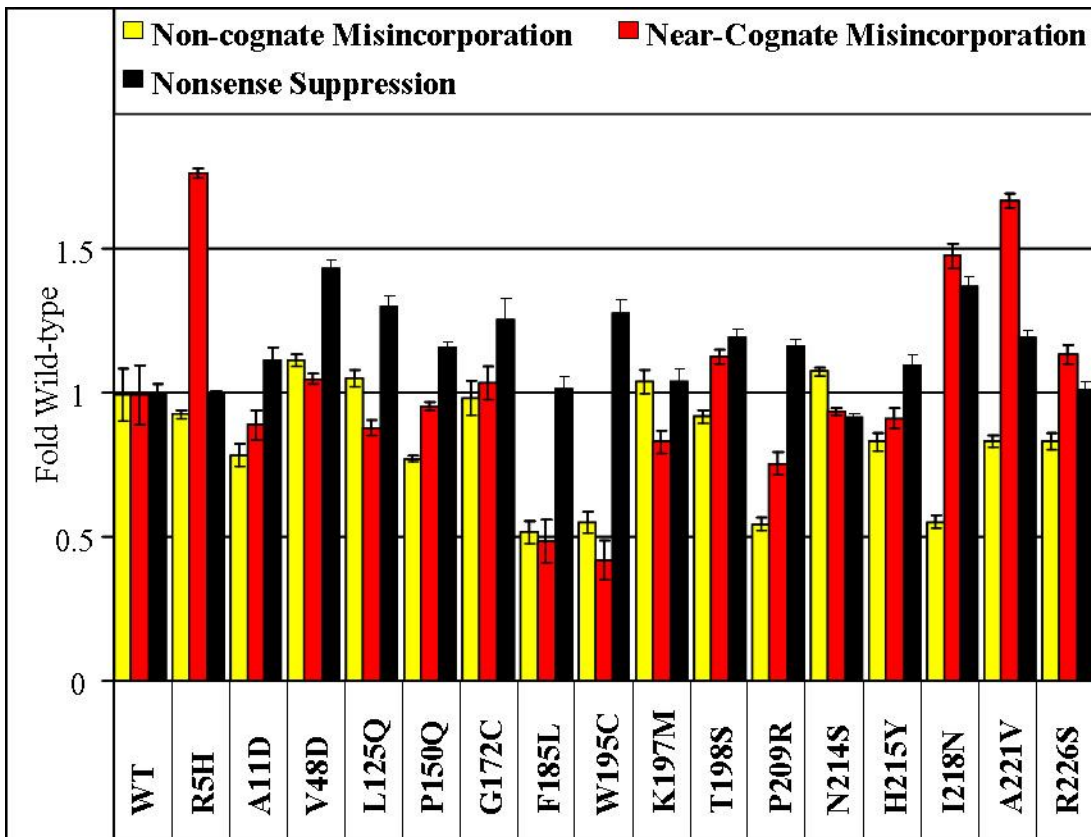


Figure 2.13: Dual luciferase measurements of translational fidelity characteristics

Effects on non-cognate (yellow) and near-cognate (red) misincorporation at codon 218 of firefly luciferase and changes in nonsense suppression (black) rates rpl2 mutation strains are depicted as fold of wild-type cells. Error bars indicate standard error.

Table 2.3: Effects of mutations in ribosomal protein L2 on rates of non- and near-cognate tRNA misincorporation

Misincorporation frequencies for non-cognate (UCU) and near-cognate (AGC) codons for each strain are reported with standard error. The fold wild-type provided is reported graphically in figure 2.12.

Strain	Non-cognate (UCU)			Near-cognate (AGC)		
	Mis-incorp (x 10 ⁻⁴)	Fold WT	P-value	Mis-incorp (x 10 ⁻⁴)	Fold WT	P-value
WT	1.66 ± 0.07	1.00	1.00	2.73 ± 0.21	1.00	1.00
R5H	1.55 ± 0.07	0.93	0.27	4.86 ± 0.35	1.78	3.72E-4
A11D	1.31 ± 0.07	0.79	8.59E-3	2.44 ± 0.16	0.89	0.70
V48D	1.86 ± 0.32	1.12	0.54	2.88 ± 0.31	1.06	0.45
L125Q	1.76 ± 0.24	1.06	0.70	2.42 ± 0.47	0.88	0.27
P150Q	1.29 ± 0.04	0.78	1.21E-4	2.62 ± 0.08	0.96	0.65
G172C	1.64 ± 0.06	0.99	0.97	2.85 ± 0.58	1.04	0.84
F185L	0.86 ± 0.11	0.52	7.33E-3	1.33 ± 0.13	0.49	3.31E-5
W195C	0.92 ± 0.16	0.55	0.01	1.16 ± 0.22	0.42	7.55E-6
K197M	1.73 ± 0.18	1.05	0.89	2.28 ± 0.39	0.84	0.31
T198S	1.53 ± 0.09	0.92	0.32	3.10 ± 0.24	1.14	0.73
P209R	0.91 ± 0.13	0.55	5.32E-3	2.08 ± 0.14	0.76	0.26
N214S	1.79 ± 0.09	1.08	0.22	2.58 ± 0.39	0.94	0.76
H215Y	1.39 ± 0.09	0.84	0.02	2.51 ± 0.08	0.92	0.37
I218N	0.92 ± 0.17	0.56	0.01	4.07 ± 0.36	1.49	4.94E-4
A221V	1.39 ± 0.14	0.84	0.18	4.59 ± 0.17	1.68	0.03
R226S	1.39 ± 0.08	0.84	0.21	3.12 ± 0.21	1.14	0.57

Table 2.4: Effects of mutations in ribosomal protein L2 on nonsense suppression rates

Nonsense suppression frequencies are reported with standard error. The fold wild-type value provided is reported graphically in figure 2.12.

Strain	Nonsense Suppression		
	Nonsense Supp. (x 10 ⁻²)	Fold WT	P-value
WT	3.41 ± 0.15	1.00	1.00
R5H	3.41 ± 0.05	1.00	0.97
A11D	3.83 ± 0.35	1.12	0.20
V48D	4.92 ± 0.20	1.44	2.78E-4
L125Q	4.46 ± 0.23	1.31	5.75E-3
P150Q	3.99 ± 0.14	1.17	0.02
G172C	4.31 ± 0.29	1.26	0.02
F185L	3.49 ± 0.40	1.02	0.72
W195C	4.39 ± 0.34	1.29	5.51E-4
K197M	3.57 ± 0.19	1.05	0.55
T198S	4.10 ± 0.31	1.20	0.03
P209R	3.99 ± 0.09	1.17	2.46E-3
N214S	3.14 ± 0.11	0.92	0.10
H215Y	3.76 ± 0.14	1.10	0.13
I218N	4.71 ± 0.55	1.38	9.43E-4
A221V	4.09 ± 0.34	1.20	0.04
R226S	3.47 ± 0.08	1.02	0.68

Polysome profiles

A subset of mutants displaying the strongest phenotypes was selected for analysis polysome profile analyses (Figure 2.14). Notably, the profile of the “wild-type” strain showed properties associated with 60S subunit defects. Specifically, these were (a) decreased 60S peak heights relative to 40S peak heights, and (b) the presence of small “shoulders” on the right sides of the 80S and polysome peaks indicative of half-mer formation. Shoulders and half-mer peaks indicate a population of mRNAs with an extra 40S subunit compared to the associated primary peak. The extra mass is due to a 40S subunit stalled at the start codon either due to a shortage of 60S subunits, or a subunit joining defect. The polysome profiles of most of the strains (F185L, W195C, N214S, H215Y, and I218N) were indistinguishable from wild type. However, the innate 60S and half-mer defects were strongly accentuated in the polysome profiles of cells expressing the V48D and L125Q mutations.

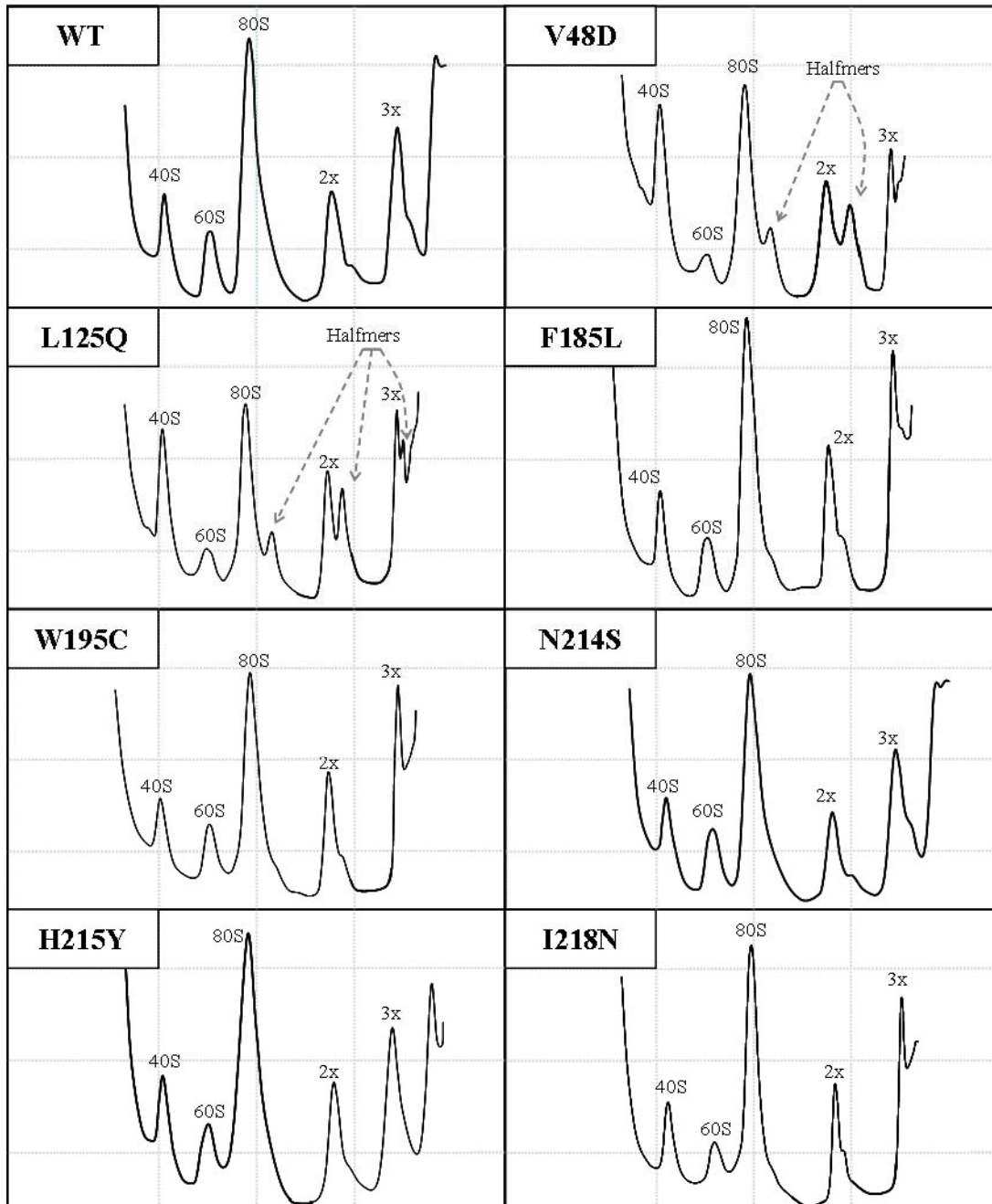


Figure 2.14: Polysome profiles of L2 mutant strains

Profiles were generated as described in the materials and methods. Cell lysates were separated through a sucrose gradient by centrifugation in a SW-41Ti rotor at 40,000 rpm for 135 minutes at 4°C. The profiles above represent the continuous read of A_{254} across the gradient as processed by an ISCO-5 gradient fractionator. Labels mark 40S, 60S, 80S and polysomal (2x, 3x, etc) peaks. Halfmer defects are apparent immediately behind 80S and polysome peaks and are indicated for the V48D and L125Q mutant strains.

Discussion

The goal of this study was to create a variety of mutants of ribosomal protein L2 in yeast and identify residues important for the structure and function of the protein. Screening for the loss of the killer virus as a general indicator of defective ribosome function allowed high throughput identification of interesting randomly generated mutants. Most of the mutants identified as losing killer were multiple mutations. While single mutation strains were selected for further study, the propensity for multiple amino acid changes itself provides information about the structure and function of L2. Ribosomal protein L2 is firmly integrated with the 25S rRNA, and the many contacts make it very robust and able to withstand multiple mutations. Possibly, the propensity for multiple mutations could have been caused by the random mutagenesis protocol utilized though this is unlikely as primer concentrations and reaction conditions were adjusted to generate primarily single mutations. Even though multiple mutations were required to generate killer phenotypes, the growth curve data reveal small but subtle changes that would make the mutants unable to compete with the wild-type. This suggests that the structure of L2 in yeast has been fine tuned to promote optimal cell growth.

The least subtle information as to the effects of the mutants was provided in the polysome profiles. The first observation is of an innate defect in 60S biogenesis visible as shoulders on all ribosome and polysome peaks in the wild-type strain due to the expression of only one isoform of L2. The strain expressing only L2A likely displays a 60S biogenesis defect which in turn causes a slight initiation defect as 40S subunits are stalled at start codons due to the insufficient supply of 60S subunits. As normal wild-

type yeast express both L2A and L2B proteins, clearly both are required for optimal ribosome function. Also, the expression of RPL2A mRNA from a cytoplasmic plasmid instead of its native chromosomal location might contribute to biogenesis issues with altered gene expression levels. Most of the strains analyzed provided profiles indistinguishable from wild-type.

The mutants harboring amino acid changes V48D and L125Q near the globular domain of the protein, demonstrated the strongest polysome defects. Extreme halfmers, indicating initiation defects, are present resulting from an apparent 60S biogenesis defect. The half-mer phenotype, which is caused by 40S subunits stalled at start codons, can also be caused by subunit joining difficulties. The poor growth characteristics of these strains in both growth curve and dilution spot assays might also be caused by a 60S biogenesis defect. These two strains also lost the killer virus, likely due to the severe biogenesis defect; though they also demonstrated a slight increase in -1 PRF, which perhaps contributed to killer virus loss.

A few other strains generated interesting phenotypes in isolated experiments. The G172C mutation displayed paromomycin sensitivity in the filter disc assay, at odds with the unperturbed growth of the strain background at all paromomycin concentrations. In all other assays, the G172C strain was remarkably similar to wild-type. Paromomycin binds at the decoding portion of the A-site on the small subunit. While the precise location of the bridge between L2 and the small subunit is unknown in yeast, it is possible that the G172C mutation is having a distal effect on the decoding center of the ribosome in the small subunit by affecting this bridge. The small subunit side of the

bridge with L2 likely involves 18S rRNA helices 22 and 23, which connect directly to the decoding center.

Two strains, harboring the F185L and W195C mutations, demonstrated hyperaccuracy phenotypes in misincorporation assays using the dual luciferase system. Interestingly, these two mutations border a highly conserved rRNA binding region of the protein. This binding interaction indirectly links to the A-site of the PTC through helices 64 and 71, potentially affecting A-site conformation and incorporation of aminoacyl-tRNAs. With the exception of an excessive growth phenotype in growth curves for the F185L strain, both mutations yielded near wild-type results.

The strain harboring mutation H215Y also lost the killer virus. Unlike the other two single mutations that encouraged loss of the killer virus, the H215Y strain is relatively healthy. The strain had a slight increase in -1 PRF and possibly a slight anisomycin resistance phenotype. The possibility of anisomycin resistance could indicate an aa-tRNA binding defect that could lead to loss of the killer virus. Also of interest is the sparsomycin resistant phenotype in the filter disc assays. The mutant is interesting as it is located in the binding pocket with H93, directly adjacent to the peptidyl transferase center. The proximity of the mutation to the PTC and the binding sites for anisomycin and sparsomycin, suggests that the mutation may be subtly changing the structural conformation of the PTC to provide resistance to both drugs. This structural aspect suggests that H215 may warrant more detailed study using a reverse-genetics approach.

This study has identified regions of ribosomal protein L2 that might be interesting for future study. Specifically, further mutation of the tip of L2 that binds helix 93 at the PTC might provide interesting information on the structure and conformation of the

active site during peptidyl transfer. Further studies will use the information gathered from this general assay to target specific amino acids across a range of biochemical properties for a more detailed analysis of L2 structure and function.

Chapter 3: Differentiating between near- and non-cognate codons in *Saccharomyces cerevisiae*

(Published: Plant et al., 2007)

Introduction

Accurate transmission of biological information is a central requirement at all levels of life. In cells, one aspect of this process is the faithful translation of the genetic code from DNA into protein. The intermediaries in the last stage of this process include mRNA, tRNAs, ribosomes and many *trans*-acting factors. The protein coding information of an mRNA is formatted as codons. The anticodon loops of aminoacyl tRNAs (aa-tRNAs) form base-pairing interactions with the codons. This enables ribosomes to add amino acids sequentially to the nascent protein. aa-tRNAs that can participate in standard Watson-Crick interactions with the first two bases in a codon and can form either canonical or non-Watson-Crick pairs at the third or “wobble” position are designated cognate-tRNAs (Crick 1966; Agris 1991). In contrast, tRNAs that do not meet these requirements are commonly referred to as near- and non-cognate tRNAs. Utilization of near- and non-cognate tRNAs is called misreading or a missense error. Misreading occurs with low frequencies of 10^{-3} and 10^{-4} per codon (Kramer and Farabaugh, 2007 and references within).

The 64 codons encode 20 different amino acids and three termination signals. In cases where one amino acid is represented by multiple codons, some tRNAs can decode more than one codon. This redundancy is facilitated by tRNA modifications and by wobble base-pairing between the anticodon and the codon (reviewed in Agris et al., 2007). Our understanding of how the ribosome achieves such a high degree of specificity

has been facilitated by both kinetic and structural analyses in bacteria (reviewed in Ogle and Ramakrishnan, 2005; Daviter et al, 2006; Sanbonmatsu, 2006). *In vitro* kinetic analyses using ribosomes, tRNAs, and the bacterial aa-tRNA binding factor EF-Tu have broken down the process of aa-tRNA selection into a series of discrete steps (reviewed in Daviter et al., 2006). These studies have identified two stages (k_2 and k_7) in this process that favor rejection of aa-tRNAs whose anticodon loops cannot base-pair with codons. A mutational analysis demonstrated that two independent mechanisms corresponding to these two steps are required for utilization of cognate aa-tRNAs (Cochella et al., 2007). Structural, biophysical, and computational analyses also show a mechanism for positive selection of cognate aa-tRNAs (Sanbonmatsu, 2006; Cochella et al, 2007; Sanbonmatsu and Joseph, 2003; Sanbonmatsu, 2006) that emphasizes the geometry of base pairing at the ribosomal decoding center (Ogle et al., 2002). Formation of an appropriately configured mini-helix in the decoding center generates an RNA minor-groove, enabling interaction with three critical bases of the small subunit rRNA. Formation of this mini-helix stimulates A1492 and A1493 of the small subunit rRNA to flip out into the minor groove forming a complex arrangement of hydrogen bonds with the tRNA/mRNA backbones in concert with G530 (Figure 3.1A). This in turn stimulates a conformational change in the aa-tRNA that transduces the information from the decoding center to activate the GTPase activity of EF-Tu (reviewed in Cochella and Green, 2005). The energy barrier for flipping out of A1492 and A1493 is sufficiently small for correct binding of aa-tRNA to shift the equilibrium in favor of the subsequent steps (Sanbonmatsu, 2006). Aminoglycoside antibiotics such as paromomycin stimulate misreading by binding to the decoding center, displacing A1492 and A1493. This forces

these bases to mimic the “flipped out” conformations that they normally assume in response to the mini-helix formation by a cognate codon:anticodon pair (reviewed in Ogle and Ramakrishnan, 2005). Together, these kinetic and biophysical mechanisms ensure the accurate utilization of cognate aa-tRNAs.

An unsettled issue remains the precise distinction between “near-cognate” and “non-cognate” tRNAs, especially in eukaryotes. This is important since the rational design or utilization of therapeutics may exploit the functional differences that exist between these two classes of tRNAs. One recent study has suggested that the relative abundances of bacterial aa-tRNAs plays a significant role in translational accuracy (Kramer and Farabaugh, 2007). By this model, highly abundant aa-tRNAs are more likely than low abundance aa-tRNAs to misread codons that are decoded by other low abundance aa-tRNAs. This study using the yeast *Saccharomyces cerevisiae* supports this competition model. However it also suggests that this is not sufficient to explain the functional differences between near- and non-cognate aa-tRNAs. Using a series of seven substitutions of a codon in the catalytic site of firefly luciferase, we show that a second critical distinction lies in the ability to form hydrogen bonding interactions at all three positions between the aa-tRNA anticodon loop and the codon in the decoding center. This is likely the result of changes in formation of the codon:anticodon mini-helix. Thus, transient formation of the mini-helix allows the rRNA and tRNA conformational changes required for activation of the GTPase activity of eEF1A, the eukaryotic homolog of EF-Tu. This is supported by the demonstration of paromomycin stimulated misreading by aa-tRNAs that are capable of forming a transient interaction. This identifies paromomycin as a functional probe to distinguish between near- and non-cognate aa-tRNAs. The

hypothetical roles in this process played by eEF1A and its associated factors, eEF1B α and eEF1B γ , were also investigated. The results suggest that the GTPase activity of eEF1A is preferentially stimulated by near-cognate codon:anticodon interactions, and point to discrete functional regions of the protein. Studies of eEF1B α , the catalytic subunit of the guanine nucleotide exchange factor (GEF) required for recycling of GTP-bound eEF1A, are consistent with a kinetic model in which limiting concentrations of eEF1A:aa-tRNA:GTP ternary complex should decrease rates of protein synthesis, resulting in increased selection against both near- and non-cognate aa-tRNAs. Interestingly, deletion of the proposed regulatory subunit of the GEF complex, eEF1B γ , tended to promote increased misreading of near-cognate codons and decreased misreading of non-cognate codons. This suggests eEF1B γ may have a regulatory function. In a final series of experiments, the potential role of the fungus-specific elongation factor eEF3 in translational fidelity was indirectly assayed through analysis of a series of mutants in the ribosomal protein L5 (rpL5). rpL5 forms part of the ribosome binding site for this factor (Andersen et al., 2006). Like the eEF1B α mutant, the ability of an rpL5 mutant to promote enhanced fidelity at both non- and near-cognate codons suggests that slowing rates of elongation by disrupting the synergy between eEF1A and eEF3 results in increased selection against both near- and non-cognate aa-tRNAs.

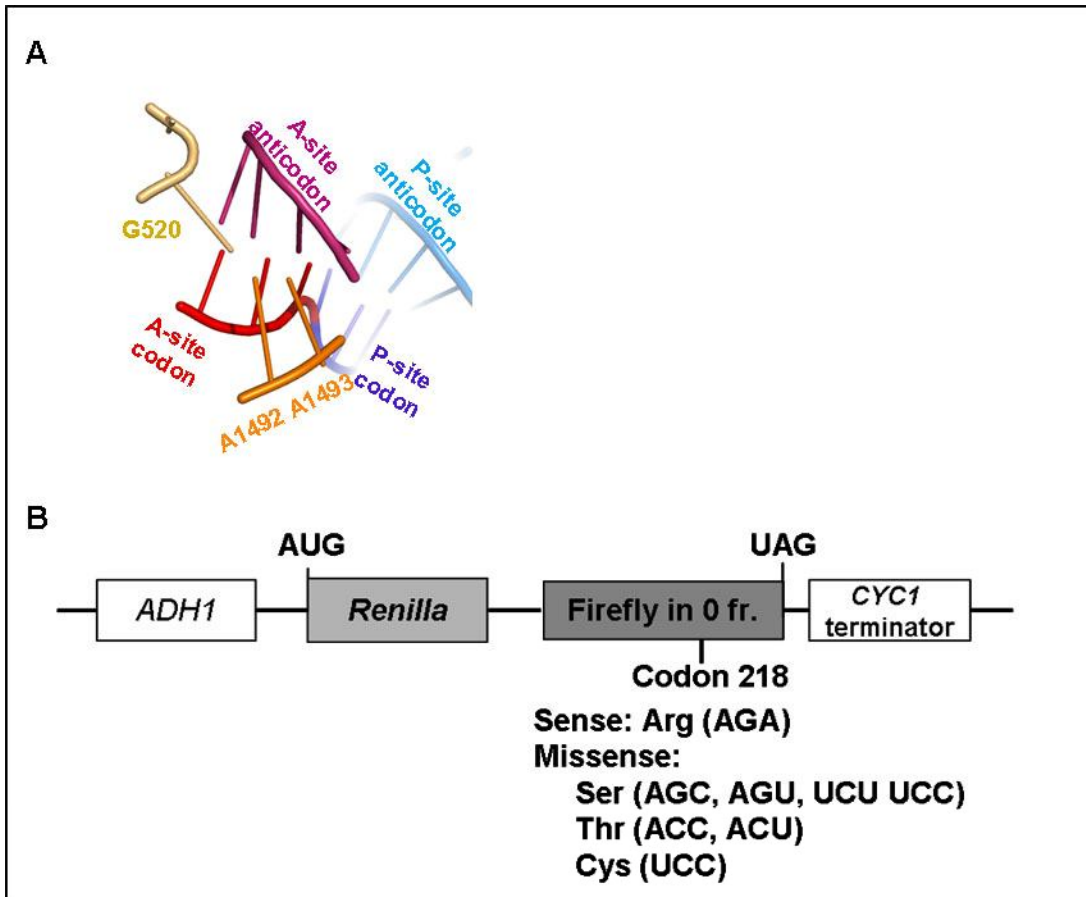


Figure 3.1: The decoding center and dual-luciferase reporters for determining rates of translational misreading in yeast

Panel A: The codon:anticodon mini-helix in the decoding center is stabilized by base-pairing at all three positions of the mini-helix favoring A-minor interactions with flipped out bases G520, A1492 and A1493. Pymol (Delano Scientific, LLC) was used to generate this figure based on the coordinates 1IBM in the RSCB Protein Data Bank. **Panel B:** In all missense reporters, transcription is initiated from the yeast *ADH1* promoter, and terminated at a sequence from the *CYC1* 3'UTR. The luciferase genes from *Renilla* and firefly are cloned in frame to produce a fusion of the two proteins. The sense reporter has the AGA codon encoding arginine at amino acid residue 218 in the catalytic site of firefly luciferase. Missense reporters contain the indicated mutations at this position, which encode the indicated amino acids. Efficiencies of missense suppression were calculated by dividing the ratio of firefly/*Renilla* luciferase generated from cells harboring the missense test vectors by the ratio of firefly to *Renilla* luciferase generated from cells harboring the sense control plasmid.

Constructs created by Ewan Plant

Materials and methods

E. coli and yeast strains and genetic methods

E. coli strain DH5 α was used to amplify plasmids. High efficiency transformations were performed as previously described (Inoue et al., 1990). The *Saccharomyces cerevisiae* strains used in this study are listed in Table 3.4. The *RPL5* strains were generously provided by Dr. John Woolford. Isogenic *TEF2*, *TEF3*, and *TEF4* yeast strains were previously described (Olareswaju et al., 2004; Anand et al, 2001; Carr-Schmid et al, 1999). Strains were cultured on YPAD or synthetic complete medium (H-) (Dinman and Wickner, 1994) and were freshly plated and incubated for two to five days at 30°C prior to transformation. Yeast were transformed with the alkali cation method (Ito et al., 1983), plated on appropriate selective media, and incubated at 30°C for four days. To assay for paromomycin sensitivity, 10-fold dilutions of logarithmically growing cells were spotted onto H-leu containing drug at a concentration of 1 mg/ml, or onto no-drug control plates, and grown at 25°C for 3 days.

Plasmid constructs

Plasmids used in this study contained a dual luciferase cassette on a yeast vector backbone with the *URA3* selectable marker. The parental pYDL-Control plasmid containing the wild-type *Renilla* and firefly luciferase genes has been described previously (Harger and Dinman, 2003). Missense mutations were introduced into the arginine codon (AGA) at position 218 in the catalytic site of firefly luciferase (Rawalska and Rospert, 2004) using variations on the following primers:

5'-ATGCGAGAANNNGACGCAGGCAGTTCTATG-3' and

5'-GCCTGCGTCN'N'N'TTCTCGCATGCCAGAGATC-3' (Integrated DNA

Technology, Coralville, IA)

where N denotes bases at codon 218 that were changed on the sense strand, and N' are the corresponding bases mutagenized on the antisense strand. Oligonucleotide site directed mutagenesis reactions were performed using the StrataGene Quikchange II kit (La Jolla, CA) according to the manufacturer's instructions. The seven mutants thus created are listed in Table 3.1. A second set of plasmids containing the yeast *TRP1* reporter were constructed by transferring the dual luciferase cassettes from the resulting plasmids as *SpeI*-*XhoI* fragments into p414 ADH (Mumberg et al., 1995).

Dual luciferase assays

Transformed yeast cells were grown overnight in selective medium at 30°C to OD₅₉₅ of 0.8 to 1.0. Cells were pelleted by centrifugation, washed twice with 0.5ml of cold lysis buffer (phosphate buffered saline containing 1 mM phenylmethylsulfonylfluoride), resuspended in cold lysis buffer and broken by agitation with glass beads (0.5 mm BioSpec). Lysates were clarified by centrifugation, and supernatants transferred to pre-chilled tubes. Luminescence reactions were initiated by addition of 50 µl of Promega DLR system to 5 µl of clarified cell lysates and measured using a Turner Design TD20/20 luminometer. At least three readings were taken for each assay and all assays were repeated (n = 3 – 12) until the data were normally distributed to enable statistical analyses both within and between experiments (Jacobs and Dinman, 2004). An unpaired two-sample *t*-test was used to test the hypothesis that two datasets

came from the same population, a rejected hypothesis indicating that the datasets were significantly different. The *P*-values from this test is the estimation of the probability of an incorrect conclusion (Jacobs and Dinman, 2004).

Results

Baseline and Paromomycin-stimulated rates of missense suppression suggest a functional difference between the near- and non-cognate tRNAs

Introduction of a missense mutation into the active site of an enzyme followed by quantitative measurement of the restoration of enzymatic activity can provide a basis to monitor translational error rates. The arginine at position 218 of firefly luciferase is located in the active site and is required for enzymatic activity. Mutation of the corresponding AGA arginine codon to either the AGC or UCU serine codon was previously used to monitor missense error rates of ribosome bound chaperone mutants in *S. cerevisiae* (Rakwalska and Rospert, 2004). The current study employed a bicistronic luciferase reporter system to monitor suppression of a series of missense mutations. This could functionally distinguish translational fidelity effects due to the inherent translatability of different codons and subsequently correlate these with *trans*-acting influences. In this assay, the gene encoding firefly luciferase is fused in frame with a downstream *Renilla* luciferase gene. Test plasmids harbored missense codons at position 218 of the firefly luciferase gene (Figure 3.1B, “Missense”) The control was identical except that it contained the wild-type AGA codon at this position (Figure 3.1B, “Sense”) Even though the two luciferase proteins are fused, the activity from each can be measured

independently as they utilize different substrates. Rates of misreading were calculated by dividing the ratio of firefly luciferase activity to *Renilla* luciferase activity generated from the missense vector in strains harboring the indicated mutant allele by the ratio generated with the sense plasmid. The results were statistically tested as previously described (Jacobs and Dinman, 2004).

Previous studies have shown that missense errors occur with frequencies on the order of 10^{-4} in both *E. coli* and in *S. cerevisiae* (Kramer and Farabaugh, 2007; Bouadloun et al., 1983; Salas-Marco and Bedwell, 2005; Stansfield et al., 1998). Consistent with the literature, the seven missense mutations assayed at position 218 demonstrated ratios of firefly to *Renilla* luciferase activities that were reduced by approximately 4 orders of magnitude in all cases (Table 3.1). Although rates of misreading are low and the differences between test and control samples are small, the sensitivity of the assay and rigor of the statistical methods enable meaningful analysis of the data. Inspection of these data revealed that rates of misreading varied over an approximately 4.5-fold range. The inability of any one amino acid (i.e. Ser, Cys, or Thr) to disproportionately influence apparent missense incorporation suggests that the assay monitored incorporation errors rather than altered luciferase activity arising from incorporation of any specific amino acid. The data reveal that the common element among the three most stimulatory codons is the potential to form a stable G•C base pair at the second position. The observation of different error rates among the four serine codons (which are decoded by different tRNA families) suggests that relative tRNA abundances are also important.

Table 3.1: Baseline levels and effects of paromomycin on suppression of missense mutations at codon 218 of firefly luciferase

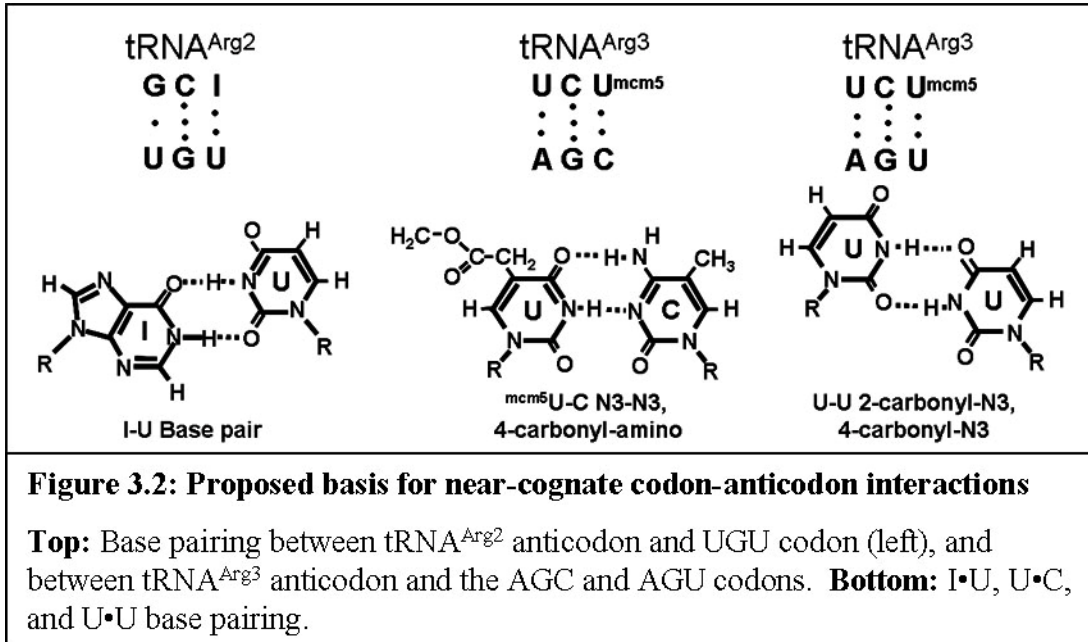
Wild-type codon is AGA Arginine.

Work performed by Ewan Plan and Phuc Nyugen

218 codon alleles	Mis-Incorporation Freq. ($\times 10^{-4}$)		Fold Change	P-value
	No Drug	+ Paromomycin		
AGC Ser	6.53 \pm 0.42	8.36 \pm 0.53	1.30	0.01
AGU Ser	2.88 \pm 0.17	3.81 \pm 0.21	1.30	2.55E-3
UGU Cys	3.56 \pm 0.28	4.89 \pm 0.28	1.40	2.99E-3
UCU Ser	2.23 \pm 0.09	2.33 \pm 0.09	1.00	0.46
UCC Ser	2.27 \pm 0.13	2.43 \pm 0.14	1.10	0.42
ACC Thr	1.92 \pm 0.29	1.55 \pm 0.06	0.81	0.25
ACU Thr	1.37 \pm 0.05	1.32 \pm 0.08	1.00	0.60

Formation of the mini-helix in the decoding center stimulates flipping out of the small subunit bases A1492 and A1493 that in combination with G530 stabilizes this structure (Figure 3.1A). Paromomycin binding to the decoding center of the small ribosomal subunit displaces A1492 and A1493, thus enhancing the frequency of missense errors (reviewed in Daviter et al, 2006). It has been hypothesized that not only does the formation of the mini-helix displace A1492 and A1493, but once displaced they sterically position the interribose bonds to maintain A-form helices (Lim et al, 2005). In the current study, translational misreading errors were significantly stimulated by paromomycin at codons that are capable of forming complete mini-helices with arginyl-tRNAs: UGU, AGU and AGC (Figure 3.2). In contrast, paromomycin did not stimulate misreading with anticodons unable to form the mini-helix, e.g. UCU, UCC, ACU and ACC. These findings suggest a functional definition for near- versus non-cognate codon:anticodon interactions. This potential to form base pairing interactions at all three positions, which is possibly nucleated by a strong Watson-Crick base pair at the second

position would allow transient formation of the mRNA:tRNA mini-helix. We propose this as the defining feature of a near-cognate interaction. In contrast, non-cognate interactions are defined by their lack of potential to form the mini-helix.



eEF1A mutants generally affect utilization of near-cognate aa-tRNAs

In eukaryotes, a ternary complex composed of eEF1A, aa-tRNA, and GTP delivers the aa-tRNA to the A-site of the ribosome. When an aa-tRNA containing the correct anticodon is sampled by the ribosome, a signal is transmitted through the body of the tRNA. This stimulates GTP hydrolysis by eEF1A and subsequent accommodation of the tRNA into the ribosomal A-site (reviewed in Ogle and Ramakrishnan, 2005; Daviter et al., 2006). eEF1A is encoded by the essential *TEF1* and *TEF2* genes in *S. cerevisiae*. A set of *TEF2* mutants expressed in a *tef1Δ tef2Δ* genetic background (Sandbaken and Culbertson, 1988) were assayed with respect to their effects on misreading using the AGC and UCU serine codons to monitor misreading of near- and non-cognate codons,

respectively. The results show allele-specific responses specifically to near-cognate codons. Strains bearing one of six alleles (E122K, E122Q, D156N, E286K, E295K, and E317K) promoted enhanced misreading of the near-cognate AGC Ser codon, but not of non-cognate UCU Ser (Figure 3.3A, Table 3.2, $p < 0.01$). In contrast, a strain expressing the T142I and to the lesser extent N153T/D156E mutant were better able to distinguish between the cognate AGA and near-cognate AGC codons. This enhanced fidelity did not extend to the non-cognate UCU codon (Figure 3.3A, Table 3.2, $p < 0.01$). In summary, it appears that near-cognate codons and not non-cognate are able to influence eEF1A activity in an allele-specific manner.

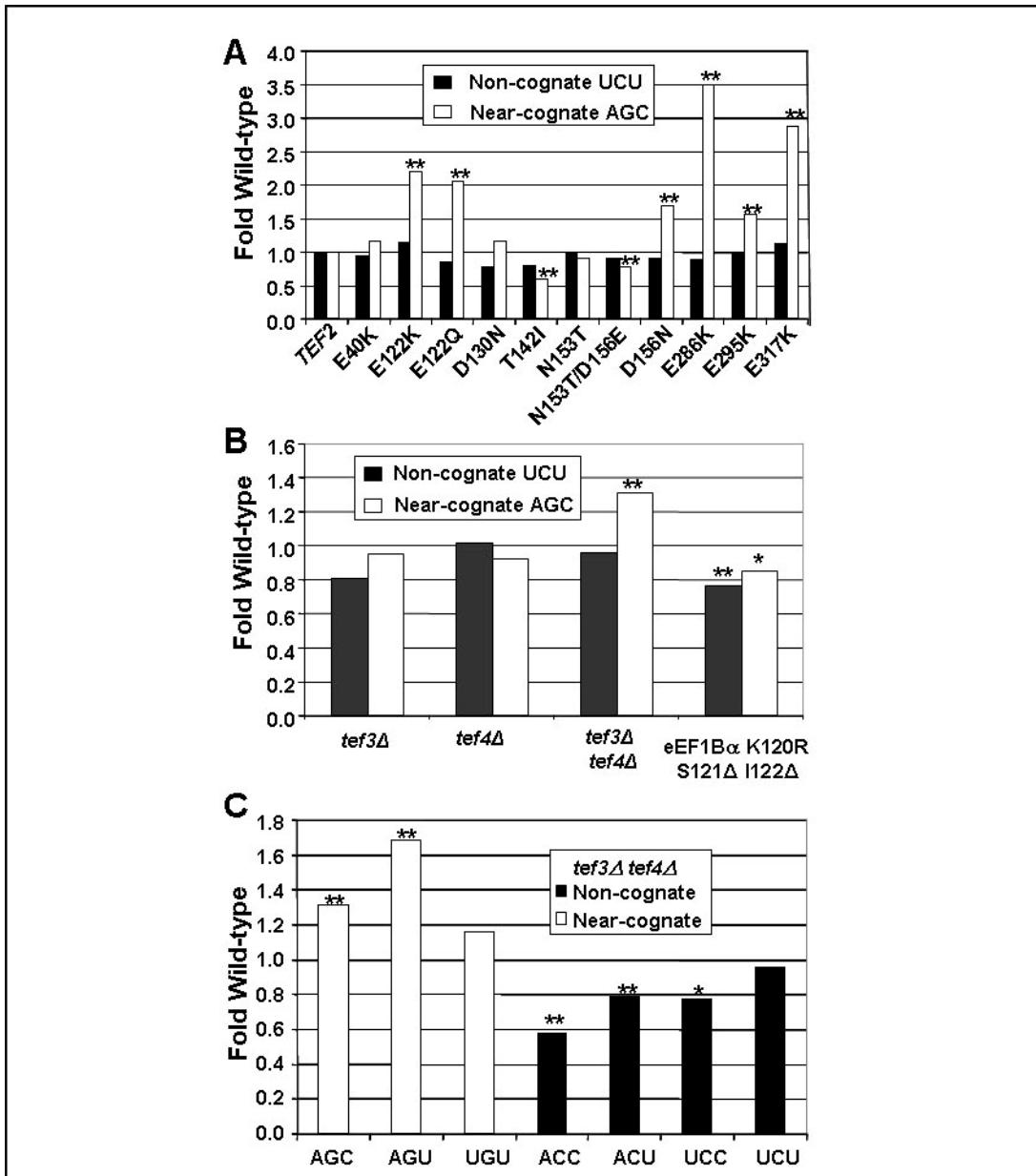


Figure 3.3: Effects of the eEF1 complex mutants on mis-reading of near- and non-cognate codons

Misreading of the non-cognate UCU and near-cognate AGC codons by mutant forms of eEF1A (**Panel A**), or by isogenic strains with *tef3Δ*, *tef4Δ*, or *tef3Δtef4Δ* double null mutants or *tef3Δ* strains expressing the K120R S121Δ I122Δ allele compared to isogenic wild-type strain (**Panel B**). **Panel C**: Misreading of all seven missense codons by cells lacking both forms of eEF1B (*tef3Δtef4Δ*). Effects of the indicated mutants are depicted as fold of isogenic wild-type cells. ** indicates *p* values of <0.01; * indicates *p* values of <0.05.

Panel A work performed by Ewan Plant and Phuc Nyugen.

Table 3.2: Effects of selected alleles of genes on mis-reading of non-cognate and near-cognate mutations at codon 218 of firefly luciferase

Portion of work performed by Ewan Plant and Phuc Nyugen

Strain	Non-cognate (UCU)			Near-cognate (AGC)		
	mis-incorp (x 10 ⁻⁴)	Fold WT	P-value	mis-incorp. (x 10 ⁻⁴)	Fold-WT	P-Value
eEF1A						
WT (<i>TEF2</i>)	2.04 ± 0.13	1.00	1.00	7.01 ± 0.49	1.00	1.00
E40K (<i>TEF2-3</i>)	1.91 ± 0.18	0.94	0.56	8.11 ± 0.72	1.16	0.22
E122K (<i>TEF2-4</i>)	2.33 ± 0.17	1.14	0.17	15.4 ± 0.55	2.20	9.76E-10
E122Q (<i>TEF2-10</i>)	1.73 ± 0.16	0.85	0.14	14.4 ± 0.79	2.05	2.43E-6
D130N (<i>TEF2-13</i>)	1.61 ± 0.12	0.79	0.02	8.16 ± 0.21	1.16	0.05
T142I (<i>TEF2-7</i>)	1.62 ± 0.14	0.79	0.03	4.20 ± 0.48	0.60	6.64E-4
N153T (<i>tef2-19</i>)	2.05 ± 0.04	1.00	0.95	6.39 ± 0.14	0.91	0.06
N153T/D156E (<i>tef2-18</i>)	1.87 ± 0.05	0.91	0.03	5.53 ± 0.20	0.79	4.92E-3
D156N (<i>tef2-17</i>)	1.85 ± 0.04	0.91	0.02	11.94 ± 0.39	1.69	3.10E-7
E286K (<i>TEF2-1</i>)	1.81 ± 0.08	0.89	0.04	24.64 ± 0.11	3.50	3.58E-8
E295K (<i>TEF2-9</i>)	2.00 ± 0.20	0.98	0.87	10.9 ± 0.95	1.55	3.09E-3
E317K (<i>TEF2-2</i>)	2.31 ± 0.04	1.13	0.06	20.1 ± 0.91	2.87	1.70E-7
eEF1Bα						
WT	3.15 ± 0.12	1.00	1.00	3.50 ± 0.14	1	1.00
K120R S121 Δ I222 Δ	2.38 ± 0.22	0.76	8.89E-3	2.98 ± 0.10	0.85	0.01
eEF1Bγ						
WT	1.22 ± 0.14	1.00	1.00	1.24 ± 0.09	1	1.00
<i>tef3</i> Δ	1.00 ± 0.04	0.81	0.15	1.18 ± 0.05	0.95	0.49
<i>tef4</i> Δ	1.25 ± 0.14	1.02	0.41	1.14 ± 0.06	0.92	0.41
<i>tef3</i> Δ <i>tef4</i> Δ	1.17 ± 0.05	0.96	0.62	1.62 ± 0.03	1.31	1.09E-5

A mutation in eEF1B α promotes general hyperfidelity

After hydrolysis of GTP, the eEF1A:GDP complex is released from the ribosome. The eEF1B α subunit (encoded by *TEF5*) is the essential nucleotide exchange factor responsible for catalytic activity in eEF1A recycling (Hiraga et al, 1993). Analysis of the role of the eEF1B α protein capitalized on the availability of the K120R S121 Δ I222 Δ mutant form of the protein that altered or deleted residues involved in critical interactions with the nucleotide binding pocket of eEF1A (Andersen et al, 2000). This mutant strain was previously shown to enhance translational fidelity by promoting lower levels of readthrough at all three stop codons (Carr-Schmid et al, 1999). In the current study, the

K120R S121Δ I122Δ eEF1B α mutant showed modest but consistent enhanced fidelity at both the UCU and AGC non- and near-cognate codons respectively (Figure 3.3B, Table 3.2, $p < 0.01$). As discussed below, we hypothesize that this may be due to limiting concentrations of eEF1A:GTP.

Codon-specific misreading in the absence of eEF1B γ

In yeast, the eEF1 complex contains a third non-essential subunit, eEF1B γ . Yeast cells express two isoforms of eEF1B γ , encoded by the *TEF3* and *TEF4* genes. The N-terminus of Tef3p exhibits structural similarity to glutathione-S-transferases and is thought to participate in the regulation of elongation during stress (Jeppesen et al., 2003; Olarewaju et al., 2004). Deletion of either eEF1B γ isoform alone had no significant effects on misreading at either the AGC near-cognate or UGU non-cognate codons (Figure 3.3B, Table 3.2). However deletion of both eEF1B γ -encoding genes caused a statistically significant increase in mis-incorporation at near- but not at non-cognate codons (Figure 3.3B, Table 3.3). These results suggest that these two proteins have redundant activities and that this factor functions in ensuring translational fidelity. To investigate this phenomenon further, misreading in the absence of eEF1B γ (*tef3Δtef4Δ*) was assayed at the remaining 5 missense codons. Although misreading of the near-cognate AGU Ser codon was also enhanced, there was no effect on recognition of the ‘near-cognate’ UGU Cys codon (Table 3.3, Figure 3.3C). In contrast, although recognition of the UCU ‘non-cognate’ codon was not affected, recognition of the other non-cognate codons (ACC, ACU, and UCC) was significantly enhanced by the absence of eEF1B γ .

Table 3.3: Survey of isogenic wild-type and mutant pairs of strains with seven different codons at codon 218 of firefly luciferase				
codon	mis-incorp (x 10⁻⁴)		Fold WT	P-value
eEF1By				
	WT	<i>tef3Δtef4Δ</i>		
AGC	9.78± 0.31	12.8± 0.23	1.31	1.1E-05
AGU	2.85 ± 0.21	4.81 ± 0.11	1.69	4.1E-06
UGU	2.81± 0.16	3.27± 0.18	1.16	0.08
ACC	1.39± 0.06	0.80± 0.06	0.58	2.2E-05
ACU	1.13± 0.05	0.89± 0.05	0.79	3.0E-03
UCC	2.07± 0.08	1.60± 0.14	0.78	0.02
UCU	3.03± 0.25	2.90± 0.13	0.96	0.62
RPL5				
	WT	K27E		
AGC	10.6± 0.51	9.39± 0.80	0.88	0.21
AGU	3.26± 0.08	2.81± 0.05	0.86	0.05
UGU	2.95± 0.14	2.50± 0.18	0.85	0.02
ACC	1.16± 0.07	0.95± 0.04	0.82	0.02
ACU	0.99± 0.05	0.76± 0.02	0.77	1.0E-03
UCC	1.59± 0.11	1.75± 0.06	1.11	0.22
UCU	2.47± 0.15	1.33± 0.09	0.54	1.5E-07

The K27E mutant of ribosomal protein L5 promotes a general enhancement of fidelity

The three-site model of the ribosome posits that preventing simultaneous occupancy of the ribosomal A- and E-sites by aa-tRNA and deacylated-tRNAs respectively helps to coordinate the elongation cycle (reviewed in Nierhaus, 1990). In fungi, the unique essential elongation factor 3 (eEF3) facilitates eEF1A-dependent A-site binding of aa-tRNA and has ATP-dependent activity required for the release of deacylated tRNA from the E site (Triana-Alonso et al., 1995). Although ribosomal protein L5 (rpL5) is far from the decoding center, it has been shown to interact with eEF3. Previous studies have characterized five temperature-sensitive alleles of the yeast

RPL5 gene encoding rpL5 (Deshmukh et al., 1995; Meskauskas and Dinman, 2001). A preliminary assay of five *rpl5* mutant strains using the near- (AGC) and non- (UCU) cognate reporters indicated that the K27E mutant of L5 tended to be generally hyperaccurate (data not shown). Analysis of all 7 missense codons revealed that the K27E mutant generally promoted greater levels of translational accuracy (Figure 3.4A, Table 3.3). Dilution spot assays revealed that rpL5-K27E is resistant to paromomycin (Figure 3.4B), consistent with the notion that this mutant is antagonistic to the action of the drug. As discussed below, these findings suggest an indirect role for rpL5 in translational decoding. This may be through its association with eEF3 and account for some differences in A-site fidelity between bacteria and fungi.

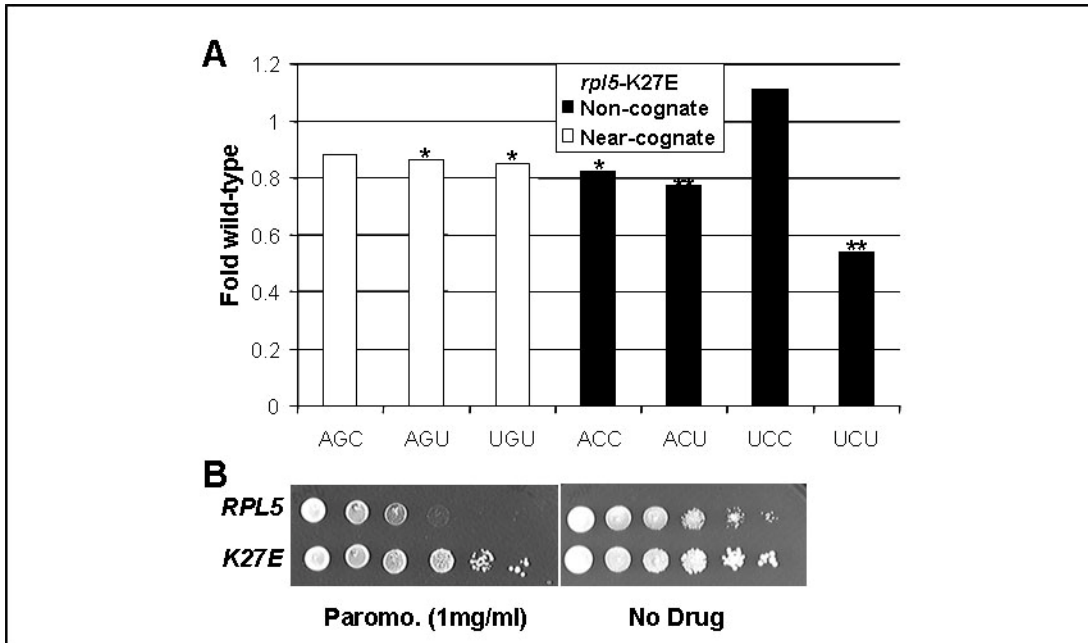


Figure 3.4: Characterization of alleles of RPL5

Panel A: Effects of the K27E *rpl5* mutant on misreading of seven missense codons. Effects on the indicated missense reporters are depicted as fold of isogenic wild-type cells. ** indicates p values of <0.01 . * indicates p values of <0.05 . **Panel B:** Paromomycin dilution spot assays. Ten-fold dilutions ($10^6 \rightarrow 10^1$ CFU) of logarithmically growing cells were arrayed onto H-leu medium containing paromomycin (1 mg/ml) or no drug control plates. Cells were grown at 25°C for 3 days.

Panel B work performed by Phuc Nyugen

Discussion

A significant number of human diseases, including sickle cell disease and a significant portion of ALS cases, are caused by missense mutations. Understanding the functional differences between mutations and drugs that result in near- versus non-cognate codon usage may inform strategies for therapeutic interventions. In the current study, codon misreading was examined in the yeast eukaryotic model system using a dual luciferase reporter in which the AGA Arg codon in the firefly luciferase catalytic site was

changed to AGC, AGU, UCU, UCC (serine); UGU (cysteine); and ACC or ACU (threonine). Each of these substitutions has a polar sidechain like arginine, but lacks the positive charge. The consistent 4-order of magnitude decrease in firefly luciferase activity with these substitutions agrees with previously characterized missense error rates. The finding that no one amino acid alters firefly luciferase activity outside a range supports that the assay monitors misincorporation of arginine. The observation that the frequency of Arg misincorporation varied over an approximately 4.5-fold range independent of the identity of the encoded amino acid suggests that misincorporation frequency is determined by other factors.

In each species, some codons are used more frequently than others. The codon bias is especially clear in highly expressed genes. Studies in *E. coli* have led to the suggestion that codon bias minimizes the deleterious effects of aberrant decoding (Stoletzki and Eyre-Walker, 2007; Najafabadi et al, 2007). Examination of codon bias in highly expressed yeast genes (see Plewniak, 2007) reveals that both the AGU and AGC Ser codons occur at a low frequency of approximately 5% of serine in the yeast genome. All of the other codons employed in this study occur with significantly higher frequencies. UGU is the most frequently used Cys codon at 84% in highly transcribed genes. Its substitution promoted even higher rates of miscoding than AGU Ser at 5% codon frequency. Thus, it is clear that codon frequency is not the sole determinant of translational fidelity. A recent study in *E. coli* suggested that competition between different tRNAs is the underlying factor influencing misreading error rates (Kramer and Farabaugh, 2007). In yeast, gene copy number for individual tRNA species correlates with initial estimates of relative tRNA content in normally growing cells, allowing the

number of functional genes encoding cognate tRNAs for each codon to be used as a proxy measure of tRNA abundance (Ikemura, 1982; Percudani et al., 1997). Examination of yeast tRNA gene copy numbers (Hani and Feldmann, 1998) reveals that AGA Arg is decoded by the highly abundant tRNA^{Arg3} (11 copies). In support of the tRNA competition model, the codons that intrinsically promoted higher levels of misreading were decoded by lower abundance tRNAs, while those at the lower end of the range are decoded by more abundant tRNAs. For example, the AGU and AGC codons are decoded by the relatively low abundance tRNA^{Ser3} (4 copies), and all Cys codons are decoded by the 4 copy tRNA^{Cys}. In contrast, the UCU and UCC codons are decoded by tRNA^{Ser2} (11 copies), and the ACC and ACU codons are decoded by the high copy tRNA^{Thr1a} (11 copies). However, tRNA competition alone cannot fully explain the observed differences. The pattern becomes more apparent when the ability of near-cognate codons to base pair with anticodons of different arginyl-tRNAs is considered (Figure 3.2). The first two bases of the AGC and AGU Ser codons could be recognized by the ^{mcm5}UCU anticodon of the highly abundant tRNA^{Arg3}. Base pairing at the wobble positions of these two codons and ^{mcm5}U is also theoretically possible through N3-N3, 4-carbonyl-amino, and 2-carbonyl-N3, 4-carbonyl-N3 hydrogen bonding respectively (see Figure 3.2). Note that although there are three possible U•U base pairs and two possible C•U couples, the geometries of the N3-N3, 4-carbonyl-amino, and of the 2-carbonyl-N3, 4-carbonyl-N3 hydrogen pairing schemes provide the most energetically favorable topologies within the constraints of the tRNA:mRNA mini-helix. Further, it has been suggested that cmo⁵ modification of U₃₄ stabilizes the shape of the anticodon loop (reviewed in Agris et al., 2007). Although the C1'-C1' distance between pyrimidine-pyrimidine nucleotide pairs is

short, and is thus destabilizing relative to that for pyrimidine-purine base pairs, biophysical analyses suggest that bridging water molecules could produce stable and planar $U_{34}\bullet U3$ and $U_{34}\bullet C3$ base pairs (reviewed in Agris et al., 2007). Of note, although biophysical analyses of RNA duplexes indicate that $U\bullet U$ base-pairing is more stable than $U\bullet C$ pairs at pH 7.0, the observation that the AGC codon promoted > 2-fold more misreading than the AGU codon suggests that this particular $U\bullet C$ base pair is more energetically permissible within the topological constraints imposed by the codon:anticodon mini-helix structure. Examination of the UGU Cys codon also reveals that it can potentially base pair at all three positions with the ICG anticodon of tRNA^{Arg2}, which is encoded by 6 genes (Figure 3.2). Although $G_{36}\bullet U1$ pairing does not normally occur in cognate codon:anticodon interactions, this has been posited to occur at the P-site in *Ty1* promoted programmed +1 ribosomal frameshifting (Belcourt and Farabaugh, 1990). The lower abundance of this tRNA in combination with the less stable $G_{36}\bullet U1$ base pair at the first position of this pair may account for the lower frequency of misreading of this codon as compared to AGC Ser. tRNA modifications that facilitate wobble position interactions are present in both bacterial and eukaryotic systems, supporting the hypothesis that the formation of a mini-helix may be central for the ribosome to distinguish between near- and non-cognate interactions across the kingdoms. Kramer and Farabaugh also noted that misreading was enhanced in the presence of paromomycin for codons where there was potential for $U\bullet U$ base-pairing. However, the frequency of misreading varies between eukaryotes and bacteria indicating that other trans-acting factors or ribosomal components are involved. We extended our analysis to examine the effects of some of these factors.

Influence of eEF1A and associated elongation factors in translational fidelity

Because eEF1A delivers aa-tRNA to the ribosome and cognate codon:anticodon interactions stimulate its GTPase activity, mutants of this factor could alter translational fidelity in two ways. First, altered affinity for the ribosome could affect the initial binding step. Second, changes in intrinsic GTPase activity could affect aa-tRNA stimulation threshold. Because initial binding is independent of codon:anticodon interactions, mutants affecting the first step would be expected to alter fidelity in response to both near- and non-cognate codons. Since such an outcome was not observed for any of the eEF1A mutants, it is unlikely that any of the mutants affected initial binding rates. In contrast, since codon:anticodon interactions between near-cognate aa-tRNAs might be more likely to induce tRNA structural changes than those between non-cognate aa-tRNAs, eEF1A mutants with increased intrinsic GTPase activity or with decreased activation thresholds would more likely be stimulated by near-cognate as opposed to non-cognate aa-tRNAs. Similarly, those having decreased intrinsic GTPase activity or increased activation thresholds would be more discriminatory when presented with near-cognate aa-tRNAs.

Examination of the mutants within the context of the structure of the eEF1A•aa-tRNA•GTP modeled as the ternary complex provides some clues with regard to which mechanism may be altered in these mutants (Figure 3.5A). The charge reversal mutants in domain 2 proposed to be involved in binding the tRNA acceptor stem (E286K, E295K and E317K) all promoted enhanced misreading of the near-cognate AGC codon. It is tempting to speculate that these mutants may promote increased aa-tRNA dissociation rates by mimicking the structural change induced by correct tRNA:mRNA interactions

and subsequently stimulating the GTPase activity of eEF1A. In contrast, the T142I mutant in domain I that interacts with the phosphate backbone of residue 61 at the base of the D-loop was more discriminatory, suggesting that this interaction is important for stimulation of GTP hydrolysis. Mutants in the vicinity of the GTP binding pocket had allele-specific effects on incorporation of the near-cognate tRNA. Charge reversal or neutralization of E122K or D156N strongly stimulated misreading. Perhaps the presence of additional positive charge in this region enhances GTP binding and/or GTPase activity. In contrast, loss of a positive charge in the N153T mutant slightly inhibited misreading. Curiously, this effect was enhanced in the N153T/D156N double mutation. Last, mutations of E40 and D130 which are not closely linked to either tRNA or GTP binding did not affect missense suppression even though they were initially isolated as +1 insertion suppressor mutants. It is also striking that genetic screens have never identified fidelity mutations in domain 3, which is also proposed to interact with aa-tRNA. This suggests that these interactions are either non-essential or irrelevant to presentation at the A-site.

The K120R S121Δ I122Δ (KSI) mutant of eEF1B α (*tef5-7*) promoted increased accuracy in decoding both the ACG near- and UCU non-cognate codons. As noted above, mutants affecting fidelity in response to both near- and non-cognate codons are likely to be due to altered affinity at the initial binding step. Previous genetic analyses showed that this mutant also promoted increased fidelity at nonsense codons, slower rates of growth and protein synthesis, and hypersensitivity to translational inhibitors (Carr-Schmid et al., 1999). Figure 3.5B shows the X-ray crystal structure of eEF1A in complex with the catalytic terminus of eEF1B α . eEF1B α binds to domain I and II of eEF1A, where KSI

amino acids are located close to the nucleotide-binding pocket in domain 1 of eEF1A. The binding site of eEF1B α to domain II overlaps the proposed aa-tRNA binding site. This is significantly different from the bacterial homolog, and may be another way in which eukaryotes and bacteria differ in maintaining fidelity and promoting aa-tRNA delivery. We propose that these residues may facilitate exchange of GDP for GTP by eEF1A. Slowing this process would serve to limit the availability of functional ternary complexes, thus affecting binding of both near- and non-cognate codons. The effects of loss of eEF1B γ shows a general trend of enhanced accuracy of non-cognate codons like an eEF1B α mutant. However, the increased misreading of a near-cognate codon is more like an eEF1A mutant. Thus, although the precise function of eEF1B γ has yet to be determined, it is reasonable to hypothesize that it may modulate eEF1B α to affect fidelity.

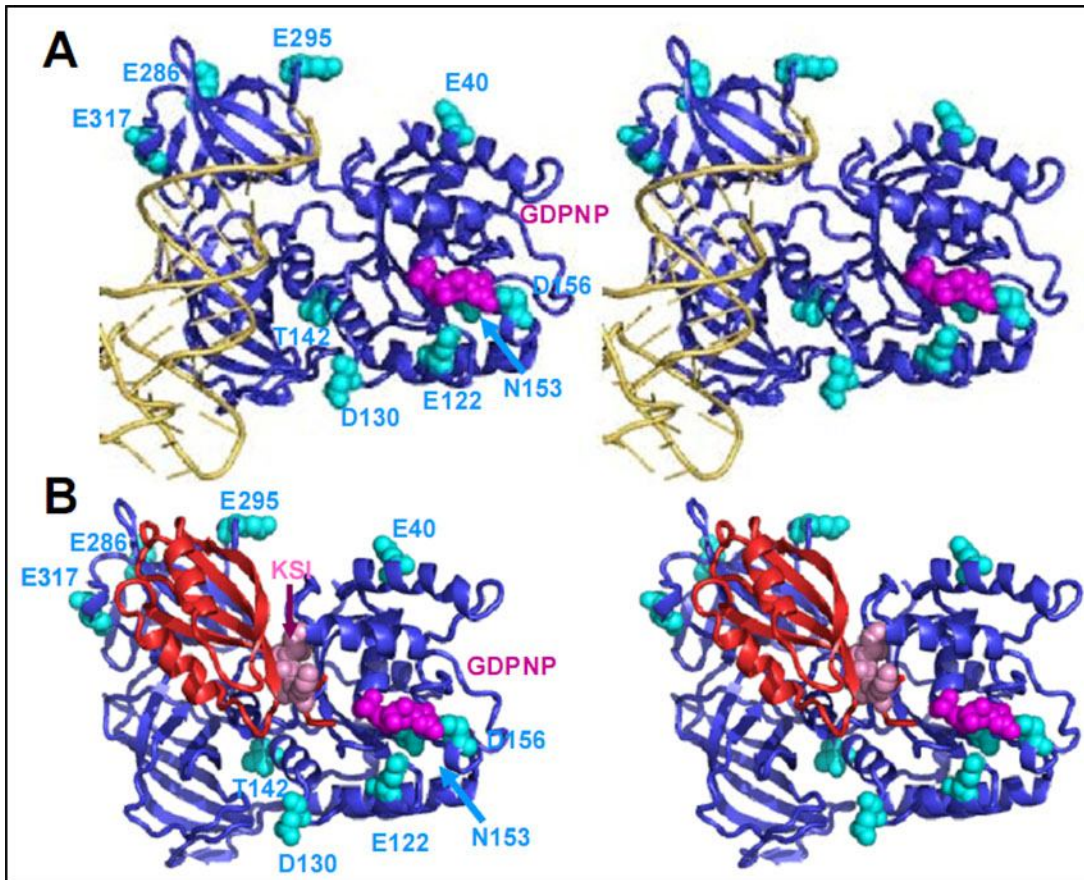


Figure 3.5: Modeling of mutations in eEF1A and eEF1B α that influence misincorporation of missense aa-tRNAs

The nucleotide exchange factor eEF1B α and the fitted aa-tRNA present clashes indicating that they do not interact with eEF1A simultaneously. Pymol (Delano Scientific, LLC) was used with the coordinates 1G7C of yeast eEF1A:eEF1B α (amino acids 114-206 in complex with GDPNP). The ribbon structure of eEF1A is shown in blue, eEF1A mutated baases are shown in cyan, and GDPNP is indicated in magenta. **Panel A:** tRNA (yellow) was fitted into the structure based on coordinates obtained from the crystal structure of the EF-Tu:Phe-tRNA^{Phe}:GDPNP complex (1TTT in the RCSN Protein Data Bank). **Panel B:** Ribbon structure of eEF1B α from 1G7C is shown in red, and the KSI residues in the mutant form used in this study are indicated in salmon.

Ribosomal protein L5: Coordination of tRNA exit from the E-site with aa-tRNA entrance at the A-site

The observation that the rpL5-K27E mutant generally promoted increased accuracy was initially surprising since this protein is located on the back of the central protuberance of the large subunit, far away from the ternary complex binding site, the ribosomal A-site, and the decoding center. In addition, a previous study implicated rpL5 in binding of peptidyl-tRNA, but not of aa-tRNAs (Meskauskas and Dinman, 2001). Nonetheless, the rpL5-K27E mutant generally promoted increased fidelity in response to almost all of the near- and non-cognate codons tested. An intriguing explanation for the allele-specific effects observed here may come from the observation that rpL5-L5 interacts with the fungal-specific elongation factor eEF3 (Andersen et al., 2006). eEF3 is an ATPase that interacts with eEF1A and catalyzes release of deacylated-tRNA from the ribosomal E-site (Triana-Alonso et al., 1995; Anand et al., 2002). It has been proposed that eEF3 and eEF1A work synergistically to remove deacylated tRNAs from the E-site and promote delivery of cognate aa-tRNA to the A-site. It is tempting to speculate that altered eEF3 binding to the K27E form of rpL5 upsets this synergy. Similar to the model proposed for the eEF1B α KSI mutant, the rpL5-K27E mutant might promote enhanced accuracy at the codon recognition step.

It should also be noted that a previous study also used a dual luciferase reporter system to examine missense suppression in yeast (Salas-Marco and Bedwell, 2005). The analyses applied in the current study cannot be directly applied to the data generated by Salas-Marco and Bedwell since that work employed eight different codons at two

positions of firefly luciferase. Since most were non-synonymous, the effects of different amino acid substitutions and their specific locations on the activity of the enzyme cannot be controlled for. Since different strain backgrounds are used in the studies and even in different sets of mutants analyzed in this work, variations in wild-type values observed requires the use of specific statistical methodology for accurate comparisons between datasets (Jacobs and Dinman, 2004). Further, relative tRNA abundance issues complicated the two instances where synonymous codons were used. Despite these differences, independent analyses, reporter constructs and strain backgrounds showed similar levels of misreading. Furthermore, specific effects on misreading were observed for mutants of ribosomal components and key factors involved in elongation and termination. These data support the universal application of this approach to studies of translational fidelity.

Kinetics: the difference between near- and non-cognate interactions may occur at the GTPase activation step

As described above, studies in the bacterial system shows accuracy during translation elongation is likely a two step process involving two distinct biophysical mechanisms: initial selection and proofreading (reviewed in Ogle and Ramakrishnan, 2005; Rodnina et al., 2005). The first step, initial binding, is mostly determined by the interaction between the ribosome and EF-Tu, and forward and reverse rates (k_1 and k_{-1}) are not affected by aa-tRNA identity (Daviter et al., 2006). However, during the next step of codon recognition, the stabilizing effects due to interactions of G530, A1492 and A1493 with the mini-helix results in dissociation rates (k_2) of near-cognate aa-tRNAs being approximately 400-fold than those of cognate aa-tRNAs (Gromadski et al., 2006).

Computational modeling suggests the existence of two major energy minima at the decoding center corresponding to the flipped-in and flipped-out conformations of A1492, and A1493, and that fast flipping between the two states provides a kinetic means to discriminate at the level of codon:anticodon interactions (Sanbonmatsu, 2006).

Formation of the stable mini-helix results in the physical transduction of information to the ternary complex, thus activating the endogenous GTPase of EF-Tu (k_3). This step acts as a kinetic trap to select for aa-tRNAs capable of forming the mini-helix. We propose that it is here that the difference between near- and non-cognate tRNA:mRNA interactions also occurs in eukaryotes. The potential of near-cognate interactions to form mini-helices, albeit at lower frequencies, provides the opportunity for stimulation of GTPase activation. The data also suggest that the presence of a canonical Watson-Crick base pair between $N_{35} \cdot N'2$ may aid in nucleating mini-helix formation, consistent with molecular dynamics modeling showing that stability testing by the kink in the mRNA between the P- and A-site codons destabilizes position 2 mismatches more severely than mismatches at the first position (Sanbonmatsu and Joseph, 2003). In contrast, non-cognate interactions cannot possibly form mini-helices, and thus are incapable of forming the kinetic trap and activating GTP hydrolysis. In a kinetic analysis comparing different codon:anticodon mismatches, one tRNA capable of participating in a non-cognate interaction was employed and stimulated GTPase activation approximately 6.7 fold less than the near-cognate codons (Gromadski et al., 2006). This is consistent with the ~ 4.5 fold increased rates of misreading promoted by near-cognate codons in the current study.

Using Paromomycin to functionally distinguish between 'near-' and 'non-cognate' codon:anticodon interactions

Binding of cognate aa-tRNA stimulates rearrangement of G530, A1492, and A1493 to establish A-minor interactions between themselves and the minor groove of the codon-anticodon helix (Ogle et al., 2002; Ogle et al., 2001). Binding of paromomycin to the decoding center stimulates similar displacement of A1492 and A1493, positioning them to stabilize codon:anticodon interactions in a promiscuous manner (Carter et al., 2000), perhaps trapping them in the flipped-out state (Sanbonmatsu, 2006). In light of the data presented here, we suggest that mini-helix formation is a precondition for paromomycin-stimulated misreading. Furthermore, paromomycin-enhanced and the potential for mini-helix formation are coordinately maximized in the decoding center. Thus, paromomycin has the potential to be used as a tool to functionally distinguish between 'near-' and 'non-cognate' codons. However, this requires expansion of the system to utilize other codons for which the encoded amino acids do not result in a partially active luciferase protein. Kramer and Farabaugh observed changes in misreading with two different aminoglycosides, paromomycin and streptomycin (Kramer and Farabaugh, 2007). Although more information about aminoglycoside-ribosome interactions has recently become available (reviewed in Hobbie et al., 2006) more experimental work needs to be performed to determine if any aminoglycosides other than paromomycin may be better sensors of cognate status.

Table 3.4: Yeast strains used in this study

Strain	Genotype	Source
JD932D	<i>MATa ade 2-1 trp1-1 ura3-1 leu2-3,112 his3-11,15 can1-100</i> [L-AHN M ₁]	Tumer et al., 1998
M213	<i>MATa leu2-3,112 his4-713 ura3-52 trp1Δ lys2-20 met2-1 tef2Δ tef1::LEU2 + pTEF2</i>	Sandbaken & Culbertson, 1988
TKY111	<i>MATa leu2-3,112 his4-713 ura3-52 trp1Δ lys2-20 met2-1 tef2Δ tef1::LEU2 + pTEF2-2 E317K</i>	Dinman and Kinzy, 1997
TKY112	<i>MATa leu2-3,112 his4-713 ura3-52 trp1Δ lys2-20 met2-1 tef2Δ tef1::LEU2 + pTEF2-3 E40K</i>	Dinman and Kinzy, 1997
TKY113	<i>MATa leu2-3,112 his4-713 ura3-52 trp1Δ lys2-20 met2-1 tef2Δ tef1::LEU2 + pTEF2-4 E122K</i>	Dinman and Kinzy, 1997
TKY114	<i>MATa leu2-3,112 his4-713 ura3-52 trp1Δ lys2-20 met2-1 tef2Δ tef1::LEU2 + pTEF2-7 T142I</i>	Dinman and Kinzy, 1997
TKY115	<i>MATa leu2-3,112 his4-713 ura3-52 trp1Δ lys2-20 met2-1 tef2Δ tef1::LEU2 + pTEF2-9 E296K</i>	Dinman and Kinzy, 1997
TKY116	<i>MATa leu2-3,112 his4-713 ura3-52 trp1Δ lys2-20 met2-1 tef2Δ tef1::LEU2 + pTEF2-10 E122Q</i>	Dinman and Kinzy, 1997
TKY117	<i>MATa leu2-3,112 his4-713 ura3-52 trp1Δ lys2-20 met2-1 tef2Δ tef1::LEU2 + pTEF2-13 D130N</i>	Dinman and Kinzy, 1997
TKY278	<i>MATa leu2-3,112 his4-713 ura3-52 trp1Δ lys2-20 met2-1 tef2Δ tef1::LEU2 + pTEF2-17 D156N</i>	Carr-Schmid et al., 1999
TKY280	<i>MATa leu2-3,112 his4-713 ura3-52 trp1Δ lys2-20 met2-1 tef2Δ tef1::LEU2 + pTEF2-19 N153T</i>	Carr-Schmid et al., 1999
TKY282	<i>MATa leu2-3,112 his4-713 ura3-52 trp1Δ lys2-20 met2-1 tef2Δ tef1::LEU2 + pTEF2-18 N153T D156E</i>	Carr-Schmid et al., 1999
TKY539	<i>MATa leu2-3,112 his4-713 ura3-52 trp1Δ lys2-20 met2-1 tef2Δ tef1::LEU2 + pTEF2-1 E286K</i>	This work
TKY677	<i>MATa ura3-52 trp1Δ101 lys2-801 his3Δ200 leu2Δ1</i>	Olarewaju et al., 2004

Table 3.4 (continued): Yeast strains used in this study

TKY678	<i>MATa ura3-52 trp1 Δ101 lys2-801 his3Δ200 leu2Δ1 tef3::LEU2</i>	Olarewaju et al., 2004
TKY679	<i>MATa ura3-52 trp1 Δ101 lys2-80 his3Δ200 leu2Δ1 tef4::TRP1</i>	Olarewaju et al., 2004
TKY680	<i>MATa ura3-52 trp1 Δ101 lys2-801 his3Δ200 leu2Δ1 tef3::LEU2 tef4::TRP1</i>	Olarewaju et al., 2004
TKY235	<i>MATα ura3-52 trp1 Δ101 lys2-801 leu2Δ1 met2-1 his4-713 tef5::TRP1 pTEF5 URA3</i>	Carr-Schmid et al., 1999
TKY243	<i>MATα ura3-52 trp1 Δ101 lys2-801 leu2Δ1 met2-1 his4-713 tef5::TRP1 pTEF5-7 K120R S121Δ I22Δ</i>	Carr-Schmid et al., 1999
JWY3742	<i>MATα ura3-52 trp1-Δ101 leu2 his3-Δ200 ade1 rpl5-Δ1::TRP1 + pRS315-RPL1-HA (RPL5)</i>	Deshmukh et al., 1995
JWY3750	<i>MATα ura3-52 trp1-Δ101 leu2 his3-Δ200 ade1 rpl5-Δ1::TRP1 + pRS315-RPL1-HA-1 (rpl5- K27E)</i>	Deshmukh et al., 1995
JWY3751	<i>MATα ura3-52 trp1-Δ101 leu2 his3-Δ200 ade1 rpl5-Δ1::TRP1 + pRS315-RPL1-HA-2 (rpl5-T28A)</i>	Deshmukh et al., 1995
JWY3749	<i>MATα ura3-52 trp1-Δ101 leu2 his3-Δ200 ade1 rpl5-Δ1::TRP1 + pRS315-RPL1-HA-3 (rpl5-V53G)</i>	Deshmukh et al., 1995
JWY3752	<i>MATα ura3-52 trp1-Δ101 leu2 his3-Δ200 ade1 rpl5-Δ1::TRP1 + pRS315-RPL1-HA-4 (rpl5-G91R)</i>	Deshmukh et al., 1995
JWY3761	<i>MATα ura3-52 trp1-Δ101 leu2 his3-Δ200 ade1 rpl5-Δ1::TRP1 + pRS315-RPL1-HA-5 (rpl5-K289E)</i>	Deshmukh et al., 1995

Chapter 4: Conclusions and future directions

Introduction

The ribosome is a complex nanomachine with many parts functioning together to perform a vital function in the cell. Understanding how the ribosome works necessitates learning how individual ingrained components of the ribosome as well as many transient associated factors contribute to translation. Exploration of various aspects of translational fidelity provides a series of lenses with which to examine the ribosome and changes in its functions as mutational changes are made in its components. At the same time, highly resolved crystal structures and increasingly informative cryo-Electron microscopy (cryo-EM) images are allowing improved analysis of ribosome structure and how changes in structure might connect to experimentally observed changes in translational fidelity.

The extension and tip of ribosomal protein L2

Ribosomal protein L2 is an integral protein in the ribosome due to both myriad 25s rRNA contacts and as a requirement for peptidyl transfer. Further mutational analysis of L2 will provide more information on its specific contributions to the ribosome structurally and functionally. This study has revealed a few specific mutations of L2 that warrant further study, and has also indicated specific regions of the protein important for its role in the ribosome.

The tip of L2 that extends furthest into the functional center of the ribosome is the most obvious candidate for further study. Until the yeast ribosome is crystallized, it is difficult to be certain of which residues are responsible for this contact with helix 93 of 25s rRNA. However, the high conservation of this region of L2 between yeast and other organisms for which crystals have been developed (*H. marismortui* in particular), provides reasonable confidence that appropriate residues are targeted. Mutations N214S, H215Y, and I218N are located in this tip of L2 and were assayed for their impact on general growth characteristics as well as various aspects of translation and fidelity (Figure 4.1). These mutations had a variety of impacts on the ribosome including Sparsomycin and Anisomycin resistance (H215Y), unchecked growth (N214S), and changes in misincorporation and nonsense suppression (I218N). These phenotypes highlight the importance of this region in maintaining the structure and function of the peptidyl transferase center, the catalytic core of the ribosome. Further work on these mutations will include measurement of A-site and P-site tRNA binding, and measurement of peptidyl transfer rates. Further work on this region should include saturating specific residues with all possible mutations, exploring which amino acid properties are responsible for maintaining optimal ribosome function. As structural data for eukaryotic ribosomes becomes more precise, it will be easier to confidently select residues impacting the structure of the peptidyl transferase center for mutation. Until then, a random saturation mutagenesis of just the tip region of L2 should produce sufficient viable mutations across the spectrum of amino acid conservation to understand the impact of this region on the ribosome.

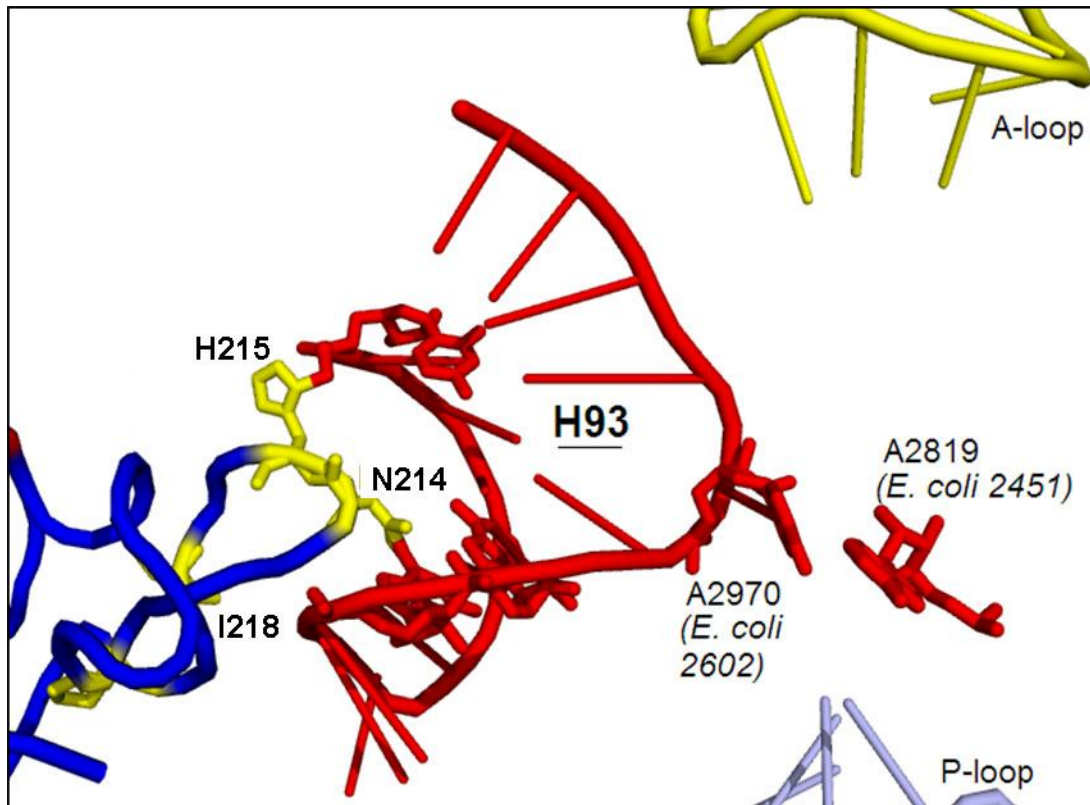


Figure 4.1: Mutated residues in the tip of L2

The locations of 3 residues at the tip of L2 that were mutated as N214S, H215Y, and I218N. This region of contact with helix 93 of the 25S rRNA is positioned to greatly impact the peptidyl transferase center. The A and P-loop rRNA elements and the conserved A2819 (2451 in *E. coli*), often thought to be involved in peptide transfer catalysis, are labeled for reference. Helix 93 is in red, and the highly conserved flipped out Adenine (2970, 2602 in *E. coli*) is labeled. RCSB protein database entry 1S1I was created by fitting *H. marismortui* crystal structure data into *S. cerevisiae* cryo-EM maps.

Other mutations in ribosomal protein L2

Several mutations yielded interesting results and demand further study though their reason for impact is more difficult to assess than those mutations in the very tip of L2. Alterations in the globular domain and the bridge region of ribosomal protein L2 provided multiple interesting results, including some severe phenotypes. For various

reasons, saturating mutagenesis of these regions may not be appropriate, but several individual mutations already created do warrant further study.

Two mutations from the highly structured globular domain of the protein generated both anisomycin resistance and aberrant polysome profiles. These mutations, V48D and L125Q, appear to cause a 60S biogenesis defect that manifests as a growth limitation as seen in dilution spots and growth curves and extreme half-mer defects in polysome profiles. As an integral protein incorporated into the ribosome early in biogenesis, disruption of the globular domain structure might affect ribosome biogenesis. A decrease in the ratio of free 60S to 40S subunits is apparent in the polysome profiles and supports the idea of the half-mer formation due to poor 60S biogenesis rather than a subunit joining defect. While neither residue is conserved (Figure 4.2), they are located near regions well conserved between *Haloarcula marismortui* and *Saccharomyces cerevisiae* and changes possibly disrupt the structure and biogenesis of the ribosome. The anisomycin resistance phenotype for these mutants is more surprising but could be attributed to a distal structural change of the PTC site where anisomycin and incoming aminoacyl-tRNAs bind. These strains could also be tested for aminoacyl-tRNA binding to provide more information for why they might show anisomycin resistance.

Another couple of mutations in the middle 'bridge' region of L2 that yielded some interesting phenotypes were F185L and W195C. These mutations are in close proximity to each other as F185 is near the end of an independent loop of amino acids that extends out from the globular domain (Figure 2.6) that brings it close to the area of W195. Interestingly, both of these mutations caused hyperaccuracy in both near- and non-cognate misincorporation studies (Figure 2.13). This indicates a potential distal

connection via 25S rRNA to the A-site side of the PTC and the channel through which aa-tRNA passes during accommodation.



Figure 4.2: Alignment of L2 from *S. cerevisiae* and *H. marismortui*

Interesting mutations made in this study are indicated in red in this clustalW alignment. Many of the mutations are at marginally conserved residues in the protein, but are often directly adjacent to well conserved features of L2. Symbols below each position indicate identical residues (*), conserved substitutions (:), or semi-conserved (.) substitutions.

An intersubunit bridge in L2

The final mutation with an interesting phenotype was G172C. This residue is just outside of the globular domain in a conserved run of glycines. This mutation was the only strain to provide any indication of paromomycin sensitivity but showed no other

phenotypes of those tested. A mutation in a run of glycines can easily impact regional structural features by introducing a larger side chain than is normally accommodated. While the exact location of the potential intersubunit bridge in L2 is unknown, the paromomycin phenotype could indicate a connection between the bridge and this region of the protein as paromomycin binds at the A-site decoding center on the small subunit of the ribosome. Understanding the location of an intersubunit bridge in yeast ribosomal protein L2 could have exciting potential for study and mutagenesis. If precisely identified in *S. cerevisiae*, this intersubunit connection could prove to impact translocation as tethering of the *E. coli* version of the intersubunit bridge was recently used to prove that intersubunit movement was necessary for translocation (Horan and Noller, 2007).

Significance of near- and non-cognate tRNA differentiation

Understanding the structural basis of how the ribosome distinguishes between cognate, near-cognate, and non-cognate tRNAs is important for development of therapeutic strategies for many human diseases. In a disease such as sickle cell anemia, which is caused by a missense mutation in the β -globin gene, the ribosome might be stimulated to misincorporate the 'incorrect' tRNA at the site of the missense mutation. A small percentage increase in proper β -globin production due to misincorporation at the missense mutation site might prove therapeutic to patients. Distinguishing differences between near- and non-cognate tRNAs would allow specific therapeutics that only affect one type of misincorporation at a time depending on what is necessary.

Misincorporation of tRNA and ribosome structure

Studying the structural implications of tRNA binding to the a-site has elucidated differences between near- and non-cognate tRNA interactions. Particularly, the potential for near-cognate tRNAs to form mini-helical structures with the A-site codon at the decoding center (Figure 3.2), provides a structural and functional difference between near- and non-cognate tRNA. Differences between near- and non-cognate tRNAs were observed in misincorporation studies using the aminoglycoside paromomycin, and in deletions of an accessory elongation factor eEF1B γ .

Many opportunities to study misincorporation and the structure and function of the ribosome are available as more and more networks of distal information transduction are uncovered. Such a distal interaction was demonstrated in the study of ribosomal protein L5. The protein connects from a far distance to the GTPase associated center through 5S rRNA, and still managed to have a significant impact as mutation K27E generated hyperaccuracy in both near- and non-cognate misincorporation studies. Understanding the complex networks of communication between integral ribosome elements as well as accessory translation factors is a large challenge. However, the mutational studies of ribosomal proteins L2 and L5 and elongation factors eEF1A, eEF1B α , and eEF1B γ already successfully demonstrate both direct and indirect effects on tRNA misincorporation. Further study of these and other elements combined with improving visualization of the eukaryotic ribosome will continue to provide more explanation for the mechanism tRNA recognition by the ribosome, and how it relates to the complex structure of the ribosome.

Appendix A: L2 mutation strains generated

Appendix A: L2 mutation strains generated				
All strain background characteristics are as in JD1315 with changes in the rpl2A ORF (MAT α his3 Δ 1 leu2 Δ 0 met15 Δ 0 ura3 Δ 0 rpl2b::KANR rpl2a::KANR + rpl2A in pRS315 K+)				
Strain Name	Nucleotide Change	Codon Change	Amino Acid Change	Source
JD1315.25	G164A	CGT-CAT	R5H	RM*
JD1315.6	C182A	GCT-GAT	A11D	SDM**
JD1315.18	T293A	GTC-GAC	V48D	RM
JD1315.16	T524A	CTA-CAA	L125Q	RM
JD1315.23	C599A	CCA-CAA	P150Q	RM
JD1315.5	G664T	GGT-TGT	G172C	SDM
JD1315.1	T703C	TTC-CTC	F185L	SDM
JD1315.3	G735C	TGG-TGC	W195C	SDM
JD1315.4	A740T	AAG-ATG	K197M	SDM
JD1315.7	A742T	ACC-TCC	T198S	SDM
JD1315.10	C776G	CCT-CGT	P209R	SDM
JD1315.41	A791G	AAC-AGC	N214S	RM
JD1315.20	C793T	CAT-TAT	H215Y	RM
JD1315.2	T803A	ATT-AAT	I218N	SDM
JD1315.8	C812T	GCT-GTT	A221V	SDM
JD1315.11	A828T	AGA-AGT	R226S	SDM
JD1315.40	G298A	GAC-AAC	D50N	RM
	G711T	AAG-AAT	K187N	RM
JD1315.39	A490T	AAC-TAC	N114Y	RM
	A610G	AAG-GAG	K154E	RM
JD1315.47	T601A	TCC-ACC	S151T	RM
	C793A	CAT-AAT	H215N	RM

Appendix A: L2 mutation strains generated (continued)				
Strain Name	Nucleotide Change	Codon Change	Amino Acid Change	Source
JD1315.14	G605A	GGT-GAT	G152D	RM
	G664T	GGT-TGT	G172C	RM
JD1315.24	G659A	GGT-GAT	G170D	RM
	T856A	TTG-ATG	L236M	RM
JD1315.34	A713G	TAC-TGC	Y188C	RM
	C833A	GCT-GAT	A228D	RM
JD1315.27	G164C	CGT-CCT	R5P	RM
	C239T	ACT-ATT	T30I	RM
	G400A	GGT-AGT	G84S	RM
JD1315.46	G164T	CGT-CTT	R5L	RM
	A395G	CAC-CGC	H82R	RM
	C812T	GCT-GTT	A221V	RM
JD1315.21	A166T	AAC-TAC	N6Y	RM
	A368T	GAA-GTA	E73V	RM
	G511T	GAC-TAC	D121V	RM
JD1315.31	A205T	ACC-TCC	T19S	RM
	A512C	GAC-GCC	D121A	RM
	A846T	CAA-CAT	Q232H	RM
JD1315.43	C224T	GCT-GTT	A25V	RM
	G475T	GGT-TGT	G109C	RM
	A740G	AAG-AGT	K197S	RM
	G741T			
JD1315.17	T242C	TTG-TCG	L31S	RM
	A255T	GAA-GAT	E35D	RM
	G559T	GGT-TGT	G137C	RM

Appendix A: L2 mutation strains generated (continued)				
Strain Name	Nucleotide Change	Codon Change	Amino Acid Change	Source
JD1315.26	G280C	GTT-CTT	V44L	RM
	G835A	GTT-ATT	V229I	RM
	G912T	TAG-TAT	YIMY ext.	RM
JD1315.29	A287G	CAA-CGA	Q46R	RM
	G508A	GGT-AGT	G120S	RM
	A611G	AAG-AGG	G154R	RM
JD1315.33	T377A	ATT-AAT	I76N	RM
	C776T	CCT-CTT	P209L	RM
	G912T	TAG-TAT	YIMY ext.	RM
JD1315.13	A422T	AAG-ATG	K91M	RM
	G735C	TGG-TGC	W195C	RM
	A740T	AAG-ATG	K197M	RM
JD1315.19	A490T	AAC-TAC	N114Y	RM
	A742T	ACC-TCC	T198S	RM
	C812T	GCT-GTT	A221V	RM
JD1315.38	G582C	AAG-AAC	K144N	RM
	C776G	CCT-CGT	P209R	RM
	A828T	AGA-AGT	R226S	RM
JD1315.42	A722C	AAG-ACG	K191T	RM
	A740T	AAG-ATG	K197M	RM
	G789T	GGT-TGT	G213C	RM
JD1315.45	C188T	TCT-TTT	S13F	RM
	G263C	GGT-GCT	G38A	RM
	A619T	ATC-TTC	I157F	RM
	A797T	CAA-CTA	Q216L	RM

Appendix A: L2 mutation strains generated (continued)				
Strain Name	Nucleotide Change	Codon Change	Amino Acid Change	Source
JD1315.22	T212C	TTG-TCT	L21S	RM
	T233C	TTG-TCG	L28S	RM
	A296G	CAC-CGC	H49R	RM
	A899G	AAG-AGG	H250R	RM
JD1315.35	C224T	GCT-GTT	A25V	RM
	T278A	ATC-AAC	I43N	RM
	A580G	AAG-GAG	K144E	RM
	G832T	GCT-ACT	A228T	RM
JD1315.30	C224T	GCT-GTT	A25V	RM
	T551A	ATT-AAT	I134N	RM
	A566G	AAC-AGC	N139S	RM
	G664A	GGT-AGT	G172S.	RM
JD1315.32	A248G	TAT-TGT	Y33C	RM
	G305A	GGT-GAT	G52D.	RM
	G628T	GAT-TAT	D160Y	RM
	A896T	CAA-CTA	Q249L	RM
JD1315.44	G328C	GTT-CTT	V60L:	RM
	T407G	TTC-TGC	F86C	RM
	A425T	AAG-ATG	K92M	RM
	G907T	GAT-TAT	D253Y	RM
JD1315.12	T377A	ATT-AAT	I76N	RM
	A572T	GAC-GTC	D141V	RM
	T703C	TTC-CTC	F185L	RM
	T803A	ATT-AAT	I218N	RM

Appendix A: L2 mutation strains generated (continued)				
Strain Name	Nucleotide Change	Codon Change	Amino Acid Change	Source
JD1315.36	C470G	CCA-CGA	P107R	RM
	A674G	GAC-GGC	D175G	RM
	T814C	TCT-CCT	S222P	RM
	T844C	TTA-TCA	L245S	RM
JD1315.15	C182A	GCT-GAT	A11D	RM
	G220A	GGT-AGT	G24S	RM
	C251G	GCT-GGT	A34G	RM
	G415A	GCC-ACC	A89T	RM
	G560A	GGT-GAT	G137D	RM
JD1315.28	G215T	AGA-ATA	R22I	RM
	A397G	ACT-TCT	T83S	RM
	A436G	AAC-GAC	N86D	RM
	G461A	GGT-GAT	G104D	RM
	T551C	ATT-ACT	I134T	RM
JD1315.37	A167T	AAC-ATC	N6I	RM
	A307G	AGA-GGA	R53G	RM
	G331A	GTC-ATC	V61I	RM
	A566T	AAC-ATC	N139I	RM
	A828T	AGA-AGT	R226S	RM
	G830A	GGT-GAT	G227D	RM
*RM = Random Mutagenesis, **SDM = Site Directed Mutagenesis				

Appendix B: Primers used in L2 study

Appendix B: List of oligonucleotide primers used in L2 study		
Non-homologous bases are lower case, added restriction sites are in italics.		
Name	Sequence	Purpose
RPL2A5F	5'-g <i>gaat</i> TCCAGCAGCATTGGCAGAG-3'	5'UTR Forward
RPL2A5R	5'-g <i>ggatcc</i> GGTTTCTTAGTTTGCTCAGAAATG G-3'	5'UTR Reverse
RPL2AOF	5'-g <i>ggat</i> CCATTAGATCAATAAGCAATGG-3'	ORF Forward
RPL2AOR	5'-g <i>actag</i> TACATAATCTAATCTTGGGTC-3'	ORF Reverse
RPL2A3F	5'-g <i>acta</i> GTAAAATAGTCATTCTTTAAGCAAG- 3'	3'UTR Forward
RPL2A3R	5'-g <i>ccgcgg</i> AACGCGTAAGGCAGAAAG-3'	3'UTR Reverse
RPL2AExtF	5'-CCCTCCTTCAATATCATTACCTCGT-3'	5' external sequencing
RPL2AExtR	5'-CTCCATGAAGCAATGCTTCACAG-3'	3' external sequencing
RPL2AIntF	5'-CCACACCAGATTGAGACAAGGT-3'	5' internal sequencing
RPL2AIntR	5'-ACCTTGCTCAATCTGGTGTGG-3'	3' internal sequencing
RPL2ARMF	5'-TTTAGCGACTAATAACCATTCTGAGC-3'	RM* - Forward
RPL2ARMR	5'-GTGTTATGTTATATTGTATTGTTTGCTTT GAGG-3'	RM - Reverse
A11D-S	5'-CGTAACCAAAGAAAGGGTGATGGTTCTA TCTTTACCTCC-3'	SDM**A11D - Forward
A11D-A	5'-GGAGGTAAAGATAGAACCATCACCCTTT CTTTGGTTACG-3'	SDM A11D - Reverse
G172C-S	5'-GTGTCATTGCCGGTGGTTGTAGAGTTGAC AAACC-3'	SDM G172C - Forward
G172C-A	5'-GGTTTGTCAACTCTACAACCACCGGCAAT GACAC-3'	SDM G172C - Reverse
F185L-S	5'-GAAGGCTGGTCGTGCTTTGCACAAGTACA GATTG-3'	SDM F185L - Forward

Appendix B: List of oligonucleotide primers used in L2 study (continued)		
Name	Sequence	Purpose
F185L-A	5'-CAATCTGTACTTGTGCAAAGCACGACCAG CCTTC-3'	SDM F185L - Reverse
W195C-S	5'-GAGGGAAGAGAAACTCTTGTCCAAAGAC CCGTGGTG-3'	SDM W195C - Forward
W195C-A	5'-CACCACGGGTCTTTGGACAAGAGTTTCTC TTCAATC-3'	SDM W195C - Reverse
K197M-S	5'-GAAACTCTTGGCCAATGACCCGTGGTGTT GC-3'	SDM K197M - Forward
K197M-A	5'-GCAACACCACGGGTCATTGGCCAAGAGTT TC-3'	SDM K197M - Reverse
T198S-S	5'-GAAACTCTTGGCCAAAGTCCCCTGGTGTT GC-3'	SDM T198S - Forward
T198S-A	5'-GCAACACCACGGGACTTTGGCCAAGAGTT TC-3'	SDM T198S - Reverse
P209R-S	5'-GAATCCAGTTGATCACCGTCACGGTGGTG GT-3'	SDM P209R - Forward
P209R-A	5'-ACCACCACCGTGACGGTGATCAACTGGAT TC-3'	SDM P209R - Reverse
I218N-S	5'-GGTGGTAACCATCAACATAATGGTAAGGC TTCTACCATC-3'	SDM I218N - Forward
I218N-A	5'-GATGGTAGAAGCCTTACCATTATGTTGAT GGTTACCACC-3'	SDM I218N - Reverse
A221V-S	5'-CATCAACATATTGGTAAGGTTTCTACCAT CTCTAGAGGTGC-3'	SDM A221V - Forward
A221V-A	5'-GCACCTCTAGAGATGGTAGAAACCTTACC AATATGTTGATG-3'	SDM A221V - Reverse
R226S-S	5'-GCTTCTACCATCTCTAGTGGTGCTGTTTCT GGTC-3'	SDM R226S - Forward
R226S-A	5'-GACCAGAAACAGCACCCTAGAGATGGT AGAAGC-3'	SDM R226S - Reverse
*RM=Random Mutagenesis, **SDM=Site Directed Mutagenesis		

Reference list

- Agrawal RK, Heagle AB, Penczek P, Grassucci RA, Frank J (1999) EF-G-dependent GTP hydrolysis induces translocation accompanied by large conformational changes in the 70S ribosome. *Nature Structural Biology* 6: 643-647.
- Agris PF (1991) Wobble position modified nucleosides evolved to select transfer RNA codon recognition: a modified-wobble hypothesis. *Biochimie* 73: 1345-1349.
- Agris PF, Vendeix FA, Graham WD (2007) tRNA's wobble decoding of the genome: 40 years of modification. *J Mol Biol* 366: 1-13.
- Anand M, Chakraborty K, Marton MJ, Hinnebusch AG, Kinzy TG (2002) Functional interactions between yeast translation elongation factors eEF1A and eEF3. *J Biol Chem* 278: 6985-6991.
- Anand M, Valente L, Carr-Schmid A, Munshi R, Olarewaju O, Ortiz PA, Kinzy TG (2001) Translation elongation factor 1 functions in the yeast *Saccharomyces cerevisiae*. *Cold Spring Harb Symp Quant Biol* 66:439-48.
- Andersen CB, Becker T, Blau M, Anand M, Halic M, Balar B, Mielke T, Boesen T, Pedersen JS, Spahn CM, Kinzy TG, Andersen GR, Beckmann R (2006) Structure of eEF3 and the mechanism of transfer RNA release from the E-site. *Nature* 443: 663-668.
- Andersen GR, Pedersen L, Valente L, Chatterjee I, Kinzy TG, Kjeldgaard M, Nyborg J (2000) Structural basis for nucleotide exchange and competition with

- tRNA in the yeast elongation factor complex eEF1A:eEF1B α . *Mol Cell* 6: 1261-1266.
- Andersen GR, Valente L, Pedersen L, Kinzy TG, Nyborg J (2001) Crystal structures of nucleotide exchange intermediates in the eEF1A- eEF1B α complex. *Nat Struct Biol* 8: 531-534.
- Ban N, Nissen P, Hansen J, Moore PB, Steitz TA (2000) The complete atomic structure of the large ribosomal subunit at 2.4 Å resolution. *Science* 289: 905-920.
- Beier H and Grimm M (2001) Misreading of termination codons in eukaryotes by natural nonsense suppressor tRNAs. *Nucleic Acids Res* 29: 4767-4782.
- Belcourt MF, Farabaugh PJ (1990) Ribosomal frameshifting in the yeast retrotransposon Ty: tRNAs induce slippage on a 7 nucleotide minimal site. *Cell* 62: 339-352.
- Bouadloun F, Donner D, Kurland CG (1983) Codon-specific missense errors in vivo. *EMBO J* 2: 1351-1356.
- Brachmann CB, Davies A, Cost GJ, Caputo E, Li J, Hieter P, and Boeke JD (1998) Designer deletion strains derives from *Saccharomyces cerevisiae* S288C; a useful set of strains and plasmids for PCR-mediated gene disruption and other applications. *Yeast*. 14: 115-132.
- Carr-Schmid A, Durko N, Cavallius J, Merrick WC, Kinzy TG (1999) Mutations in a GTP-binding motif of eukaryotic elongation factor 1A reduce both translational fidelity and the requirement for nucleotide exchange. *J Biol Chem* 274: 30297-30302.

- Carr-Schmid A, Valente L, Loik VI, Williams T, Starita LM, Kinzy TG (1999) Mutations in elongation factor 1beta, a guanine nucleotide exchange factor, enhance translational fidelity. *Mol Cell Biol* 19: 5257-5266.
- Carter AP, Clemons WM, Brodersen DE, Morgan-Warren RJ, Wimberly BT, Ramakrishnan V (2000) Functional insights from the structure of the 30S ribosomal subunit and its interactions with antibiotics. *Nature* 407: 340-348.
- Christianson TW, Sikorski RS, Dante M, Shero JH, Hieter P (1992) Multifunctional yeast high-copy-number shuttle vectors. *Yeast* 110: 119-122.
- Cochella L, Brunelle JL, Green R (2007) Mutational analysis reveals two independent molecular requirements during transfer RNA selection on the ribosome. *Nat Struct Mol Biol* 14: 30-36.
- Cochella L, Green R (2005) Fidelity in protein synthesis. *Curr Biol* 15: R536-R540.
- Cooperman BS, Wooten T, Romero DP, and Traut RR (1995) Histidine 229 in protein L2 is apparently essential for 50s peptidyl transferase activity. *Biochem Cell Biol* 73: 1087-1094.
- Craig AW, Haghghat A, Yu AT, Sonenberg N (1998) Interaction of polyadenylate-binding protein with the eIF4G homologue PAIP enhances translation. *Nature* 392: 520-523.
- Crick FHC (1966) Codon-Anticodon Pairing - Wobble Hypothesis. *Journal of Molecular Biology* 19: 548-555.

- Daviter T, Gromadski KB, Rodnina MV (2006) The ribosome's response to codon-anticodon mismatches. *Biochimie* 88: 1001-1011.
- DeLano WL (2002) The PyMOL Molecular Graphics System, www.pymol.org
- Deshmukh M, Stark J, Yeh LC, Lee JC, Woolford JL, Jr. (1995) Multiple regions of yeast ribosomal protein L1 are important for its interaction with 5 S rRNA and assembly into ribosomes. *J Biol Chem* 270: 30148-30156.
- Diedrich G, Spahn CM, Stelzl U, Schafer MA, Wooten T, Bochkariov DE, Cooperman BS, Traut RR, and Nierhaus KH (2000) Ribosomal protein L2 is involved in the association of the ribosomal subunits, tRNA binding to the A and P sites and peptidyl transfer. *EMBO Journal* 19: 5241-5250.
- Dinman JD (1995) Ribosomal Frameshifting in Yeast Viruses. *Yeast* 11: 1115-1127.
- Dinman JD, Icho T, Wickner RB (1991) A -1 ribosomal frameshift in a double-stranded RNA virus forms a Gag-pol fusion protein. *PNAS* 88: 174-178.
- Dinman JD, Kinzy TG (1997) Translational misreading: Mutations in translation elongation factor 1 α differentially affect programmed ribosomal frameshifting and drug sensitivity. *RNA* 3: 870-881.
- Dinman JD, Ruiz-Echevarria MJ, Czaplinski K, Peltz SW (1997) Peptidyl transferase inhibitors have antiviral properties by altering programmed -1 ribosomal frameshifting efficiencies: development of model systems. *PNAS* 94: 6606-6611.
- Dinman JD, and Wickner RB (1992) Ribosomal frameshifting efficiency and gag/gag-pol

ratio are critical for yeast M1 double-stranded RNA virus propagation. *J Virology* 66: 3669-3676.

Dinman JD, Wickner RB (1994) Translational maintenance of frame: mutants of *Saccharomyces cerevisiae* with altered -1 ribosomal frameshifting efficiencies. *Genetics* 136: 75-86.

Farabaugh PJ (2000) Translational frameshifting: implications for the mechanism of translational frame maintenance. *Prog Nucleic Acid Res Mol Biol* 64: 131-170.

Farabaugh PJ, Zhao H, Vimaladithan A (1993) A novel programmed frameshift expresses the POL3 gene of retrotransposon Ty3 of yeast: frameshifting without tRNA slippage. *Cell* 74: 93-103.

Fourmy D, Recht MI, Blanchard SI, and Puglisi JD (1996) Structure of the A-site of *E. coli* 16 S rRNA complexed with an aminoglycoside antibiotic. *Science* 274:1367-1371.

Fourmy D, Yoshizawa S, and Puglisi JD (1998) Paromomycin binding induces a local conformational change in the A-site of 16s rRNA. *JMB* 277: 333-345.

Frank J and Agrawal RK (2000) A ratchet-like inter-subunit reorganization of the ribosome during translocation. *Nature* 406: 318-322.

Gabashvili IS, Agrawal RK, Grassucci R, Squires CL, Dahlberg AE, Frank J (1999) Major rearrangements in the 70S ribosomal 3D structure caused by a conformational switch in 16S ribosomal RNA. *EMBO J* 18: 6501-6507.

Grifo JA, Tahara SM, Morgan MA, Shatkin AJ, Merrick WC (1983) New initiation factor activity required for globin mRNA translation. *J Biol Chem* 258: 5804-5810.

- Gromadski KB, Daviter T, Rodnina MV (2006) A uniform response to mismatches in codon-anticodon complexes ensures ribosomal fidelity. *Mol Cell* 21: 369-377.
- Hani J, Feldmann H (1998) tRNA genes and retroelements in the yeast genome. *Nucleic Acids Res* 26: 689-696.
- Hansen JL, Moore PB, and Steitz TA (2003) Structures of five antibiotics bound at the peptidyl transferase center of the large ribosomal subunit. *J Mol Biol* 330: 1061-1075.
- Harger JW, Dinman JD (2003) An in vivo dual-luciferase assay system for studying translational recoding in the yeast *Saccharomyces cerevisiae*. *RNA* 9: 1019-1024.
- Harger JW, Dinman JD (2004) Evidence against a direct role for the Upf proteins in frameshifting or nonsense codon readthrough. *RNA* 10: 1721-1729.
- Harger JW, Meskauskas A, and Dinman JD (2002) An 'integrated model' of programmed ribosomal frameshifting and post-transcriptional surveillance. *Trends Biochem Sci* 27: 448-454.
- Hiraga K, Suzuki K, Tsuchiya E, Miyakawa T (1993) Cloning and characterization of the elongation factor EF-1 beta homologue of *Saccharomyces cerevisiae*. EF-1 beta is essential for growth. *FEBS Lett* 316: 165-169.
- Hobbie SN, Bruell C, Kalapala S, Akshay S, Schmidt S, Pfister P, Bottger EC (2006) A genetic model to investigate drug-target interactions at the ribosomal decoding site. *Biochimie* 88: 1033-1043.

- Horan LH and Noller HF (2007) Intersubunit movement is required for ribosomal translocation. *Proc Natl Acad Sci USA* 104(12): 4881-4885.
- Ikemura T (1982) Correlation between the abundance of yeast transfer RNAs and the occurrence of the respective codons in protein genes. Differences in synonymous codon choice patterns of yeast and *Escherichia coli* with reference to the abundance of isoaccepting transfer RNAs. *J Mol Biol* 158: 573-597.
- Inoue H, Nojima H, Okayama H (1990) High efficiency transformation of *Escherichia coli* with plasmids. *Gene* 96: 23-28.
- Ito H, Fukuda Y, Murata K, Kimura A (1983) Transformation of intact yeast cells treated with alkali cations. *J Bacteriol* 153: 163-168
- Jacobs JL, Dinman JD (2004) Systematic analysis of bicistronic reporter assay data. *Nucleic Acids Res* 32: e160-e170.
- Jacks T, Madhani HD, Masiarz FR, Varmus HE (1988). Signals for ribosomal frameshifting in the Rous sarcoma virus gag-pol region. *Cell* 55: 447-458.
- Jacks T and Varmus HE (1985) Expression of the Rous sarcoma virus pol gene by ribosomal frameshifting. *Science* 230: 1237-1242.
- Jasnos L, Sliwa P, and Korona R (2005) Resolution and repeatability of phenotypic assays by automated growth curve analysis in yeast and bacteria. *Analytical Biochemistry* 344: 138-140.
- Jeppesen MG, Ortiz P, Shepard W, Kinzy TG, Nyborg J, Andersen GR (2003) The crystal structure of the glutathione S-transferase-like domain of elongation

factor 1Bgamma from *Saccharomyces cerevisiae*. J Biol Chem 278: 47190-47198.

Katunin VI, Muth GW, Strobel SA, Wintermeyer W, Rodnina MV (2002) Important contribution to catalysis of peptide bond formation by a single ionizing group within the ribosome. Mol Cell 10: 339-346.

Kawakami K, Paned S, Faioa B, Moore DP, Boeke JD, Farabaugh PJ, Strathern JN, Nakamura Y, Garfinkel DJ (1993) A rare tRNA-Arg(CCU) that regulates Ty1 element ribosomal frameshifting is essential for Ty1 retrotransposition in *Saccharomyces cerevisiae*. Genetics 135: 309-320.

Klein DJ, Moore PB, and Steitz TA (2004) The Roles of Ribosomal Proteins in the Structure Assembly, and Evolution of the Large Ribosomal Subunit. J Mol Biol 340: 141-177.

Kozak M (1980) Role of ATP in binding and migration of 40S ribosomal subunits. Cell 22: 459-467.

Kramer EB, Farabaugh PJ (2007) The frequency of translational misreading errors in *E. coli* is largely determined by tRNA competition. RNA 13: 87-96.

Laughrea M (1981) Speed-accuracy relationships during in vitro and in vivo protein biosynthesis. Biochimie 63: 145-168.

Le H, Tanguay RL, Balasta ML, Wei CC, Browning KS, Metz AM, Goss DJ, Gallie DR (1997) Translation initiation factors eIF-iso4G and eIF-4B interact with the poly(A)-binding protein and increase its RNA binding activity. J Biol Chem 272: 16247-16255.

- Lim VI, Curran JF, Garber MB (2005) Ribosomal elongation cycle: energetic, kinetic and stereochemical aspects. *J Mol Biol* 351: 470-480.
- Ludwig A and Tenhaken R (2001) Suppression of the ribosomal L2 gene reveals a novel mechanism for stress adaptation in soybean. *Planta* 212: 792-798.
- Meskauskas A, Dinman JD (2001) Ribosomal protein L5 helps anchor peptidyl-tRNA to the P-site in *Saccharomyces cerevisiae*. *RNA* 7: 1084-1096.
- Moazed D and Noller HF (1987) Interaction of antibiotics with functional sites in 16S ribosomal RNA. *Nature* 327: 389-394.
- Muhlrad D, Hunter R, and Parker R (1992) A rapid method for localized mutagenesis of yeast genes. *Yeast* 8: 79-82.
- Mumberg D, Muller R, Funk M (1995) Yeast vectors for the controlled expression of heterologous proteins in different genetic backgrounds. *Gene* 156: 119-122.
- Nakagawa A, Nakashima T, Taniguchi M, Hosaka H, Kimura M, and Tanaka I (1999) The three-dimensional structure of the RNA-binding domain of ribosomal protein L2; a protein at the peptidyl transferase center of the ribosome. *EMBO Journal* 18(6): 1459-1467.
- Najafabadi HS, Lehmann J, Omid M (2007) Error minimization explains the codon usage of highly expressed genes in *Escherichia coli*. *Gene* 387: 150-155.
- Nierhaus KH (1990) The allosteric three-site model for the ribosomal elongation cycle: features and future. *Biochemistry* 29: 4997-5008.

- Nissen P, Hansen J, Ban N, Moore PB, and Steitz TA (2000) The structural basis of ribosome activity in peptide bond synthesis. *Science* 289: 920–930.
- Nissen P, Kjeldgaard M, Thirup S, Polekhina G, Reshetnikova L, Clark BF, Nyborg J (1995) Crystal structure of the ternary complex of Phe-tRNAPhe, EF-Tu, and a GTP analog. *Science* 270: 1464-1472.
- Ogle JM, Brodersen DE, Clemons WM, Jr., Tarry MJ, Carter AP, Ramakrishnan V (2001) Recognition of cognate transfer RNA by the 30S ribosomal subunit. *Science* 292: 897-902.
- Ogle JM, Murphy FV, Tarry MJ, Ramakrishnan V (2002) Selection of tRNA by the Ribosome Requires a Transition from an Open to a Closed Form. *Cell* 111: 721-732.
- Ogle JM, Ramakrishnan V (2005) Structural Insights into Translational Fidelity. *Annu Rev Biochem* 74: 129-177.
- Olarewaju O, Ortiz PA, Chowdhury W, Chatterjee I, Kinzy TG (2004) The translation elongation factor, eEF1B, plays a role in the oxidative stress response pathway. *RNA Biology* 1: 12-17.
- Peltz SW, Hammell AB, Cui Y, Yasenchak J, Puljanowski L, and Dinman JD, (1999) Ribosomal Protein L3 Mutants Alter Translational Fidelity and Promote Rapid Loss of the Yeast Killer Virus. *Mol Cell Biol* 19: 384-391.
- Percudani R, Pavesi A, Ottonello S (1997) Transfer RNA gene redundancy and translational selection in *Saccharomyces cerevisiae*. *J Mol Biol* 268: 322-330.

- Petrov A, Meskauskas A, Dinman JD (2004) Ribosomal Protein L3: Influence on Ribosome Structure and Function. *RNA Biol.* 1: 59-65.
- Plant EP, Jacobs KLM, Harger JW, Meskauskas A, Jacobs JL, Baxter JL, Petrov AN, Dinman JD (2003) The 9-Å solution: How mRNA pseudoknots promote efficient programmed -1 ribosomal frameshifting. *RNA* 9:168–174.
- Plant EP, Nguyen P, Russ JR, Pittman YR, Nguyen T, Quesinberry JT, Kinzy TG, Dinman JD (2007) Differentiating between Near- and Non-Cognate Codons in *Saccharomyces cerevisiae*. *PLOS one* 6(e517): 1-11.
- Planta RJ and Mager WH (1998) The list of cytoplasmic ribosomal proteins of *Saccharomyces cerevisiae*. *Yeast* 14(5): 471-477.
- Plewniak F (2007) GCG Documentation.
http://www.vet.gla.ac.uk/GCGdoc/Data_Files/codon_freq_tables.html.
- Rakwalska M, Rospert S (2004) The Ribosome-Bound Chaperones RAC and Ssb1/2p Are Required for Accurate Translation in *Saccharomyces cerevisiae*. *Mol Cell Biol* 24: 9186-9197.
- Rao MS, Hirsch F, Wu BC, Spohn WH, Busch H (1977) Comparative studies on the '5'-cap' and in vitro translational activity of cytoplasmic and nuclear poly A(+) RNA1. *Mol Cell Biochem* 15: 3-13.
- Rodnina MV, Gromadski KB, Kothe U, Wieden HJ (2005) Recognition and selection of tRNA in translation. *FEBS Lett* 579: 938-942.
- Sachs AB, Sarnow P, Hentze MW (1997) Starting at the beginning, middle, and end: translation initiation in eukaryotes. *Cell* 89: 831-838.

- Salas-Marco J, Bedwell DM (2005) Discrimination between defects in elongation fidelity and termination efficiency provides mechanistic insights into translational readthrough. *J Mol Biol* 348: 801-815.
- Sambrook J, Fritsch EF, and Maniatis T (1989) *Molecular cloning, a laboratory manual.*, C.Nolan, N.Ford, and M.Ferguson, eds. (Cold Spring Harbor, NY: Cold Spring Harbor Press).
- Sanbonmatsu KY, Joseph S, and Tung CS (2005) Simulating movement of tRNA into the ribosome during decoding. *Proc Natl Acad Sci USA* 102: 15854-15859.
- Sanbonmatsu KY (2006) Energy landscape of the ribosomal decoding center. *Biochimie* 88: 1053-1059.
- Sanbonmatsu KY (2006) Alignment/misalignment hypothesis for tRNA selection by the ribosome. *Biochimie* 88: 1075-1089.
- Sanbonmatsu KY, Joseph S (2003) Understanding discrimination by the ribosome: stability testing and groove measurement of codon-anticodon pairs. *J Mol Biol* 328: 33-47.
- Sandbaken MG, Culbertson MR (1988) Mutations in elongation factor EF-1 α affect the frequency of frameshifting and amino acid misincorporation in *Saccharomyces cerevisiae*. *Genetics* 120: 923-934.
- Schmeing TM, Huang KS, Strobel SA, Steitz TA (2005) An induced-fit mechanism to promote peptide bond formation and exclude hydrolysis of peptidyl-tRNA. *Nature* 438: 520-524.
- Shatkin AJ (1976) Capping of eucaryotic mRNAs. *Cell* 9: 645-653.

- Sievers A, Beringer M, Rodnina MV, Wolfenden R (2004) The ribosome as an entropy trap. *Proc Natl Acad Sci USA* 101: 7897-7901.
- Sikorski RS and Hieter P (1989) A system of shuttle vectors and yeast host strains designed for efficient manipulation of DNA in *Saccharomyces cerevisiae*. *Genetics* 122: 19-27.
- Somogyi P, Jenner AJ, Brierley I, and Inglis SC (1993) Ribosomal pausing during translation of an RNA pseudoknot. *Mol Cell Biol* 13: 6931–6940.
- Song H, Mugnier P, Das AK, Webb HM, Evans DR, Tuite MF, Hemmings BA, Barford D (2000) The crystal structure of human eukaryotic release factor eRF1—mechanism of stop codon recognition and peptidyl-tRNA hydrolysis. *Cell* 100: 311-321.
- Spahn CMT, Beckmann R, Eswar N, Penczek PA, Sali A, Blobel G and Frank J (2001) Structure of the 80S ribosome from *Saccharomyces cerevisiae* – tRNA-ribosome and subunit-subunit interactions. *Cell* 107: 373-386.
- Spahn CM, Gomez-Lorenzo MG, Grassucci RA, Jorgensen R, Andersen GR, Beckmann R, Penczek PA, Ballesta JP, Frank J (2004) Domain movements of elongation factor eEF2 and the eukaryotic 80S ribosome facilitate tRNA translocation. *EMBO J* 23: 1008-1019.
- Stansfield I, Jones KM, Herbert P, Lewendon A, Shaw WV, Tuite MF (1998) Missense translation errors in *Saccharomyces cerevisiae*. *Journal of Molecular Biology* 282: 13-24.
- Stoletzki N, Eyre-Walker A (2007) Synonymous codon usage in *Escherichia coli*: selection for translational accuracy. *Mol Biol Evol* 24: 374-381.

- Sumpter VG, Tate WP, and Nierhaus KH (1990) The complex between ribosomal proteins and aminoacyl-tRNA: the interactions and hydrolytic activities are not confined to the proteins L2 and L16 of *Escherichia coli* ribosomes. *Biochimica et Biophysica Acta* 1048: 265-269.
- Toussant M, Levasseur G, Gervais-Bird J, Wellinger RJ, Elela SA, and Conconi A (2006) A high-throughput method to measure the sensitivity of yeast cells to genotoxic agents in liquid cultures. *Mutation Research* 606: 92-105.
- Triana-Alonso FJ, Chakraborty K, Nierhaus KH (1995) The elongation factor 3 unique in higher fungi and essential for protein biosynthesis is an E site factor. *J Biol Chem* 270: 20473-20478.
- Tu C, Tzeng TH, and Bruenn JA (1992) Ribosomal movement impeded at a pseudoknot required for frameshifting. *Proc Natl Acad Sci USA* 89: 8636-8640.
- Tumer NE, Parikh B, Li P, Dinman JD (1998) Pokeweed antiviral protein specifically inhibits *TyI* directed +1 ribosomal frameshifting and *TyI* retrotransposition in *Saccharomyces cerevisiae*. *J Virol* 72: 1036-1042.
- Uhlein M, Weglohner W, Urlaub H, and Wittmann-Liebold B (1998) Functional implications of ribosomal protein L2 in protein biosynthesis as shown by in vivo replacement studies. *Biochem J* 331: 423-430.
- Vicens Q and Westhof E (2001) Crystal Structure of Paromomycin Docked into the Eubacterial Ribosomal Decoding A Site. *Structure* 9: 647-658.
- Warrington J and Blomberg A (2003) Automated screening in environmental arrays allows analysis of quantitative phenotypic profiles in *Saccharomyces cerevisiae*. *Yeast* 20: 53-67.

- Weinger JS, Parnell KM, Dorner S, Green R, Strobel SA (2004) Substrate-assisted catalysis of peptide bond formation by the ribosome. *Nat Struct Mol Biol* 11: 1101-1106.
- Wickner RB (1974) Chromosomal and nonchromosomal mutations affecting the “killer character” of *Saccharomyces cerevisiae*. *Genetics* 76: 423-432
- Wickner RB and Leibowitz MJ (1976) Two chromosomal genes required for killing expression in killer strains of *Saccharomyces cerevisiae*. *Genetics* 82: 429-442.
- Wills N, Moore B, Hammer A, Gesteland RF, Atkins JF (2006) A Functional -1 Ribosomal Frameshift Signal in the Human Paraneoplastic Ma3 Gene. *J Biol Chem* 281: 7082-7088.
- Willumeit R, Forthmann S, Beckmann J, Diedrich G, Ratering R, Stuhmann HB, and Nierhaus KH (2001) Localization of the Protein L2 in the 50 S Subunit and the 70 S E. coli Ribosome. *J Mol Biol* 305: 167-177.
- Wilson W, Malim MH, Mellor J, Kingsman AJ, and Kingsman SM (1986) Expression strategies of the yeast retrotransposon Ty: a short sequence directs ribosomal frameshifting. *Nucleic Acids Res.* 14: 7001-7016.
- Wilson KS and Noller HF (1998) Molecular movement inside the translational engine. *Cell* 92: 337-349.
- Wintermeyer W, Peske F, Beringer M, Gromadski KB, Savelsbergh A, Rodnina MV (2004) Mechanisms of elongation on the ribosome: dynamics of a macromolecular machine. *Biochem Soc Trans* 32: 733-737.
- Winzeler EA, Shoemaker DD, Astromoff A, Liang H, Anderson K, et al. (1999)

Functional characterization of the *Saccharomyces cerevisiae* genome by gene deletion and parallel analysis. *Science* 285: 901-906.

Wittmann-Liebold B, Uhlein M, Urlaub H, Muller E, Otto A, Bischof O (1995) Structural and functional implications in the eubacterial ribosome as revealed by protein-rRNA and antibiotic contact sites. *Biochem. Cell Biol.* 73: 1187-1197.